University of Pretoria

In vitro study of *in silico* designed sirtuin 1 and bromodomain 4 inhibitors on human neuroblastoma SH-SY5Y and acute myeloid leukemia U937 cells

by
Monique Otto

Submitted in partial fulfilment of the requirements for the degree
Master of Science degree in Human Physiology

Department of Physiology
School of Medicine
Faculty of Health Sciences
University of Pretoria

Supervisor: Dr BA Stander
Co-supervisors: Prof P du Toit, Prof AD Cromarty

2018

MSc candidate:
Miss M Otto
12028054
Department of Physiology
University of Pretoria
Tel: +27 12 332 4558
E-mail address: moniqotto@gmail.com

Supervisor:
Dr BA Stander
Department of Physiology
University of Pretoria
Tel: +27 12 319 2241
Fax: +27 12 321 1679
E-mail address: andre.stander@up.ac.za

Co-supervisor:
Prof P du Toit
Department of Physiology
University of Pretoria
Tel: +27 12 420-2536
E-mail address: peet.dutoit@up.ac.za

Co-supervisor:
Prof AD Cromarty
Department of Pharmacology
University of Pretoria
E-mail address: duncan.cromarty@up.ac.za

Declaration

University of Pretoria
Faculty of Health Sciences
Department of Physiology

Title of Project:

In vitro study of *in silico* designed sirtuin 1 and bromodomain 4 inhibitors on human neuroblastoma SH-SY5Y and acute myeloid leukemia U937 cells.

I, Monique Otto **(**Student number: 12028054), declare that:

I understand what plagiarism is and am aware of the University's policy in this regard.
I declare that this project is my own original work. Where other people's work has been used, this has been properly acknowledged and referenced in accordance with departmental requirements.
I have not used work previously produced by another student or any other person to submit as my own.
I have not allowed, and will not allow, anyone to copy my work with the intention of presenting it as their own.

Signature

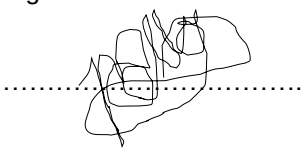

Acknowledgements

I wish to express my sincerest appreciation towards the following persons and institutions upon the completion of this degree:

To my Supervisors;
Dr A Stander, my main supervisor; my sincerest thanks for your endless patience, guidance and advice from the first day of my third year physiology classes to the last day we laboured to complete this project. I am so thankful to have had you as my 'teacher' and friend throughout this time. To Prof P du Toit, my co-supervisor and dear mentor from my second year physiology classes to (hopefully) forever; I cannot thank you enough for all your kind words and gentle encouragement, as well as for the opportunities this year to work for you by means of the HFPA to gain experience. I will be forever grateful to you. To Prof D Cromarty, thank you for sharing your NRF student funds and for your studious advice towards improving this thesis.

To my friends and colleagues;
My lab mates Desiree Frazer, Stephan Basson, Trophimus Thembo, Jessie Chang, Vangi Nortje and all other students who were constantly coming and going; thank you for all the work discussions we had, for your assistance and advice and for accepting mine, and mostly for all the kindness have received from you throughout this time and the laughs we shared at the end of a hard day's work. To the Department of Physiology; thank you everyone for the time we shared these three years, for your friendly greetings in the hall on 25 hour days and for all your help when I needed it, especially when I started at the department as a new MSc student who had completed an honours degree elsewhere. Thank you for being such splendid people to work with; Prof A Joubert, Dr M van Rooy, Dr M Coetzee, Dr C Grobbelaar, Dr P Bipath, Dr A Koorts, Ms D Crafford, Mr M Kleynhans, Mr A Kasonga, Ms M Mabena, Mr C Ramphisa and every other member – thank you! To my friends from other departments and faculties; Prof E Chirwa, Mohammed Hamad and everyone else; thank you for your endless support and friendship. You are all dear to me.

To the campus administration and security on both the Hatfield and Prinshof campuses; thank you for being helpful, supportive and friendly. Receiving assistance with a smile and a kind word had meant a great deal to me.

To my funding bodies; the NRF, UP Postgraduate and the Thuthuka fund; thank you for enabling me to undertake this project and for your empowering support throughout these years of study. Please know that you hold my sincerest appreciation.

To my family; my mother and father, E M Otto and J L Otto, to my grandmother, A Roos and my uncle Carel and everyone else who financially or otherwise supported my work throughout the years of

study. A special thanks in remembrance also to my dear grandfather, F Roos and my grandmother and grandfather, MSJ Otto and GA Otto. Please accept my sincere thanks and appreciation.

To my special friend, Jacques v d Merwe; thank you for your unfailing devotion. Thank you for every uplifting word, every kind gesture and for every day that your love carried my steps.

To my Lord Jesus, my ever present friend and confidant; thank you for your mercy, your daily gifts and for blessing me with life and opportunity. Thank you for your nearness throughout this time, for your daily strength and forgiveness. Thank you for seeing me and knowing me, and for your endless love.

I dedicate this work
to every precious person living with cancer or sharing the heavy load of a loved one.

“..when pain is to be born, a little courage helps more than much knowledge, a little human sympathy more than much courage, and the least tincture of the love of God more than all.”

— C.S. Lewis, The Problem of Pain

“May the God of hope fill you with all joy and peace in believing, so that by the power of the Holy Spirit you may abound in hope.”

— Romans 15:13

Summary

In this novel study, the effects of newly *in silico* designed bromodomain 4 and sirtuin 1 inhibitors on cellular growth and death was investigated in the neuroblastoma SH-SY5Y and acute myeloid leukemia U937 cell lines. The investigated bromodomain 4 compounds were found to be not as potent when compared to the sirtiun 1 inhibitor, W137. Therefore, the anti-proliferative effects and mechanistic action of W137 on the two human cancer cell lines were investigated.

The regulation of cancer associated gene expression may be possible in SIRT1-advantaged cancers such as in neuroblastoma and acute myeloid leukemia through the inhibition of SIRT1, which functions by deactivating or down-regulating anti-cancer proteins through deacetylation. Crystal violet DNA staining was applied to study the effect of W137 on cell numbers of SH-SY5Y cells and inhibition of cell proliferation was achieved in a concentration dependent manner. An $IC_{50(SIRT1)}$ value of 20 µM for the SH-SY5Y cells and 25 µM for U937 cells was determined after 48 h exposure. The $IC_{50(SIRT1)}$ values obtained for the compound as tested on the two cell lines were comparable to other well-known SIRT 1 and 2 inhibitors and low enough to merit further experimentation. Qualitative studies on cell morphology employing fluorescent microscopy and triple dye staining indicated a decrease in cell density and loss of cellular membrane integrity. A slight increase in propidium iodide staining of DNA after 48 h exposure to the W137 compound suggested either necrosis and/or late stages of apoptosis.

Employing flow cytometry and propidium iodide to study the progression of the cell cycle revealed increased cell numbers in the sub-G_1 phase in SH-SY5Y and U937 cells, suggesting cell death is induced by W137 after 24 and 48 h respectively. No significant cell cycle block in either the G_1 or G_2/M phase was observed, suggesting that the compound does not work by modulating the cycle in SH-SY5Y cells. The efficacy of W137 does not vary significantly after 24 h exposure compared to 48 h exposure for the SH-SY5Y cell line, while an increase in compound efficacy seems to be observed after an extended exposure period (48 h) for the U937 cell line.

Flow cytometry employing propidium iodide in conjunction with Annexin V was used to analyse cell death induced via apoptosis and/or necrosis and 24 h as well as 48 h exposure to the W137 compound revealed an increase in early and late apoptosis with a slight increase in necrosis, in SH-SY5Y cells. Analysis of the U937 cell line indicated a slight population shift towards early apoptosis after 24 h exposure and a slight shift towards late apoptosis and necrosis after 48 h. These findings confirm that cell death occurs via apoptosis in the SH-SY5Y as well as in the U937 cell line when exposed to W137. SH-SY5Y (Control: 22.32% vs exposed: 26.53%) and U937 (Control: 24.52% vs exposed: 43.07%) cells exhibited increased mitochondrial membrane depolarization and therefore the intrinsic mitochondrial pathway is the likely means by which apoptosis is achieved. Therefore, apoptosis is the mechanism by which cell death is achieved in both cell lines, as confirmed by cell cycle studies, analyses of cell death and mitochondrial membrane permeability studies in both cell lines. Levels of hydrogen peroxide (H_2O_2) generated within W137-exposed cells after 48 h was measured using DH2CF-DA and flow cytometry. After 48 h exposure, a statistically significant decrease in DCF-fluorescence SH-SY5Y cells (Control: 40 vs exposed: 13.4) but not U937 cells (Control: 251.4 vs exposed: 259.8) was observed, suggesting that increased ROS levels was not induced in response to W137 exposure after 48 h.

To study the effect of exposure to the W137 compound on the expression of the *p53* and *C-MYC* genes, both key factors in healthy and cancerous cells, the quantitative reverse transcriptase polymerase chain reaction (qRT-PCR) technique was employed. The SH-SY5Y cell line indicated a decrease in *C-MYC* levels upon Actinomycin D and W137 exposure after 24 h, while expression of the *p53* gene was decreased after 24 h Actinomycin D exposure. Exposure to W137, however, increased *p53* expression after 24 h as well as 48 h. *p53* is crucial in programming cells for death and probably induces SH-SY5Y cells to enter apoptosis. Significant increase in *C-MYC* gene expression was observed in U937 cells after Actinomycin D exposure after 24 h and 48 h (p-value <0.05). Repression of SIRT1 therefore possibly resulted in the activation or increased expression of the pro-apoptotic gene *p53*, possibly enhancing cancer cell susceptibility to death and repair mechanisms. MYC oncoproteins, which are commonly up-regulated in human cancers of different organ origins, exert oncogenic effects by modulating gene and protein expression.

ELISA (Enzyme-linked Immunosorbent Assay) was employed to test for change in p53 protein K382 acetylation and activity following 48 h exposure to W137. The active, acetylated p53 protein is a crucial component in cell maintenance, damage detection and programmed cell death, and inhibition or down-regulation of p53 has been detected in many cancer types (1-3). Deacetylation of p53 by SIRT1 results in protein deactivation or down-regulation and therefore SIRT1 inhibition is expected to result in p53 being in the acetylated stage and active (4). Following 48 h exposure, analyses of the SH-SY5Y cells indicated a small but statistically significant increase in the expression of K382 acetylated p53 protein in Actinomycin D (1.17-fold) and W137 exposed cells (1.12-fold) (p-value <0.05).

In conclusion, the novel dual SIRT1 and 2 inhibitor W137 therefore inhibited cell proliferation in both the U937 and SH-SY5Y cell lines in a dose-dependent manner through the inhibition of cell growth and the induction of cell death *in vitro*. The two cell lines exhibited different reactions to the compound in some experiments but similar reactions in others, motivating the importance of further study into the cell line specificity and mechanistic variation of W137. The confirmation of these results by that obtained from the fluorescent microscopy study leads to the conclusion that apoptosis is the most likely cause of cell death for these cell lines. The current study contributes to the unravelling of the *in vitro* molecular mechanisms associated with and influenced by SIRT1 and SRT2 providing a basis for further research on this multi-functional cellular component and its diverse role in disease regulation. The W137 compound could potentially be an effective component in a drug designed to treat more than one type of cancer.

Keywords: Anti-cancer, acute myeloid leukemia (AML), neuroblastoma, sirtuin 1 (SIRT1), U937, SH-SY5Y, flow cytometry, apoptosis, cell cycle, mitochondrial membrane potential (MMP), reactive oxygen species (ROS), gene expression, qRT-PCR, protein acetylation, ELISA, *p53*, *C-MYC*.

Table of Contents

List of Abbreviations

ADP	Adenosine diphosphate
AML	Acute myeloid leukemia
AIDS	Acquired Immunodeficiency Syndrome
AIF	Apoptosis inducing factor
ATCC	American Type Culture Collection
ATK	Protein kinase B
ATP	Adenosine triphosphate
ATPase	Adenosine triphosphosphate-phosphatase
BAD	Bcl-2 antagonist of cell death
BAK	Bcl-2 homologous antagonist/killer
BAX	Bcl-2-associated X protein
BCA	Bicinchoninic acid assay
Bcl-2	B-cell CLL/lymphoma 2
Bcl-xL	B-cell lymphoma-extra large
Bcl-w	B-cell lymphoma-wee (Scottish slang word meaning ‘small’)
BH3 motif	Bcl-2 homology domain 3
BRD4	Bromodomain 4
Ca2+	Calcium ion
CDK	Cyclin Dependent Kinases
CDK1	Cyclin Dependent Kinase 1
CDK2	Cyclin Dependent Kinase 2
CDK4	Cyclin Dependent Kinase 4
CDK6	Cyclin Dependent Kinase 6
cDNA	Complimentary DNA
C-MYC	V-MYC myelocytomatosis viral oncogene homolog
CO2	Carbon dioxide
CV	Crystal violet
DiOC6(3)	3,3'-Dihexyloxacarbocyanine Iodide
D-MEM	Dulbecco’s minimum essential medium eagle
DMSO	Dimethyl sulfoxide
DNA	Deoxyribonucleic acid
DSB	Double-strand breaks

E2F	Elongation factor 2
EDTA	Ethylenediaminetetraacetic acid
ELISA	Enzyme-Linked ImmunoSorbent Assay
ER	Endoplasmic reticulum
ERK	Extracellular signal-regulated kinases
FCS	Fetal calf serum
FITC	Fluorescein isothiocyanate
FSC	Forward Scatter Channel
GAP	GTPase activating protein
H2DCFDA	2′,7′-Dichlorodihydrofluorescein diacetate
HiF-1α	Hypoxia-inducible factor 1-alpha
HiF-2α	Hypoxia-inducible factor 2-alpha
HIV	Human Immunodeficiency Virus
HK2	Hexokinase-2
IC50	Half maximal inhibitory concentration (Inhibitory Concentration of 50%)
IGF1/2	Insulin-like growth factors 1 and 2
IMDM	Iscove's Modified Dulbecco's Medium
Lys382	Lysine amino acid residue 382
Max	MYC-associated factor X
Mcl-1	Myeloid cell leukemia-1
MKP3	Mitogen-activated protein kinase phosphatase 3
miR-34a	MicroRNA 34a
MMP	Mitochondrial Membrane Potential
mRNA	Messenger RNA
m-Tor	Mammalian/Mechanistic target of rapamycin
NAD+	Nicotinamide adenine dinucleotide
NADH	Reduced nicotinamide adenine dinucleotide
NFKB	Nuclear Factor-kappa B
NOXA	Phorbol-12-myristate-13-acetate-induced protein 1
N-MYC	V-MYC myelocytomatosis viral oncogene homolog
PB	Phosphate buffer
PBS	Phosphate buffered saline
PCR	Polymerase chain reaction
PI3K	Phosphoinositide 3-kinase

pRb	Retinoblastoma protein
PS	Phosphatidylserine Phospholipid
q-RT PCR	Quantitative reverse transcription polymerase chain reaction
P-TEFb	Positive transcription elongation factor B
PUMA	p53 up-regulated modulator of apoptosis
RAS	Rat Sarcoma
RNA	Ribonucleic acid
ROS	Reactive oxygen species
SIRT1	Sirtuin 1
SIRT2	Sirtuin 2
SIRT3	Sirtuin 3
SIRT4	Sirtuin 4
SIRT5	Sirtuin 5
SIRT6	Sirtuin 6
SIRT7	Sirtuin 7
SSC	Side Scatter Channel
STAT1	Signal transducer and activator of transcription 1
TBS	Tris buffered saline
TNF	Tumor necrosis factor
Tris	Hydroxymethylaminomethane
Tris HCl	Hydroxymethylaminomethane hydrochloride
UV	Ultra-violet
VDAC	Voltage dependent anion channel
WR	Working reagent

List of Figures

List of Tables

Chapter 1: Literature Review

Cancer and cancer incidence

Cancer is a group of specialized molecular heterogenic diseases characterized by malignant, ill-regulated proliferation of cells resulting in either a solid tumour mass or other abnormal cellular conditions (5-7). Cancer cells reproduce uncontrollably, bypassing normal cell regulatory controls and often metastasize to distant parts of the body. Cancer arises from a single normal cell or groups of cells which suffer genomic or epigenomic mutation that cannot be repaired by cell rehabilitation mechanisms or the cell does not die due to one or other regulatory dysfunction. When a mutation activates a proto-oncogene (such as *C-MYC*) (8) to become an oncogene or inhibits a tumour suppressor gene (such as *p53*) (1), cancer arises.

Annually there are approximately 7.4 million cancer related deaths worldwide and the disease is classified among the leading causes of severe illness related morbidity and mortality (5). In first world countries, cancer has been shown to be the number one cause of death and the second major contributor in developing countries (9). In 2011 alone, approximately 14 million new cases of cancer and 8.2 million cancer related deaths were reported worldwide (5-7). Over the next two decades, an increase of 70% in the number of new cases is expected due to high risk lifestyle choices, increased levels of air-, water-, and food carcinogens, increased occurrence of immune-compromising conditions such as human immunodeficiency virus (HIV) infection, rising stress levels in the general population and disease evolution (5, 6, 9). Cancer can affect any organ and tissue type in almost any part of the body. The leading causes of cancer related death are cancers of the lung, liver, stomach, colorectal, breast, and oesophagus (5, 9). Current therapies for the treatment of cancer include chemotherapy, immunotherapy, chemoradiotherapy and surgery to excise the tumorigenic mass.

Acute myeloid leukemia and neuroblastoma

Acute myeloid leukemia (AML) is a genetically heterogeneous blood cancer affecting the haematopoietic myeloid progenitor cells (myeloblasts) resulting in the affected cells losing the ability to grow, proliferate and differentiate normally (10, 11). This results in accumulation of non-functional, un-matured myeloblasts with a high metabolic rate and abnormal functionality (10, 11). The disease is characterized by uncontrolled proliferation resulting in a high level of anomalous blood cells in the bone marrow and the blood, as well as accumulated in other organs in the body. This interferes with normal hematopoietic function (12, 13). Research indicates that disease incidence increases with age since the norm of 3,8 cases per 100 000 in patients under 64 years rises to 17,9 cases per 100 000 in patients older than 64 years (14). As with all other cancers, risk factors such as exposure to carcinogenic chemicals (benzene from cigarette smoke etc.), ionizing radiation and cytotoxic chemotherapy aimed at treating tumours increases the chances of acquiring AML. Of all cancer patients treated with chemotherapy, 10-15% have subsequently been diagnosed with AML (10). This type of cancer is therefore often considered as being a secondary condition to other malignancies, as it occurs more commonly compared to other cancers and possibly due to commonly occurring risk factors. Prognosis is frequently poor despite treatment.

Neuroblastoma is a brain tumour of neural crest origin that affects immature neurons and occurs in young children but rarely found in children older than 10 years (6, 15, 16). It is the most common form of childhood cancer but is often only diagnosed after it has metastasized to other areas of the body where more apparent cancer symptoms are elicited. Neuroblastomas occur in thesympathetic nervous system and therefore form tumorous masses in any organ enervated by sympathetic nerve tracts (15). The adrenal glands are the source of approximately a third of all neuroblastoma cases while a quarter of all cases have their origins in the sympathetic nerve ganglia of the lower abdomen (6, 15, 16). The remaining cases originate in the spinal cord, neck or chest. Neuroblastoma is also a cancer associated with poor prognosis, often due to late discovery when the disease has reached advanced stages, with intensive metastasis and limited treatment options that are rarely more than marginally effective (6, 15, 16).

The hallmarks of cancer

The six biological capabilities that can be acquired during the multistep development of human tumours are referred to as the hallmarks, or characteristic features, of neoplastic disease (6, 17). For normal cells to become tumorigenic and ultimately metastatic, these hallmark capabilities need to be acquired in a progressive order (6, 17). The six hallmarks include sustaining proliferative signalling, the evasion of growth suppressors, resisting cell death induction mechanisms, enabling indefinite replication, promoting angiogenesis and inducing tissue invasion and metastasis. Instability of the genome, which generates the genetic diversity that allows the characteristics to be acquired, as well as chronic inflammation, which promotes several of the hallmark functions, lies at the essence of the fundamental hallmarks (18, 19). Researchers have also recently named two emerging cancer characteristics as being significant in promoting cancer development, namely the reprogramming of cell energy metabolism and evasion of the immune system (6, 17)(Figure 1.1.3.1).

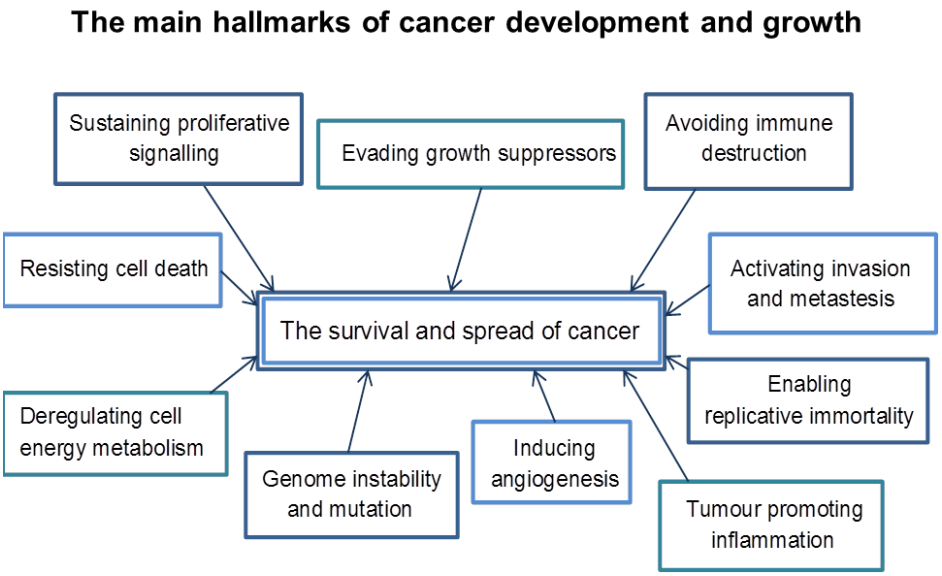

Figure 1.1.3.1: Schematic representation of the hallmarks of cancer. The prime characteristics cells need to acquire in order to cause disease include mechanisms of unhindered growth and spread to other tissues and organs, routes of cell maintenance evasion and deviation of cellular pathways to create increased energy supply for cells and blood supply for cancer tissue (18, 19).

Solid tumours contain a complex repertoire of recruited, seemingly normal cells that are important in establishing the tumour microenvironment (20). Tumours are not insular masses of proliferating cancer cells but rather a complex of multiple distinct

cell types continually participating in heterotypic interactions with one another (21, 22). The wide variety of tumour types that exist, all possess histopathological variation as well as genetic and epigenetic distinctions, complicating the understanding of the disease and the establishment of effective therapies (21, 22).

The targeting of the cancer pathogenesis mechanism as a treatment is thought to be one of the most noteworthy findings relating to human cancer research over the decades (6, 17). Cancer hallmarks as mechanistic targets are central to this treatment approach and that of future therapies. The increasing number of existing targeted therapeutics can be categorized according to the specific cancer hallmark or hallmarks that are targeted (21, 22). Treating cancer based on specific characteristics and measuring the efficacy of drugs based on the changes in these characteristics in response to treatment, serves as validation of that specific hallmark for that specific cancer. If a cancer hallmark is crucial to the biology of the tumour, then tumour growth and progression may be impaired by inhibiting of that specific hallmark (21, 22).

Most hallmark-targeting cancer drugs developed thus far have been directed to target specific components of cellular pathways involved in enabling particular capabilities (6). Treatments specific to cancerous cells have been considered fundamental in cancer therapy as it presents inhibitory activity against the dysfunctional target while being less toxic towards healthy cells (23, 24). The molecular, metabolic, structural and functional differences between cancerous and non-cancerous cells contributes to normal cells being less susceptible to certain anti-cancer drugs (23). As an example, cells that undergo normal cell division have been reported to be less sensitive to mitotic inhibitors compared to cancer cells where proliferation occurs much faster (23).

Each of the core hallmarks is thought to be regulated by partially redundant and highly specialized, ultra-communicative signalling pathways (6, 17). Therefore, by targeting a single key pathway during therapy, a critical capability may not be completely eradicated. Some cancer cells may subsequently survive and their progeny eventually evolve towards the selective pressure imposed by the applied therapy and become resistant (25). Such adaptation, accomplished by epigenetic

reprogramming, mutation and remodelling of the stromal microenvironment, can re-establish tumour growth and clinical relapse (6, 17).

Cancer cells may also gain resistance to a drug by systematically reducing their dependence on the particular hallmark being targeted by the therapy, resulting in cells becoming more dependent on adjacent cells for support. Solid tumours obtain blood flow through the secretion of angiogenic factors (cytokines) that induce the formation of a network of vascular capillaries for the tumour mass, contributing to its self-efficiency (26, 27). In selected preclinical models where potent angiogenesis inhibitors succeed in suppressing this capability, tumours have been reported to adapt and shift from a dependence upon continued angiogenesis to increasing invasiveness and cancer metastasis (6, 28). Hypoxic cancer cells evidently gain access to pre-existing tissue vasculature to obtain oxygen by invasion of neighbouring cells, rendering anti-angiogenic drugs ineffective against these cells. This form of adaptive resistance strategy is apparent in the increased level of invasion and local metastasis that is seen when human glioblastomas are treated with angiogenesis inhibiting drugs (29). How this mechanism dominates in other human cancers is yet to be established.

Analogous adaptive shift in dependence from one hallmark to another may also negatively influence the efficacy of analogous hallmark-targeting therapies (6). The deployment of apoptosis-inducing drugs, for example, may induce cancer cells to up-regulate mitogenic signalling, resulting in compensation for the initial reaction triggered by treatments through an increased rate of mitosis and reproduction (30, 31). Therefore, multiple biochemical pathways linked to each hallmark should be considered when developing drugs and designing treatment protocols. Multiple core and emerging hallmarks and enabling characteristics should be simultaneously targeted by means of mechanism-orientated combination therapeutics. New research and treatment strategies should be aimed at more effective and durable therapies for human cancer through the incorporation of knowledge regarding established hallmarks as well as additive capabilities (6). New anti-cancer drugs should be developed while continuously taking drug resistance, mechanistic bypassing strategies and undiscovered neoplastic characteristics into consideration. Future research may render it possible to therapeutically target the majority of

cancer cell supporting pathways simultaneously, therefore preventing the development of adaptive resistance and eventual disease relapse (6, 17).

The cell cycle

1.4.1 An overview of the stages and progression of the cell cycle and the mechanism of cancer

The period between the formation of one cell as a product of cellular division to when that cell undergoes division to create the next generation, is known as the cell cycle (32, 33). During this process, the DNA of the cell and all other cellular components are duplicated in order to produce two identical daughter cells, which are also genetically identical to the parent cell. In eukaryotes, such as human beings, the cell cycle is divided into four phases, namely G_1 (gap 1), S (synthesis), G_2 (gap 2) and M (mitosis). Cells that had not entered the cell cycle are referred to as being in a quiescent or sedentary stage called the G_0 phase. Mitosis is the stage when a somatic parent cell divides once to form two identical daughter cells through appropriate segregation and separation of chromosomes and other cellular components. The main purpose fulfilled by the cell cycle and mitosis is to enable the organism to grow, adapt to changing conditions and to replace damaged or old cells. Figure 1.1.4.1 illustrates an overview of the main phases of the cell cycle (blue) and the phase transition checkpoints (red):

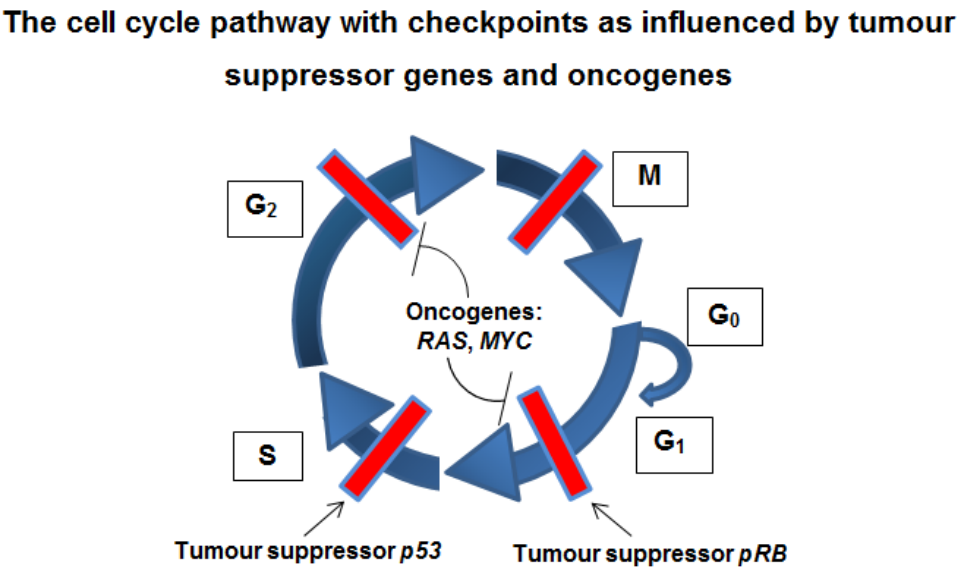

Figure 1.1.4.1: The phases of the cell cycle (blue); G_1 (gap1), S (DNA synthesis/replication), G_2 (gap 2) and M (mitosis). G_1 prepares the maturing cell for DNA synthesis which takes place during the S phase. The cell continues to grow and prepare for division through the G_2 phase, cell components start to divide and chromatin condenses to form chromosomes that separate during mitosis (32). Cells withdraw from the cell cycle upon damage detection at the DNA checkpoints (red) and are either rectified by repair machinery or undergo programmed cell death (34). Tumour suppressors that are active at the G_1/S and S/G_2 checkpoints, respectively, as well as oncogenes that allow damaged cells to bypass the G_1/S and G_2/M checkpoints, respectively, are indicated.

Cells in G_0 (Gap 0 or quiescent) are non-dividing, metabolically active cells that are functional but in a resting, non-proliferating state (32). Cells re-enter the G_1 phase from G_0 if the appropriate growth factors are present and the cell cycle is initiated. Eukaryotic cell division is a highly regulated process and cells can also enter senescence, an irreversible state of arrest to prevent proliferation of harmful cells, from the G_0 phase. Proteins and enzymes needed for DNA replication only accumulate when the cell is preparing to undergo division (35). When specific growth inhibitory signals are detected or there is an absence of appropriate mitogenic signalling, proliferation is paused and cells enter the G_0 phase to be repaired or to enter programmed cell death (apoptosis). A highly conserved family of multifunctional enzymes, referred to as cyclin dependent kinases (CDKs), mediates cell cycle progression by means of binding to and modifying protein substrates (35). When CDKs bind to specific regulatory subunits referred to as a cyclins, active cyclin/CDK complexes are formed. The complexes are central in cell cycle regulation

and progression, with specific cyclin complexes controlling a specific stage of the transition from one phase to the next (35). The rate of cell division also depends on the location of the cells in the body, the tissue type, the age of the organism as well as whether the cells are normal or cancerous (34).

In normal, healthy cells, CDK expression occurs throughout the cell cycle and each cyclin protein has a tightly regulated, limited time-frame of expression (Figure 1.1.4.1). This highly synchronised expression and time of activity is mediated through cell cycle-dependent regulation on both the cyclin gene transcription level and protein degradation (Figure 1.1.4.1). For CDK activation to occur, binding to a specific cyclin protein at a specific stage needs to take place. The integrity of the resulting cyclin/CDK complex is tightly regulated by covalent modification by cyclin activating kinases and by dephosphorylation (mediated by members of the Cdc25 family) events resulting in activation and inhibition of protein kinase activity only when required (Figure 1.1.4.1). The CDK activating kinase (CAK) is responsible for mediating activation by phophorylation of CDK1, CDK2, CDK4 and CDK6. The CAK protein complex consists of the 3 subunits, namely CDK7, cyclin H and MAT1 (35). Cyclin degradation by the ubiquitin proteasome system also plays a role in the progression of cells through the cell cycle. Two families of CDK inhibitors exist, namely the INK4 inhibitors (inhibits CDK4 and CDK6 activity during the G_1 phase) and the Cip/Kip inhibitors (inhibit CDK activity during all phases of the cell cycle). Both families are influenced by various forms of cell stress and growth inhibitory pathways and can initiate cell cycle arrest in the G_1 phase through CDK inhibition and prevention of their ability to phosphorylate pRb (Retinoblastoma protein) and other pRb-family proteins (Figure 1.1.4.1).

Throughout eukaryotic cell cycle progression, signalling pathways monitor the successful completion of events in one phase of the cycle before proceeding into the next phase. These regulatory pathways and spaces of maintenance are commonly referred to as cell cycle checkpoints (36). Cell processes can be temporarily halted at cell cycle checkpoints to allow for repair of cellular damage or cycle arrest can be initiated due to unavailability of essential growth factors, hormones or nutrients. When cellular damage is beyond repair or cell stress is too intensive, checkpoint signalling halts progression and potentially hazardous cells are eliminated through

permanent cell cycle arrest and/or apoptosis (Figure 1.1.4.1). When cells pass the screening and transition through a checkpoint, the cell cycling continues irreversibly until the next checkpoint. Four main checkpoints exist, including the G_1/S checkpoint, the S phase checkpoint, the G_2/M checkpoint and the spindle checkpoint. The cell cycle checkpoint pathways are operational during the entire cell cycle and may slow progression at any stage during the four phases if internal (within a cell itself) or external (signals, stress, hormones etc.) irregularities are detected.

The most significant change in a cancerous cell compared to a normal cell is the loss of control of the cell cycle, resulting in uncontrolled proliferation progressively followed by the other hallmarks of cancer (32, 37). The G_1/S checkpoint determines the integrity of the DNA and therefore, whether the cell continues to enter the S phase where DNA is duplicated (38). If damage is detected, the cell cycle is halted and repair mechanisms are initiated, if rescue is possible, or programmed cell death is induced. Cellular proliferation is regulated and maintained by tumour suppressor genes (Figure 1.2) that preserve cellular integrity through the checkpoints and can initiate a block in cell cycle progression when DNA damage is detected. Repair mechanisms are activated in order to fix the DNA damage and apoptosis may be initiated if the damage is beyond repair. Aberrations in tumour suppressor genes lead to desensitization of damage detection mechanisms and DNA abnormalities are subsequently carried through the cell cycle and inherited by the next generation (39). The retinoblastoma (*Rb*) gene, which encodes for retinoblastoma protein (pRb), is a tumour suppressor gene active during mitosis. The pRb protein plays a major role at the G_1/S checkpoint and therefore in tumour inhibition by negatively regulating the cell cycle when damage is detected (40). The fundamental importance of tumour suppressor genes such as *Rb* is emphasized when mutations that inactivate *Rb* result in uncontrolled cell division and the formation of retinoblastoma, a rare malignancy of the retina for which young children are especially susceptible (34). The same major risks to cellular health are present with the inactivation or under-expression of the cell cycle maintaining tumour suppressor gene *p53* (34).

Equally fundamental in the formation of cancerous cells, but through positive regulation rather than negative regulation, are oncogenes. Proto-oncogenes (managerial genes with the potential of becoming pro-cancerous) are re-classified as

oncogenes when they are de-regulated and then promote uncontrolled cell growth and division (34). These genes are normal components of cell genomes where they play important regulatory, metabolic and survival roles but can lead to the proliferation and essentially the immortality of cancer cells when they are up-regulated and over-expressed. One such example is the *C-MYC* proto-oncogene which, in healthy cells, encodes for a multi-functional protein which acts as a transcription factor that directly binds to DNA and activates transcription, induces the addition of acetyl groups to lysine residues on chromatin to modify gene expression and regulates the cell's progress through the cell cycle (41, 42). Mutations often result in over-expression of the C-MYC or N-MYC proteins, de-regulation of cellular proliferation and tumour formation or cancer maintenance (43). The fundamental role of *C-MYC* in the survival of cancerous cells and its abnormal expression that is associated with many tumours has been a subject of intensive study (44, 45).

Chromosomal DNA is tightly packed to form a stable structure coiling around histone proteins that maintain the shape and structure of the chromatin (46). This form of packaging serves as the primary control over DNA access to transcription factors and other components. The structure of chromatin and all the stages of its packaging are tightly regulated by several reversible epigenetic modifications that either promote or inhibit access to the DNA (47, 48). Acetylation occurs when the addition of an acetyl group to specific lysine residues on a histone reduces the positive net charge on the histone molecule and relaxes the tight coils of the chromatin. In most cases this makes DNA (and therefore the target genes) more accessible to transcription factors and many other binding proteins containing acetyl binding sites (49). Sirtuin 1 (SIRT1) functions as a NAD^+ dependent protein modifying enzyme which plays critical roles in gene expression through chromosomal structure and gene accessibility through deacetylation of lysine as well as ADP-ribosylation or, in some instances, deacetylation (50).

Cancer cells require increased levels of oxygen and nutrients from energy sources to maintain an increased metabolism (over-expression of genes and proteins, increased proliferation, etc.) (51). The Warburg effect describes the preferred method for cancer cells to acquire energy and is defined as the production of energy by cancer cells through glycolysis and lactic acid fermentation in the cytosol of the

cell, rather than through the mitochondria. In cancer cells, this process sometimes occurs even in the presence of oxygen, therefore metabolizing glucose to lactic acid at a high rate (51). Normally, glycolysis is followed by the oxidation of pyruvate in the mitochondria of the cell in the presence of oxygen (52). Cancer cells, however, have been found to harbour decreased numbers of mitochondria compared to normal cells (53). The mitochondria that are present have a high abundance of membrane bound hexokinase-2 (HK2) iso-enzymes, expressed predominantly in cancerous cells (53). HK2 is involved in regulating the glycolytic pathway through the conversion of glucose into pyruvate and then to lactic acid (by another cycle), rendering the enzyme essential for the bioenergetics and therefore, the survival of cancer cells (53). When HK2 binds to the voltage dependent anion channel (VDAC) in the mitochondrial membrane, the feedback inhibition of glucose-6-phosphate is bypassed and can enter the mitochondria to produce ATP (54). This constant and mechanistically combinational supply of ATP helps the cancer cells to maintain the high levels of energy needed to proliferate (54). Therefore, to therapeutically destroy cancer cells through their energy metabolism, both glycolysis as well as mitochondria must be targeted. Binding of HK2 to the VDAC also prevents the Bcl-2-associated X protein (BAX) from being transported to the outer mitochondrial membrane (55). As BAX is a pro-apoptotic protein which works in conjunction with p53, the prevention of its translocation affects mitochondrial permeability negatively and desensitizes cells to programmed death signals (55).

Reactive oxygen species (ROS) are chemically reactive molecules which contain oxygen and are natural products or by-products of cellular processes such as metabolic respiration (56, 57). These highly reactive molecules, such as peroxides, hydroxyl radicals, and singlet oxygen, positively and negatively impact the life of cells. ROS have important roles in redox signalling and homeostasis but also negatively impact the aging process and can be damaging to mitochondria and DNA structure. Mitochondria are important sources of ROS, such as superoxide and hydrogen peroxide (56, 57). The mitochondria are critical to energy production in cells as well as in the control of apoptosis as previously explained. Pro-apoptotic proteins (such as cytochrome *c*) are released into the cytosol upon increased mitochondrial permeability (depolarization) of the mitochondrial membrane, possibly resulting in death of a healthy cell. Excessive quantities of ROS can cause damage

to the mitochondrial membrane and therefore lead to changes in the mitochondrial membrane potential (36). When applied therapeutically, increased mitochondrial permeability allowing pro-apoptotic proteins to be released into the cytosol induces cell death in cancer cells (58, 59). This renders mitochondrial membrane permeability and ROS levels produced in a cell as a measure of the efficacy of treatment drugs against cancer cells.

1.4.2 Cell transition from the G_1 phase to the S phase

During the G_1 phase many signals coalesce to accelerate the processes leading to cellular development and preparation for division (36). Diverse metabolic, stress and environmental factors are interpreted during this period to control the machinery of the cell to direct entry into the S phase or to halt further progression. Once the G_1 phase is initiated, extracellular stimuli (such as hormones, growth factors, etc.) result in elevated levels of D-type cyclins (cyclins D1, D2, and D3) which binds to and activates CDK4 and CDK6. This in turn stimulates quiescent cells to actively re-enter the cell cycle or proliferating cells to continue undergoing changes needed to grow and reproduce (36). Following the increase in formation and subsequent activation of the cyclin D/CDK4/6 complexes, cyclin E levels increase. Binding of cyclin E units to CDK2 substrates results in Cyclin E/CDK2 complexes (60).

The commitment to enter the S phase is made mid to late G_1 phase at a stage referred to as the restriction point, or the G_1/S checkpoint (61). Once the commitment is made to replicate DNA and divide cell material, the process is irreversible until the following G_1 phase of the next cycle is reached (61). The retinoblastoma (*Rb*) family of cancer influencing genes are translated into proteins (pRb, p107, and p130) that serve as crucial molecular switches when bound to the elongation factor 2 (E2F) family of transcription factors (35, 62). The E2F family serve as transcription mediators of genes required in DNA synthesis, including the genes which are transcribed and translated to form cyclin E, A and B as well as the enzymes dihydrofolate reductase and thymidine kinase (63). Hypophosphorylated pRb represses E2F-dependent transcription of S phase genes while pRb phosphorylation results in E2F and pRb dissociation and halting of the inhibitory

effect of pRb on E2F. The cell is then allowed to enter the S phase (61). Phosphorylation of pRb is mediated by the cyclin D/CDK4/6 and cyclin E/CDK2 complexes (62). pRb can also be regulated through acetylation mediated by histone acetylases such as p300/CBP which are under cell cycle control and prevent efficient pRb phosphorylation (62).

During the S phase highly regulated DNA replication is initiated to produce an identical copy of the full genome of the cell, ensuring accurate inheritance of genetic information (64). The initiation of DNA replication during the S phase takes place at multiple highly conserved sites on the chromosomes which are referred to as the origins of replication (64). The origin recognition complex (ORC) marks the position of replication origins in the genome and serves as a point of assembly for a multiprotein, pre-replicative complex (pre-RC) at these origins. The pre-RC is assembled during the exit from mitosis of the precious cycle and is activated by the cyclin-dependent kinase family and the Cdc7-Dbf4 kinase family of proteins (65). Thereafter, the ORC protein complex at each origin changes to a post-replication state (post-RC) and DNA replication is activated while further activation events from the same origins are prevented for the rest of the cell cycle (64). The mini chromosome maintenance protein complex (66) binds to the chromatin during the final step of pre-RC formation and serves as crucial factors in limiting eukaryotic DNA replication to only one event per cell cycle (67). After ORC activation, DNA polymerases, human replication protein A (PRA) and proliferating cell nuclear antigen (PCNA) assemble at the origins and the transition to the DNA duplication phase of the cell cycle is irreversibly completed (67). As cells progress through the S phase, maintenance of pRb hyperphosphorylation is required for DNA replication to be successfully completed. A group of functionally related proteins called CDK inhibitors regulate the phosphorylation status of CDK proteins (67, 68). The cyclin E/CDK2 complexes regulate the transition from the G_1 phase into the S phase (Figure 1.1.4.2) (68). Shortly after cyclin E stimulation, induction of cyclin A expression occurs and cyclin A then binds to CDK2 in the S phase and to CDK1 in the G_2 and mitotic phases (68). Cyclin A is a crucial regulator during cell entry into the S phase and is also important in the G_2 phase and mitosis.

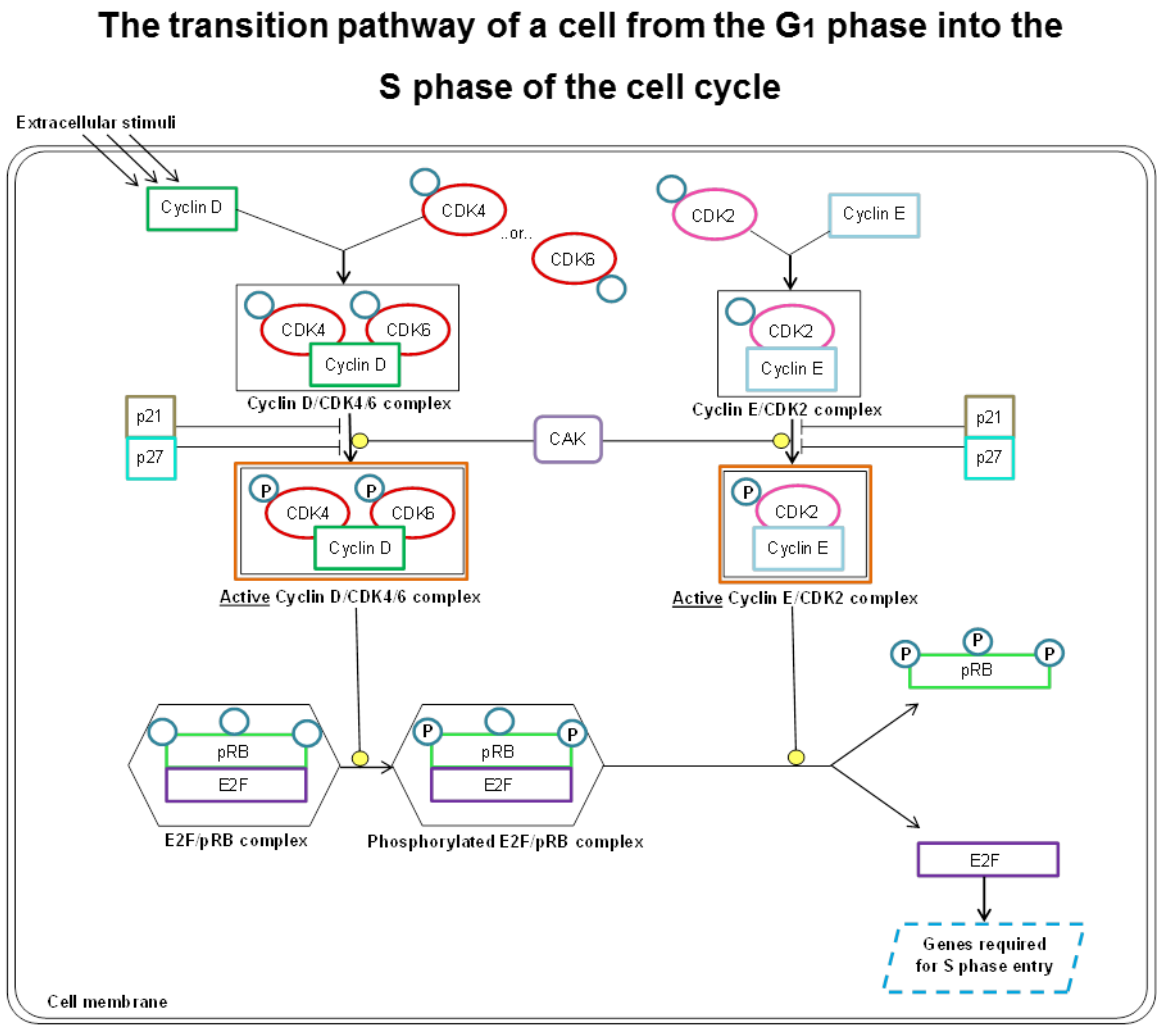

Figure 1.1.4.2: The cell cycle transition from the G_1 to the S phase. During the G_1 phase, CAK (CDK activating kinase) activates the newly formed cyclin D/CDK4/6 and cyclin E/CDK2 complexes through phosphorylation (68). The active complexes stimulate the sequential phosphorylation of the transcription factor pRb at different stages. The hypopolarized pRb/E2F complex serves to halt the progression of the cell into the S phase. Once hyperphosphorylation is achieved, pRb (in its hyperpolarized form), dissociates from the E2F transcription factor, which can then stimulate the activity of genes crucial to cell entry into the S phase. The INK4, Cip/Kip and other inhibitor families can halt cell cycle progression by inhibiting cyclin/CDK complexes and thereby lead to G_1/S phase arrest (61).

1.4.3 Cell transition from the G_2 phase to Mitosis

The process of cells passing the checkpoint from the G_2 phase entering into mitosis is under strict control of the B type cyclins, which also associate with CDK1 (Figure 1.1.4.3). After duplication of the genome in S-phase, cells transition through G_2 and prepare for division during mitosis. As cells enter into G_2 phase, the mitosis

promoting factor (MPF) complex forms through the combination of cyclin B and CDK1. The CDK1 protein is present throughout the cell division cycle, but is specifically activated by protein-protein interactions and reversible phosphorylation at the exact time points and stages when and where required (69).

At the end of G_2 phase, cyclin B/CDK1 complexes are activated by dephosphorylation and cells enter into mitosis (70). CDK1 activity is inhibited by kinase phosphorylation of two residues, Thr14 and Tyr15, through the action of Wee-1 and Myt-1 kinases (70). Wee-1 and Myt-1 activity is upregulated by phosphorylation through checkpoint kinase 1 and 2 (Chk1, Chk2). The checkpoint kinases are proteins that function in DNA structure checkpoint signalling (Figure 1.1.4.3). Activation of CDK1 occurs after the simultaneous phosphorylation of the Thr161 residue by cyclin activating kinase (CAK) and dephosphorylation of the Thr14 and Tyr15 residues through the activity of dual-specificity phosphatases Cdc25C and Cdc25B (Figure 1.1.4.3). Cdc25C is phophorylated and activated Polo-like kinase 1 (Plk-1) and active CDK1, creating a positive feedback loop between Cdc25C and CDK1 (Figure 1.1.4.3). The activity of Plk-1 is in turn regulated by DNA structure checkpoint signalling via the ATM (Ataxia Telangiectasia Mutated) and ATR (Rad3-related) cell signalling complexes as well as by Chk1 and Chk2 (Figure 1.1.4.3) (70).

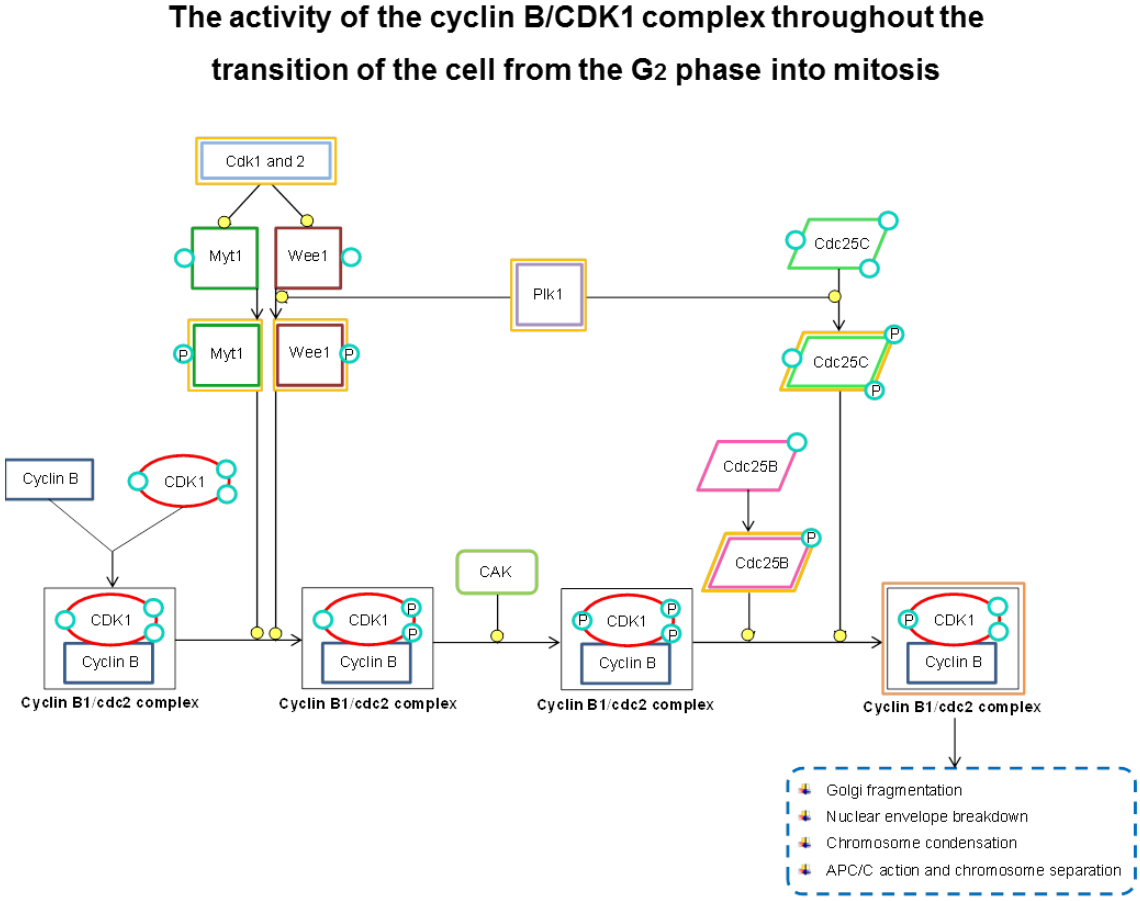

Figure 1.1.4.3: The cyclin B/CDK1 complex as a mediator of cell transition from the G_2 phase into mitosis. CDK1 activity and association with cyclin B is maintained through consecutive stages of phosphorylation and dephosphorylation (70). Mediators include Myt1, Wee1, CAK and Cdc25B and Cdc25C, also stimulated through phosphorylation induced activation and deactivation. Factors Wee1 and Myt1, as well as Cdc25B and Cdc25C compete for the phosphorylation status of the same amino acid residues (S216, T130 etc.) (not shown). DNA damage and upstream integrity regulators of Wee1, Myt1 and Cdc25C, including Plk1 and Chk1/2 (not shown), determines the balance in phosphorylation status of the amino acid residues. CDK activation is crucial for phosphorylation, and therefore subsequent activation, of several proteins important in the cell division process including mediators of chromosome condensation and separation, APC/C complex activity and spindle machinery assembly (70).

Following the transition into mitosis, the maturation promoting factor (MPF) complex plays a crucial role in all the stages required for division of the genetic material, organelles and the cell itself to form the next generation (71). Activated cyclin B/CDK1 complexes can phosphorylate numerous substrates required for cell division including condensins and various histones resulting in chromosome condensation, various Golgi matrix components resulting in Golgi fragmentation and various

proteins involved in spindle dynamics and chromosome movements including kinesins and stathmin (70-73). Furthermore, the cyclin B/CDK1 complex contributes to regulate the anaphase-promoting complex/cyclosome (APC/C), the core component of the ubiquitin-dependent proteolytic machinery which controls the timely degradation of critical mitotic regulators (such as inhibitors of anaphase onset securins and cyclins) at specified times (72).The APC/C is a multiprotein complex consisting of at least 11 core subunits and two cofactors namely Cadherin 1 (Cdh1) and cdc20 (72). MPF function is finely regulated by location and the presence of stimulants. The complex accumulates in the cytoplasm when in association with microtubules and centrosomes until late prophase when translocation to nucleus takes place as required for nuclear envelope breakdown (71).

During mitosis, also referred to as the M phase, the cell goes through five stages to ensure that each daughter cell will have a complete and identical set of chromosomes (32). The five main stages of mitosis are prophase, pro-metaphase, metaphase, anaphase and telophase, each encompassing a series of events required for the impeccable dividing of replicated genetic material and the other components of the cell (70). The MPF complex plays a crucial role during mitosis, serving as an orchestrator of chromosome condensation (during prophase), nuclear envelope breakdown (pro-metaphase) and also controls spindle dynamics and centrosome separation (meta-anaphase transition) (71). During the closing stages of mitosis, sister chromatid separation (anaphase), spindle disassembly, and cytokinesis (telophase) is mediated by APC/C. Phosphorylation of APC/C subunits regulates both the function and the assembly of the mature complex. The result of one successfully completed somatic cell division cycle is two genetically identical cells completely capable of entering the cell cycle once they have exited mitosis (70).

Cell death

1.5.1 Apoptosis

Cells naturally undergo death during organism growth and development, when cells are damaged beyond repair, when cells are senescent or when dying is part of the role played by the cell as in the immune system and blood clotting (74-76). Apoptosis is when cellular death is induced as a result of the activation of intracellular chemical programming with the purpose of resulting in cell death. This controlled process occurs without cells undergoing lysis and therefore avoiding damage toward neighbouring tissue. Apoptosis serves as a natural barrier to cancer development (74-76) and is triggered in response to various physiological stress conditions experienced by cells during the process of tumorigenesis or as a result of anti-cancer therapy. Many tumours that successfully progress to high stages of malignancy and drug resistance have been found to do so even in the presence of apoptosis inducing stress (74, 75).

The apoptotic machinery of human cells consists of both upstream regulators and downstream effector components (74, 75). The components are divided into two major regulatory circuits, one which receives and death-inducing signals from outside the cell (the extrinsic apoptotic program) and another which senses and integrates a variety of signals originating from inside the cell itself (the intrinsic program, thought to be more widely implicated as a tumorigenesis barrier). Each circuit results in the activation of specific proteases (caspases 8 and 9, respectively) that are latent under normal circumstances, but which initiates a cascade of effector caspases responsible for the execution phase of apoptosis through proteolysis. At this stage, the cell is disassembled through an orderly stepwise procedure and then consumed by its neighbours and by phagocytic cells deigned to remove apoptotic remnants (6).

When apoptosis is triggered, signals are conveyed between the regulator and the effector proteins involved in the process. Balance is thought to be maintained through mediation of pro- and anti-apoptotic members of the Bcl-2 family of regulatory proteins (74, 75). Bcl-2 and its relatives Bcl-xL, Bcl-w, Mcl-1, and A1 are apoptosis inhibitors and mainly function through suppressing BAX and BAK, two pro-

apoptotic trigger proteins linked to the mitochondria. Physical interactions occur through BH3 motifs (protein-protein interaction domains) shared between BAK/BAX and Bcl-2-like proteins (74, 77). When BAK, imbedded in the outer mitochondrial membrane, is not inhibited, BAX is recruited and the integrity of the outer mitochondrial membrane is disrupted. Pro-apoptotic signalling proteins are subsequently released. Upon release from the mitochondria, pro-apoptotic signalling protein cytochrome c activates a cascade of proteolytic caspases, inducing the multiple cellular changes associated with the programmed cellular death.

Several major abnormality sensors important in tumour development have been found to be sensitive to cellular conditions and to trigger apoptosis, one of which is the tumour suppressor gene 53 (*p53*) (74, 75, 78). The p53 protein, acting as a transcription factor, induces apoptosis through up-regulating the expression of the NOXA and PUMA BH3-only pro-apoptotic proteins. This is initiated in response to substantial levels of DNA double strand breaks and other irreparable chromosomal abnormalities. Hyperactive signalling by certain oncoproteins, such as C-MYC, also leads to apoptosis unless counterbalanced by anti-apoptotic factors or if the *p53* gene is mutated or the pathway is dysfunctional (74, 75, 78). Insufficient signalling, abnormal expression or the dysfunction of survival proteins (such as survivin and β-catenin) could also result in apoptosis even in the absence of over-expressed pro-apoptotic factors (4).

Apoptosis is tightly controlled in normal, healthy cells (Figure 1.1.5.1). However, certain neurodegenerative disorders as well as neoplastic cells possess complex strategies to limit or circumvent apoptosis. Most often tumour cells escape apoptosis through limiting, decreasing or loss of p53 tumour suppressor function, which is a critical component of the apoptosis-inducing circuitry. Tumours may evade apoptosis by increasing the expression of anti-apoptotic regulators, such as the Bcl-2 family, heightened survival signals, such as IGF1/2 or through the down-regulation of the pro-apoptotic factors BAX, BAK and PUMA. (1). The numerous apoptosis-avoiding mechanisms employed by cancer cells are an indication of the complexity and diversity of apoptosis-inducing signals that need to be evaded by cancer cell populations during the pathway to malignancy (1).

The cell maintenance pathway controlling cell death or repair upon damage detection

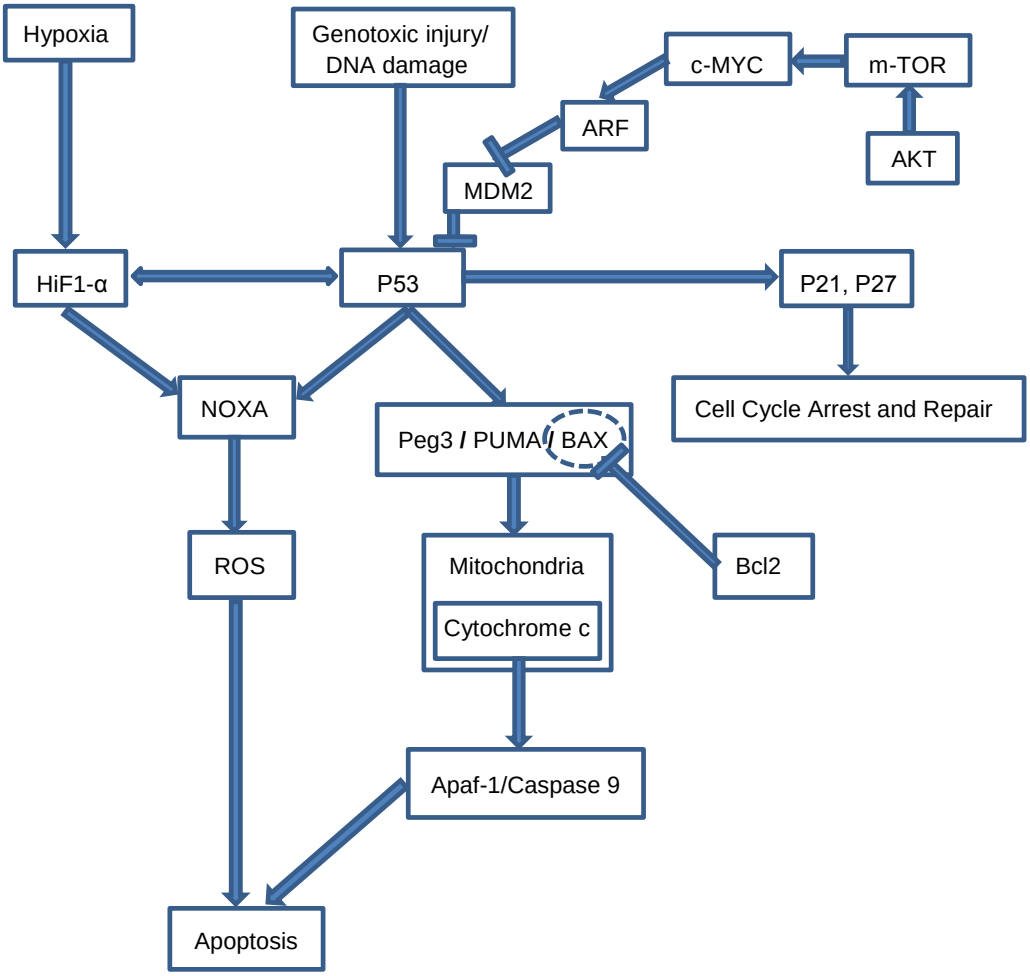

Figure 1.1.5.1: The cell maintenance pathway of non-cancerous cells when affected by damage or stress resulting in cell cycle arrest and reparation of the damage on molecular level or cell death. HiF1-α and p53 stimulation occurs upon cellular damage, the NOXA pathway is stimulated to lead to the release of reactive oxygen species into the cytoplasm resulting in apoptotic cell death or BAX/BAK is stimulated to enter the mitochondria and stimulate cytochrome c dissociates from the inter-mitochondrial membrane, exiting the mitochondria and entering the cytoplasm as part of the electron transport chain, leading to cell death (74, 77). When the C-MYC oncoprotein, transcription stimulated by m-TOR and induced by ATK, is over-expressed, the repression of p53 can be produced through MDM2 inhibition, which is a crucial component of p53 stimulation. This is the case in many cancers, resulting in over-expression of C-MYC and under-expression of complete repression of p53. Cell survival is optimized through the resistance to cell death- and repair mechanisms. The cell can then reproduce optimally for cancer growth and eventual metastasis (74, 75, 78).

Linkages at the molecular level between cell death, cell survival and the cell cycle have been researched intensively in recent years (74, 77). The formation of a tumour, consisting of various cancerous cell types is a dynamic process that is driven by complex interactions between oncogene activation, tumour suppressor inactivation and responses to cellular stress. The selection whether to undergo cell cycle arrest and/or repair, to initiate apoptosis, necrosis, autophagy or mitotic catastrophe in response to anticancer agents is critical in the successful application of treatment. The molecular mechanisms by which anticancer drugs induce apoptosis, when this is indeed the mechanism of action of the drugs used by the patient, are mediated by mitochondrial dysfunction, which is regulated by the balance of pro-apoptotic and anti-apoptotic proteins in the Bcl-2 family. When there is DNA damage within cancer cells, the activation of pro-apoptotic proteins such as BAX and BAK is induced in a p53 dependant manner (79). Translocation of the proteins from the cytosol into mitochondria takes place, while other proteins and molecules are translocated back to the cytosol causing mitochondrial membrane depolarization and subsequent cell death (74, 77).

When a pro-apoptotic protein is under-expressed or dysfunctional or an anti-apoptotic protein (pro-survival) is over-expressed, apoptotic resistance occurs as seen in tumorigenic cells of many cancer types (80). Non-apoptotic cell death in cells lacking apoptotic machinery is mainly attributed to autophagy and in some cases oncosis (a three-stage cell death process sometimes initiated upon cellular injury). The mechanism of action of many chemotherapeutic agents is the induction of autophagic cell death and it has been reported that treatment with commonly prescribed anticancer drugs such as paclitaxel and vinblastine induced both autophagic cell death and apoptotic cell death. Oncotic cell death can also be induced directly through receptor-mediated pathways which result in the release of ROS followed by mitochondrial damage, therefore causing metabolic catastrophe through cell swelling and ultimately cell death through oncosis (80).

Oncosis can also be induced when autophagy is insufficient and cells are under metabolic stress, resulting in insufficient energy production through catabolism and loss of function of organelles that are degraded and used as an energy resource (81, 82). Cancer cells often have a defect in a specific cell death pathway but can die through any other mechanisms and pathways that are still functional. However, the

nature of the defective cell death mechanism ultimately affects the specific treatment that is applicable to the specific cancer as well as the clinical outcome of treatment. Many questions still remain unanswered concerning the interactions between apoptotic and non-apoptotic cell death pathways and whether they overlap to any degree. It is as of yet still unclear if such responses occur successively or simultaneously and whether one mechanism can compensate for another that is inactivated by a tumorigenic mutation. If these cell death pathways overlap significantly and are modified during cancer progression, then anticancer therapies that are designed to restore function to a key program will restore all programs simultaneously and therefore improve the efficacy of the treatment (81, 82). However, if these cell death mechanisms are independent, identifying and targeting the single pathway that most efficiently inactivates the cancer cells in question, and therefore will have the greatest influence on the disease, might be the most effective approach.

1.5.2 Autophagy

Autophagy mediates both tumour cell survival and death, and, like apoptosis, normally operates at basal levels when not induced and is an important physiological mechanism inside cells (83, 84). When cells are under certain states of stress, mostly severe nutrient deficiency, autophagy is hyperactivated (83, 84). The activation of this mechanism results in cells breaking down cellular organelles such as ribosomes and mitochondria to supplement the cells nutrition. The molecules resulting from the catabolism are then used for biosynthesis and cell metabolism. Intracellular vesicles referred to as autophagosomes envelope intracellular organelles and then fuse with lysosomes to enzymatically degrade the components. This results in small metabolites with low molecular weights that support survival in cells that are under stress and need to survive in nutrient-limited environments, as often experienced by cancer cells (83, 84).

Autophagy machinery has both regulatory and effector components, like apoptosis, including proteins that organize autophagosome formation and mediators of delivery to lysosomes (83, 84). It has also been proposed that the regulatory circuits of autophagy, apoptosis, and cellular homeostasis interact at certain stages. The

signalling pathway involving the PI3-kinase, AKT and mTOR kinases, for example, is stimulated by survival signals that block apoptosis as well as similarly inhibiting autophagy (85). Also, when survival signals are insufficient to suppress death inducing signals, the PI3K signalling pathway is down-regulated (86). This results in autophagy and/or apoptosis possibly being induced through interacting regulatory circuits possessing entirely different purposes in maintaining cellular balance (83, 87, 88).

1.5.3 Necrosis

Differently from apoptosis, where cells contract and reduce to a silent corpse that is consumed by neighbouring cells, necrotic cells undergo system breakdown, become bloated and explode (89). The cell contents are subsequently released into the surrounding tissue microenvironment. Necrotic cell death has been shown to be under genetic control in some instances and is not a random, undirected process (82, 90, 91). Pro-inflammatory signals are released into the surrounding microenvironment, which does not occur during apoptosis and autophagy. This results in the recruitment of immune inflammatory cells that evaluate the extent of the tissue damage rendered and remove the necrotic debris from the site (90, 92, 93). In the case of cancer tissue, however, repetitive lines of evidence have portrayed immune inflammatory cells as active tumour promoting entities; given that such cells are capable of cancer cell proliferation, mediating angiogenesis as well as tissue invasiveness. Necrotic cells can also release bioactive regulatory factors (IL-1α, etc.) which can directly stimulate neighbouring viable cells to proliferate, potentially facilitating cancer progression (92, 94). While first seemingly beneficial in counterbalancing cancer-associated hyperproliferation, necrotic cell death may indeed prove advantageous to cancerous cells. The toleration of a certain degree of necrotic cell death may be advantageous to incipient neoplasias and potentially invasive and metastatic tumours. The recruitment of tumour-promoting inflammatory cells supplying growth-stimulating factors to the surviving cells within the tumour mass is highly advantageous. Necrosis is therefore termed as having pro-inflammatory and tumour-promoting potential rather than anti-proliferation affects as initially suspected (92).

Current treatments for AML and neuroblastoma

The most often prescribed therapeutic drugs for the treatment of various cancer types, including leukemia and neuroblastoma, are anti-mitotic agents such as paclitaxel, docetaxel and vincristine that function by disrupting microtubule structures of tumorigenic cells which undergo a higher rate cell division and are therefore more susceptible to mitotic inhibition (6, 15, 16).

Cancer specific therapy for treating AML includes repeated cycles of high-dose cytarabine, a widely prescribed chemotherapeutic drug which acts through DNA damage, and hematopoietic stem-cell transplantation which reduces the risk of relapse. Stem-cell transplantation is a high risk form of therapy with 15 to 25% treatment-related mortality (95). The highly negative statistics mentioned above enforce the need to research and develop therapies that decrease this risk, which is continually being investigated by scientists. Targeted therapies that are intensely specific to cancerous cells are needed to reduce the number of AML cases, especially those acquired through chemotherapy, as well as to increase the effectiveness of treatment (6, 15, 16). Also, new combinational therapies targeting various cancer survival mechanisms simultaneously as well as gene therapy targeting oncogenes and their connected pathways and effector proteins are proving to be promising methods of inhibition (95-97).

Neuroblastoma is currently treated with cytotoxic chemotherapy, retinoids, immunotherapy, surgery and combination therapies, the most commonly prescribed chemotherapeutic drugs being anti-mitotic chemicals such as vincristine, cisplatin and doxorubicin (3, 95-97). Side effects of chemotherapy include severe nausea, fatigue, increased chances of infection and easy bleeding or bruising (95-97). Research is therefore ongoing to find anti-cancer agents that are less harmful to other bodily systems while maintaining a maximum level of efficacy against cancer cells. High-risk neuroblastoma (stage IV patients, older than 1 year at diagnosis, and stage III patients, with *N-MYC* amplification and/or unfavourable histopathology) is treated with multi-agent chemoradiotherapy and purged autologous bone marrow transplantation to improve the treatment outcome. The lethality of high-risk neuroblastoma is still above 50%, mainly due to progressive disease that is resistant to further therapy and often associated with acquired loss of p53 expression and

function. Neuroblastoma relapse, as well as others cancers, often occurs in hypoxic tissues where chemotherapy and radiotherapy activity has been reported to be lower. Therefore, new anti-cancer agents aimed at treating neuroblastoma need to maintain cytotoxicity toward cancer cells while in reduced-oxygen environments and be p53-independent for use in the treatment as neuroblastoma is possibly p53 sensitive (95-97).

Targeting Sirtuins: AML and neuroblastoma

The sirtuin family (SIRT1-7) is a group of NAD^+ dependent protein-modifying enzymes with genetically conserved cores and diverse functions in the cellular nucleus and mitochondria (50). Sirtuins play critical roles in cellular stress response, gene expression, DNA damage repair and cell survival through deacetylation of lysine as well as ADP-ribosylation and deacylation (98, 99). The diverse roles of these enzymes in maintaining genome integrity, regulating cell metabolism, proliferation and avoiding apoptosis classify them as complex tumour promoting as well as tumour suppressing entities, and as promising targets for cancer therapeutics (98, 99). Sirtuins are thought to act as cancer suppressors in normal cells and cancer promoters in tumorigenic cells in most cases (98, 99).

The particularly bifurcated roles of sirtuin 1 (SIRT1), a class lll histone and non-histone deacetylase primarily located in the nucleus, seems to be dependent on cell- and tumour type as well as the nature of the maintenance genes in the genome (Figure 1.1.7.1). SIRT1, the most thoroughly studied member of the sirtuin family, shares the greatest homology with yeast SIR2, a protein crucial to the replicative life span, cellular metabolism and epigenetic regulation of yeast cells and higher eukaryotes (4).

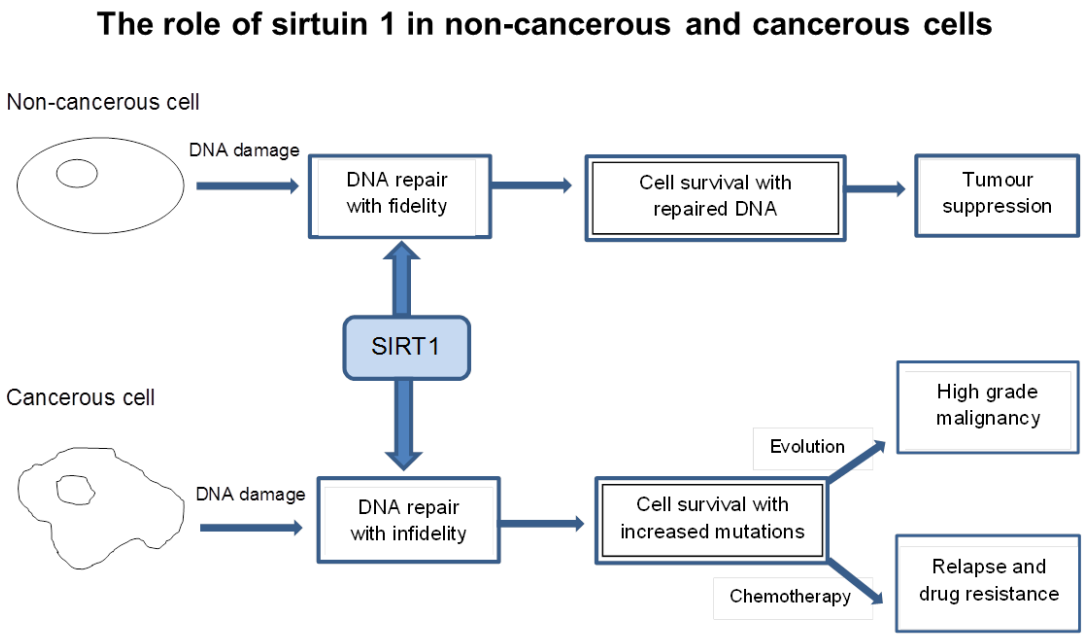

Figure 1.1.7.1: A model for the bifurcated roles of SIRT1 in cancer through genome maintenance. SIRT1 promotes genome maintenance in both normal and cancer cells under genotoxic stress and DNA damage. Activation of DNA repair with high fidelity in normal cells improves genome stability and suppresses tumour formation (98, 99). Activation of DNA repair with low fidelity in cancer cells prevents catastrophic genomic events and renders cancer cell survival, but allows cancer cells to accumulate non-fatal lesions and more mutations to evolve towards high grade malignancy and drug resistance under chemotherapy. The fidelity of a DNA polymerase is the result of accurate replication of a desired template (4).

SIRT1 targets both histones and non-histone proteins for lysine deacetylation, therefore functioning in transcription regulation and the molecular activities of proteins and playing crucial roles in cellular metabolism, survival, development and differentiation and the stress response (100-102). Through lysine acetylation, SIRT1 regulates cellular activities by influencing chromatin structure (such as the promotion of heterochromatin formation) and the expression of genes on the transcription level (such as NF_kB transcription inhibition and insulin secretion) as well as enzymatic activity within the cell. The functionality of SIRT1 is therefore intimately involved in the epigenetic health and regulation of the cell (4).

SIRT1 deacetylates the genome guardian p53 at its C-terminal Lys382 residue, alleviating its transactivation activity and thereby inhibiting its tumour suppressor functions. Cell cycle arrest upon damage detection, senescence and the ability of the

cell to stimulate the initiation of apoptosis is therefore suppressed (4). Enhanced acetylation at specific lysine residues is an indispensable event for p53 activation and is crucial for subsequent recruitment of p53 to promoter regions of target genes to result in rescue gene activation in response to cellular stress signals. Up-regulated SIRT1 (as detected in a variety of cancers such as leukemia and skin melanomas and carcinomas) negatively regulates p53 translation to the nucleus where it functions as a transcription factor and thereby antagonizing the cell rescue action of p53 (103). SIRT1, however, is also regulated by p53 in a positive feedback loop through the inhibition of SIRT1 expression when p53 binds to the promoter region (4, 104). Also, p53 stimulates the expression of miR-34a, a highly conserved micro-RNA family functional in tumour suppression, which represses SIRT1, thereby preventing p53 lysine deacetylation by SIRT1, rendering the p53 protein active. It is therefore concluded that the p53-SIRT1 loop is highly implicated in cancer development (103).

SIRT1 also plays a role in inflammation attenuation through the regulation of NF_kB, a protein complex crucial to transcriptional control, cytokine regulation and cell survival (4). When the RelA/p65 subunit of the complex is deacetylated at Lys 310 by SIRT1, transcription activity is repressed and cells are sensitized to TNF-α-induced apoptosis (4, 104). When cells are under hypoxic stress, SIRT1 binds to and deacetylates HiF1-α leading to inhibition of the protein and its control over glycolysis. SIRT1 therefore negatively regulates the growth and angiogenesis of fibrosarcoma tumours *in vivo*. HiF-2α, closely related to HiF-1α structurally but with different transcriptional targets, is also deacetylated by SIRT1. Oppositely, during hypoxia, HiF-2α signalling is activated through deacetylation, resulting in the corresponding hypoxic stress response. During a deficiency in oxygen a decrease in NAD molecules occurs and the activity and expression of SIRT1 gradually decreases. This might trigger the crossover between HiF-1α and HiF-2α thereby coordinating hypoxic stress response and metabolism during hypoxia, ensuring that cells respond accordingly to hypoxic conditions while still maintaining survival as far as possible (4).

The SIRT1 protein can also promote cellular survival and proliferation by forming a positive feedback loop with the oncoprotein C-MYC, as seen in many cancers (44, 45, 105). Transcription of SIRT1 is directly activated by the *C-MYC* oncogenes, while C-MYC activity is actively enhanced when the protein is deacetylated. A positive

feedback loop has therefore been reported to form through the deacetylation of *C-MYC* and the enhancement of its protein stability by SIRT1, resulting in SIRT1 mainly being classified as a pro-cancer enzyme, among other diverse functions (44, 45, 105). Apoptosis and senescence is inhibited and cell survival enhanced through this SIRT1-C-MYC axis.

Amplification of *N-MYC* is reported to be correlated to advanced as well as angiogenic neuroblastoma (106, 107). SIRT1 positively regulates *C-MYC* gene and protein expression via deacetylation of chromatin and subsequent activation of gene expression (44). It remains unclear whether *C-MYC* is also up-regulated in neuroblastoma and if this cancer would therefore be sensitive to inhibitory treatment targeted at the C-MYC protein. In neuroblastoma, N-MYC oncogenesis is promoted by SIRT1 through a positive feedback loop with MKP3 and ERK. The dual specificity mitogen-activated protein kinase phosphatase MKP3 down-regulates mitogenic signalling through dephosphorylation of ERK (extracellular signal-regulated). However, unlike C-MYC, N-MYC is not a deacetylase substrate of SIRT1 but a transcriptional repressor complex is formed by N-MYC and SIRT1 at the gene promoter of MKP3. This leads to repression of expression and ERK protein phosphorylation as well as N-MYC phosphorylation and stabilization (3, 4). This mechanism thereby serves as an example of tumour promoting transcription factors regulated by SIRT1.

During active leukemogenesis, C-MYC forms a heterodimer with Max (MYC-associated factor X) to transactivate downstream target genes essential for cancer cell differentiation and disease progression (108, 109). Cancerous cells are also characterized by altered epigenetic landscapes which influence gene expression, and often exploit the chromatin regulatory machinery to control specified oncogenic gene expression. As leukemia is C-MYC sensitive, SIRT1 is once more classified as a motivated target for anti-cancer therapeutics.

Studies have indicated that SIRT1 inhibition or knockout leads to p53 hyperacetylation and subsequent senescence-like cellular growth arrest and apoptosis, often by inhibition of the survival mechanisms of oncogenes such as *C-MYC*, in selected cancers. The *p53* molecule (on DNA, mRNA and protein level) is therefore rendered as an invaluable cancer treatment target (84). Numerous studies

have unearthed complex tumour promoting and inhibitory functions of the human sirtuins under a variety of conditions. The commonly obtained result of SIRT1 inhibitors stabilizing p53 protein levels in selected tumour types classifies sirtuin inhibitors as pro-apoptotic and anti-cancerous entities (4, 104).

Targeting bromodomains: AML and neuroblastoma

Bromodomains (BRDs) are conserved structural modules found in proteins associated with gene expression and function. The function is to recognize post-transcriptional lysine acetylation on histones and other proteins as required in various mechanisms of action (110). Acetylation occurs when the addition of an acetyl group to specific lysine residues reduce the positive net charge on the histone (or non-histone) molecule and thereby lessens the tension in the coils of the chromatin. This open structure results in improved access to DNA and, therefore, increased accessibility of target genes (49). The binding of BRD-containing proteins to acetyl-lysine and its subsequent alterations is an important mechanism in the transcription of a multitude of genes as well as chromosomal regulation (by opening chromatin structure) (86, 111). The inhibition of this molecular binding mechanism could allow the regulation of specific gene expression and subsequent maintenance of diseases such as cancer and inflammation, rendering BRDs as valid targets for a variety of treatment outcomes.

One specific gene target of BRD binding and activation is the nuclear, multifunctional, proto-oncogene *C-MYC* which is essential to cell cycle regulation and fundamental in many cancer types (41). *MYC* (*C-MYC* and *N-MYC* family of mostly anti-apoptotic oncogenes) expression is tightly correlated with cell-cycle progression in normal tissues and unchecked *MYC* expression is among the most prominent hallmarks of the hyper-proliferation associated with most forms of cancer (41). *MYC* contributes to the genesis and maintenance (biomass accumulation, enhanced cellular bioenergetics etc.) of various cancers including mammary carcinomas, Burkitt lymphoma and leukemia (41). *MYC* expression is highly regulated and many transcriptional regulatory motifs within the proximal promoter region contribute to its expression. The roles of C-MYC in tumour maintenance result in cell addiction to the protein as well as to nutrients, resulting in reduced

proliferation and in some cases apoptosis upon *MYC* knockdown (41, 66). Additional mutagenic alterations combined with *MYC* de-regulation (through gene amplification, loss of regulation or chromosomal translocation) are required to enable tumorigenesis. However, contrasts have also been reported in the expression of the *C-MYC* gene in cells programmed to die or in cells resistant to death during, especially in disease regulation (45, 66). Findings have suggested that cells constitutively expressing *C-MYC* are more resistant to cell death induced by certain chemotherapeutic drugs that work by blocking cell division, such as seen in many cancer types (41). Other studies have suggested a causal connection between the expression of the *C-MYC* gene and ensuing cell death through apoptosis, especially in cells that are prevented from entering cellular division or after the withdrawal of growth factors (112-114). A recent study by Gibson *et al.* (1995) has examined the frequency of cell death in several Chinese hamster ovary cell lines that contain 20 to 30 copies of the human *C-MYC* gene and that express high levels of human *C-MYC* mRNA and protein. It was found that constitutive C-MYC expression in cells incubated at highly specific conditions correlated with increased cell death due to apoptosis. The discussion of the findings concluded that the over-expression of C-MYC protein can promote cell death under some but not all conditions of stress that block cell division. It was also concluded that C-MYC may, in some cases, accelerate but not necessarily initiate apoptosis (112). Research has also shown that the over-expression of *C-MYC* may sensitize cells to apoptosis through a wide variety of coordinated stimuli (113). The event leading to the decision of apoptosis initiation as well as the mechanism of the apoptotic response is regulated, when stimulated by *C-MYC*, is highly dependent on the type and physiological status of the cell. Multiple cooperating molecular pathways of cell survival and apoptosis determine whether a cell lives or dies. Understanding how *C-MYC* interfaces with these pathways to influence the survival of cells is crucial in understanding disease (113, 115). The study of tumour initiation and progression and the elucidation of novel treatment regimens aimed at new treatment targets is crucial in treating the highly complex and evolving malignancy that is cancer.

MYC protein expression is finely monitored in normal cells. The over-expression of C-MYC results in the apoptosis inducer p53 and other maintenance molecules activating the negative feedback mechanism to normalize C-MYC levels (113, 114,

116). However, mutations in these checkpoints and molecules or in their pathways often occur in cancer cells, rendering C-MYC potentially tumorigenic. Mutations in the *p53* gene have been found in more than half of all documented human tumour types (113, 114, 116).

BRD proteins play a role in the activation of C-MYC and bromodomain inhibitors could therefore result in *in vivo* tumour inhibition and even apoptosis. The transcriptional regulator bromodomain 4 (BRD4) (117) was recently found to play a crucial role in *C-MYC* transcription through promoter interactions and by targeting transcriptional elongation complexes (41). BRD4 binds to acetylated histones on BCP (BRD-containing proteins) through the BRD and facilitates chromatin-dependent signalling and the transcription at target loci (118). By inhibiting the interaction between BRD4 and acetylated histones of the activation proteins, the levels of C-MYC proteins and their effectors will be reduced by negative control of the transcription of the *C-MYC* gene itself (119).

BRD4 acetyl-lysine binding is also required for activation of the apoptosis regulator Bcl-2, which suppresses apoptosis in cell systems such as factor-dependent lymphohematopoietic and neural pathways as well as cell death regulation by maintenance of mitochondrial membrane permeability (116). Bcl-2 also inhibits caspase activity by prevention of cytochrome c release from the mitochondria and/or by binding to apoptosis-activating factor 1 (APAF-1). Therefore, chemical inhibition of the BRD4 binding domain in cancer cells inhibits both the expression of C-MYC and Bcl-2 and its subsequent roles in *in vivo* tumorigenesis in selected cancers (116).

Another promising opportunity for a BRD to be targeted for inhibition in cancer therapeutics is in the regulation of the cell cycle regulator CDK9 (cyclin dependent kinase 9) by BRD4 (120). CDK9 is associated with the positive transcription elongation factor P-TEFb, recruited by BRD4 to the transcriptional target site through the recognition of acetylated lysine residues. The P-TEFb complex as a potential target for therapy would prove especially relevant in the treatment of leukemia where up-regulation of the associated genes have previously been reported (120).

Acute myeloid leukaemia (AML) is regularly associated with aberrant chromatin states, and as such, the protein BRD4 has been identified as being critical to disease maintenance (2). The effects of BRD4 suppression have been partially attributed to

its role in sustaining *C-MYC* expression to promote cancer cell self-renewal and progression. BRD4 is therefore a promising therapeutic target in AML and potentially other cancers as C-MYC is classified as being a ubiquitous cancer contributing factor (2). Amplification of *N-MYC* is reported to be correlated to advanced and angiogenic neuroblastoma (3, 121). BRD4 positively regulates *C-MYC* expression via deacetylation of chromatin and subsequent activation of gene expression (2, 41). It remains unclear whether *C-MYC* is also up-regulated in neuroblastoma and if this cancer would therefore be sensitive to inhibitory treatment targeted to this protein.

Newly designed BRD4 and sirtuin inhibitors

The SIRT1 inhibitory compound W137 and the BRD4 inhibitory compounds tested in this project, CC2 and CC6, are novel compounds designed by Dr BA Stander in collaboration with Professor AD Cromarty. This study is the first to investigate the efficacy of these compounds the U937 and the SH-SY5Y cell lines.

The inhibitory effects of the SIRT1 inhibitor W137 as well as the BRD4 inhibitors CC2 and CC6 were assessed to determine the IC_{50} values on both the U937 and the SH-SY5Y cell lines. Further testing throughout this research project was conducted only on the selected compound with the lowest IC_{50} values for both cell lines (W137).

The findings will be used to motivate further *in vivo* efficacy studies that are to follow based on the conclusions drawn from the data acquired. The results may also indicate that the compounds are cell line specific and therein provide direction for specified future research.

Relevance and aim of the study

The first aim of the study is to determine the anti-proliferative effects of the SIRT1 and BRD4 inhibitors W137, CC2 and CC6 on the human acute myeloid leukemia (U937) and the neuroblastoma (SH-SY5Y) transformed cell lines. The second aim of this study is to provide an understanding of the cell death-inducing properties, mechanism of action and other *in vitro* effects of these selected *in silico* designed inhibitor compounds. Through the inhibition of BRD4, which features in many

mechanisms by recognizing acetylated lysine that increases gene accessibility and/or the inhibition of SIRT1 which functions by deacetylation, resulting in anti-cancer protein deactivation or down-regulation of cancer associated gene expression may be possible. If the activity of the *C-MYC* oncogene and the tumour suppressor gene *p53* can be regulated by the administration of a SIRT1 and/or BRD4 inhibitory drug, cancer cell survival and cell death evasion, mutation and metastases could potentially be treated. *C-MYC*, which is often observed to be over-expressed in a variety of cancers, is crucial for survival and *p53*, which is often down-regulated or inhibited in cancer cells, is crucial for cell death in many cancers. The acquired loss of *p53* expression and protein function, as often observed in a wide range of human cancers, renders SIRT1 and BRD4, which each plays a mechanistic role in p53 activity or has a part in p53 functional pathways as a possible cancer treatment target.

This research entails an *in vitro* mechanistic study of the SIRT1 and BRD4 inhibitory compounds. The 50% inhibitory concentration (IC_{50}) was determined for each compound on the two test cell lines respectively. This was not a comparative study but to determine whether either of the test compounds were effective against the two cancer cell lines. A qualitative study analysing the morphology of the adhesive SH-SY5Y cells by means of triple staining and fluorescent microscopy as well as light microscopy through haematoxylin and eosin staining provided insight into morphological changes undergone by test compound exposed cells compared to Actinomycin D exposed positive control samples and untreated negative control samples. Loss of membrane integrity and cells undergoing apoptosis would indicate cell death by necrosis or apoptosis respectively. To elucidate the dominant mechanism, the influence of the test compounds on the cell cycle was tested because re-activation or up-regulation of p53 (through C-MYC down-regulation, and/or other mechanisms) may lead to a cell cycle blockade at one or more of the cycle checkpoints. Staining with DNA binding propidium iodide indicated at which cell cycle stage(s) the cell division is halted. The apoptosis stimulating effect of the test compounds was determined by Annexin V and propidium iodide staining, indicating whether the cells are undergoing an early or late stage of apoptosis or if the cells are dying through necrosis. An increase in apoptosis due to p53 up-regulation and/or C-MYC down-regulation in response to test compound exposure would render SIRT1

and/or BRD4 as valuable treatment targets and the compound(s) tested as potential future anti-cancer drugs. The loss of mitochondrial membrane potential (studies through 3,3'-dihexyloxacarbocyanine Iodide ($DiOC_6(3)$ fluorescence) as well as reactive oxygen species formation by cells under stress (using 2',7' – dichlorodihydrofluorescin diacetate (DCHF-DA), which only fluoresces upon oxidation by H_2O_2) was measured as potential parameters resulting in cell death and serves to determine the mechanism by which an inhibitor initiates cell proliferation inhibition or death.

Furthermore, the expression of the *C-MYC* and *p53* genes, which are fundamental to cancer inhibition (by *p53* up-regulated and/or *C-MYC* down-regulated) and survival (often but not always by *C-MYC* up-regulation and *p53* down-regulation), was determined using qRT-PCR to quantify the transcribed mRNA in exposed and control cells. ELISA analysis was used to analyse the amount of translated p53 protein produced by test compound exposed cells compared to non-exposed and control cells to determine whether more p53 is indeed produced and *C-MYC* suppressed in treated cells. The p53 protein is active when acetylated. By inhibiting the deacetylation enzyme SIRT1 and/or the acetylation recognition motif BRD4, this study hoped to find increased expression of p53 and to identify a promising candidate compound for future anti-cancer treatment. This study also set out to determine cell line specificity of the tested compound(s), in order to establish whether the human cancer cell lines tested will possibly be treatable by drugs created from the studied compounds.

Chapter 2: Materials and Methods

All experiments were conducted in the Department of Physiology of the University of Pretoria with the exception of flow cytometry analysis which was conducted at the department of Pharmacology of the University of Pretoria. The ethics approval number is 244/2017.

Cell lines

Cancer cell lines are well characterised commercially available model cells that keep dividing and growing indefinitely when maintained under specific laboratory conditions. The cells can then be used in cell culture to study cancer biology and to test the efficacy of potential cancer therapies as well as the diverse and adverse effects of established chemotherapeutic drugs (7). The availability of an expanded variety of such experimental models is crucial for studying cancer pathology, uncovering the genetic and epigenetic alterations and their effects as well as for testing specificity for cancerous cells (122). Cell lines are used to assess the effects of certain genetic manipulations that would otherwise be complicated by ethical and practicality issues (123). When compared to other models, cell lines in research are easy to characterize on a molecular basis (assuming no code alterations such as mutations during repetitive culturing had taken place) as well as to uncover critical genes in complex pathway studies and aid research into the cancer related methylation reactions (123). When testing the efficacy of new drugs or in the discovery of novel putative drug targets, cancer cell line profiling has largely become the model of choice over the past decade (7, 124, 125).

The effects of the W137 compound were investigated in the following cell lines:

a) SH-SY5Y: This is a thrice cloned sub-line of the neuroblastoma SK-N-SH cell line which was established in 1970 from a metastatic bone tumour. The patient was female and four years of age. The cells are partially suspended and partially adherent under standard cell culturing conditions and grow as clusters of neuroblastic cells with multiple short neurites at 37 °C. The cells aggregate and form

floating clumps upon trypsinization. Figure 1.11.1 is from the ATCC website information and purchase page (ATCC).

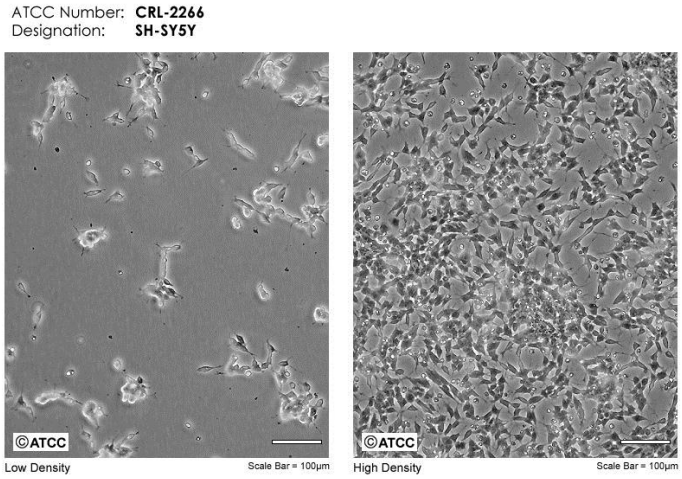

Figure 1.11.1: Photomicrograph representation of the SH-SY5Y cell line as illustrated by the ATCC (ATCC® CRL-2266™)
(http://www.lgcstandards-atcc.org/products/all/CRL-2266.aspx?geo_country=za)

b) U937: Derived by Sundstrom and Nilsson from malignant cells obtained from a pleural effusion of human myeloid lymphocytes. The patient was male and 37 years of age. The cells are rounded and non-adherent when incubated under standard cell culturing conditions and grow at 37 °C. Figure 1.11.2 is from the ATCC website information and purchase page (ATCC):

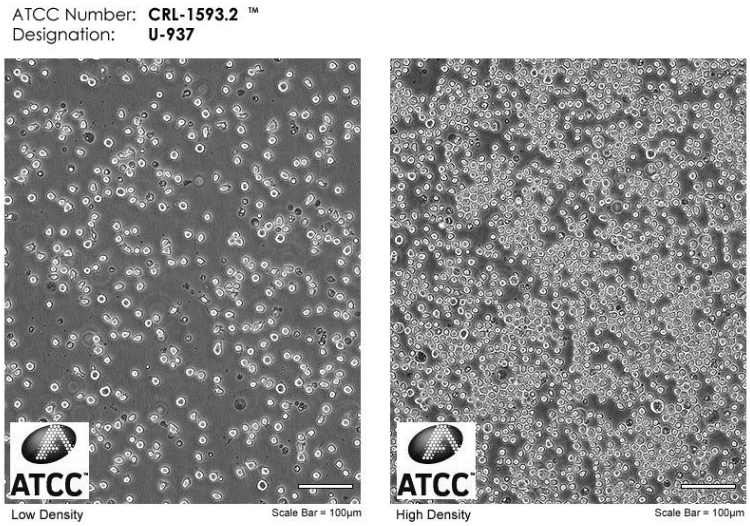

Figure 1.11.2: Photomicrograph representation of the U937 cell line in culture as illustrated by the ATCC (ATCC® CRL-1593.2™)

(http://www.lgcstandards-atcc.org/products/all/CRL-1593.2.aspx?geo_country=za).

General laboratory procedures

1.12.1 Materials

Dulbecco's Modified Eagle Medium (DMEM), Trypsin-EDTA and crystal violet were purchased from Sigma Chemical Co. (St. Louis, United States of America). Heat-inactivated foetal calf serum (FCS), sterile cell culture flasks and plates were obtained through Sterilab Services (Kempton Park, Johannesburg, South Africa). Penicillin, streptomycin and fungizone were purchased from Highveld Biological Pty (Ltd) (Sandringham, SA). All other chemicals were of analytical grade and were purchased from Sigma Chemical Co. (St. Louis, United States of America), Southern Cross Biotechnology Pty (Ltd) (Cape Town, SA), Amersham Biosciences Pty (Ltd) (Pittsburgh, PA, USA) and Agilent Technologies Pty (Ltd) (Palo Alto, CA, USA).

1.12.2 General cell culture procedures

Aseptic techniques were applied throughout, with all work being carried out in a laminar flow cabinet from Labotec (Midrand, South Africa), all solutions were filtered-sterilized (0.22 µm pore size) and all glassware and non-sterile equipment sterilized by autoclaving (20 min, 120 °C, 15 psi). The effects of the *in silico* designed inhibitors were investigated on a neuroblastoma cell line (SH-SY5Y) (American Tissue Culture Collection (ATCC), Maryland, USA)) and on an acute myeloid leukemia (AML) cell line (U937) (American Tissue Culture Collection (ATCC), Maryland, USA)). The SH-SY5Y cells were supplemented with 10% foetal bovine serum in DMEM-F12 medium (50% Dulbecco's Modified Eagle Medium (DMEM) and 50% Ham's F12 medium) and 1% antibiotics (100 U/mL penicillin G, 100 µg/mL streptomycin and 250 µg/L fungizone). The U937 cells were supplemented with 10% foetal bovine serum in Iscove's Modified Dulbecco's Medium (IMDM) and 1% antibiotics (100 U/mL penicillin G, 100 µg/mL streptomycin and 250 µg/L fungizone).

Cell were grown and maintained in 25 cm^2 tissue culture flasks in the humidified atmosphere of a water-jacketed incubator Forma Scientific (Ohio, United States of America), set at 37 °C, 5% CO_2. Cells were seeded into 24 well plates not exceeding 50 000 cells per well, in 96-well plates not exceeding 5000 cells per well and 25 cm^2 (25 mL) flasks not exceeding 1 000 000 cells per flask. Cell counting and viability

testing was performed using the MUSE Cell Analyser by Merck (Merck, Dramstadt, Germany).

Phosphate buffered saline (0.1M, PBS) was prepared by diluting a ten times concentrated solution consisting of 80 g/L NaCl, 2 g/L KCl, 2 g/L KH_2PO_4 and 11.5 g/L Na_2HPO_4 (all purchased from Merck (Munich, Germany)) to a 1 times concentrated solution. The diluted PBS solution was autoclaved (20 min, 120 °C, 15 psi) before use. Hydroxymethylaminomethane (Tris) buffered saline (TBS) was prepared by diluting a ten times concentrated solution (pH = 7.4) consisting of 61 g/L Tris (purchased from Sigma Chemical Co. St. Louis, USA) and 90 g/L NaCl, (purchased from Merck (Darmstadt, Germany) to a 1 times concentrated solution. The pH was adjusted to 7.4 with 1 N HCl.

The growth medium of the cells was replaced at one to three day intervals, depending on the proficiency of cell growth. In the case of the attached SH-SY5Y cell line, cells were trypsinized when confluent by removing the growth medium, washing with cold, sterile PBS and then with cold, sterile trypsin/versene for 20 sec or as long as it takes for cells to detach and appear rounded. The trypsin solution was removed and the tissue culture flask was gently tapped against a hard surface to aid in cell detachment. The detached cells were re-suspended in fresh, warmed medium and either divided into subcultures, used in experiments or frozen away in cryotubes in a -80 °C freezer. The freeze medium consists of 10% growth media, 10% DMSO and 80% FCS. Compound W137 was synthesized by WuXi AppTec (Shanghai, China) (>95% pure as per HPLC) and a stock solution of 50 mM was prepared. The final concentration of DMSO on the cells was not greater than 0.1% (*v*/*v*).

1.12.3 General experimental procedures

For experiments using the SH-SY5Y cell line, cells were incubated for 24 h to allow for attachment after which medium was removed and the cells were exposed to the compound in a range of concentrations, namely 6.25 µM, 12.5 µM, 25 µM, 50 µM and 100 µM. Cells were harvested by trypsinisation as described above and were counted by making use of the MUSE Cell Analyser (Merck, Darmstadt, Germany), or by using a haemocytometer whereby a volume of 20 µl of the suspended cells where mixed with 80 µl PBS and 100 µl Trypan blue to give a concentration of cells with 10

times dilution factor. Dead cells take up the dye and are consequently stained blue, which is then left uncounted. For experiments using the U937 cell line, cells were free floating and directly counted using the MUSE Cell Analyser (Merck, Darmstadt, Germany).

When using the haemocytometer and Trypan blue to determine the number of viable cells per mL, the following formula is applicable:

Cells/mL = Average count of viable cells in the corner squares x dilution factor x 10^4

Computer-Aided Drug Design

This component (Section 2.3) of the work reported in this study was completed by Dr. B A Stander (Department of Physiology) and is included here for the sake of clarity and completeness in the context of the rest of the dissertation.

1.13.1 Software and computer system

The following software packages were used on an Ubuntu 14.04 LTS computer system with an Intel Core i7-5820K CPU with a GeForce GTX 980 GPU (Table 1.13.1):

Table 1.13.1: Software packages used for *in sito* drug design.

Software	Purpose
Chimera (126),	Visualization and figure generation
Chemsketch (127)	2D molecule preparation and SMILES generation
Open Babel 2.3.2 (128)	Converting SMILES strings to 3D structures.
Balloon, (129, 130)	Enumeration of ligands
Autodock Vina (131), rDOCK (132) and Autodock (133)	Docking
GROMACS 4.6.5 (134)	Molecular dynamics simulations
AMBER99sb force field (135)	Protein, water and ion forcefield parameters
The Stockholm lipids forcefield (136)	Lipid forcefield parameters
CUDA 7.0 (137)	GPU accelerarion of molecular dynamics

	simulations
ACPYPE (138) using antechamber from the AMBER 14 suite (139) and	Ligand forcefield parameters.
g_mmpbsa (140).	MMPBSA free energy calculations

1.13.2 Docking Methodology

An ensemble docking study was carried out using the following receptors: X-ray structures of sirtuin 3 including 4jsr, 4jt8 and 4jt9. Homology models of these proteins for sirtuin 1 and sirtuin 2 were generated using the SWISS-MODEL (141). In Autodock Vina the exhaustiveness was set to 15 with the rest of the parameters set on default (142). For Autodock, the Lamarckian genetic algorithm for conformational searching was used in Autodock with the ga_pop_size and ga_num_evals parameters set to 250 and 2500000 respectively. A minimum of 30 runs were carried out for each potential ligand. For rDOCK a cavity of radius 15Å centered on the structure of the ligand from 4jsr (1NQ) was used to define the docking volume. Each compound was subjected to 50 docking runs and the poses were sorted according to its docking score.

Ligand-binding assay: Sirtuin 1, 2 and 3

A biochemical assay against human SIRT1, 2 and 3 were performed by Reaction Biology Corp. (RBC) (Malvern, PA, USA; http://www.reactionbiology.com). Full-length human SIRT1 and 2 and catalytically active human SIRT3 were expressed in *Escherichia coli* and purified. A fluorogenic peptide from p53 residues 379-382 (Ac-RHK-K(Ac) for SIRT1–3 was used as a substrate to perform the assay. The assay generally consists of a two-step reaction. First a deacetylated substrate was produced which is then cleaved to release the fluorogenic 7-amino-4-methylcoumarin (AMC) used to label the substrate. Suramin (SIRT1 and 2 inhibitor) and nicotinamide (SIRT3 inhibitor) were used as positive controls. To determine the $IC_{50(SIRT1)}$ values, the fluorescence produced by serial dilution of the compounds was analysed. The percentages of enzyme activity (relative to DMSO controls) are calculated. The $IC_{50(SIRT1)}$ values were calculated from the resulting sigmoidal dose–response curves using Dr Fit.

Cell growth studies

1.15.1 SH-SY5Y cell line: Crystal violet assay and spectrophotometry

a) Materials

Glutaraldehyde, crystal violet and Triton X-100 were purchased from Merck (Darmstadt, Germany).

b) Methods

Quantification of fixated monolayer cells were determined using crystal violet as a DNA stain and spectrophotometry analysis. Staining cell nuclei of fixed cells with crystal violet allows for rapid, accurate and reproducible quantification of cell number in cultures grown in 96-well plates (143, 144). Absorbance of the dye measured at 570 nm corresponds to cell numbers. According to Berry *et al.* (1996) crystal violet staining of samples containing an abnormally high proportion (>30%) of stationary binucleated cells yields apparently higher cell concentrations than trypan blue or Coulter counter methods (145).

For crystal violet assays, exponentially growing SH-SY5Y cells were seeded in 96-well tissue culture plates at a cell density of 5000 cells per well. Cells were incubated at 37 °C for 24 h to allow for attachment. After 24 h attachment the medium was discarded and the cells were exposed to a range of concentrations namely 6.25 µM, 12.5 µM, 25 µM, 50 µM and 100 µM of W137 compound, and incubated for a further 48 h, before the crystal violet assay was performed.

After 48 h the medium was discarded and 100 µl of 1% glutaraldehyde (in PBS) was added to each well and incubated at room temperature for 15 min. The glutaraldehyde solution was discarded and 100 µl 0.1% crystal violet (in PBS) was added and left at room temperature for 30 min. The crystal violet solution was discarded and the microtiter plates were immersed under running tap water for 10 min and left overnight to dry. A volume of 200 µl 0.2% Triton X-100 was added to solubilize the cells and incubated at room temperature for 30 min. A volume of 100 µl of this solution was transferred to a clean microtiter plate and the absorbance was read at 570 nm with an Epoch^{TM} microplate spectrophotometer from Bio-Tek Instruments Inc. (Vermont, USA).

Cell counting was done using the MUSE Cell Analyser (Merck, Darmstadt, Germany) for accurate and reproducible quantification of cell numbers and viability measurements (146). Dose-dependent studies were conducted to determine the growth inhibitory effect of the compounds on the SH-SY5Y cell line. Time-dependent studies were carried out after 24 and 48 h in order to observe the progression of cell growth over time in response to exposure to the compounds. Excel and Graphpad Prism 5.0 (GraphPad Software, Inc., CA, USA) was used to analyse raw data. The $IC_{50(SIRT1)}$ value was be calculated as follows:

$$IC50 = \frac{Number\ of\ cells\ exposed\ to\ test\ condition}{Number\ of\ cells\ exposed\ to\ vehicle - treated\ condition} * 100 = 50$$

The obtained growth inhibitory constant of 50% (SIRT1-IC_{50}) was used henceforth as a concentration constant for the compounds throughout this study. The compound that generated the lowest SIRT1-IC_{50} value for both cell lines, namely the SIRT1 inhibitor W137, was selected for further analysis throughout this project.

1.15.2 U937 cell line: Cell counting using flow cytometry

a) Materials

Cell Count and Viability Solution is a product of the MUSE Cell Analyser from Merck, Germany. Ethanol was also purchased from Merck, Germany.

b) Methods

Cell quantification was done using the MUSE Cell Analyser (Merck, Darmstadt, Germany) for accurate and reproducible quantification of cell numbers and viability measurements. The MUSE Cell Analyser system applies the principles of propidium iodide cell penetration, clearly distinguishing between live and dead cells (viability percentages and live cell counting). The same procedure as described in this section was planned for human peripheral blood lymphocytes (HPBL) but the low viability was detected upon repeated testing and had therefore been excluded from the project henceforth.

An amount of 5 000 U937 AML cells per well were seeded into 96-well plates and incubated at 37 °C for 15 min to allow cells to adjust in suspension. Wells were then designated to different concentrations of the inhibitor compounds, namely 6.25 µM,

12.5 µM, 25 µM, 50 µM and 100 µM (three biological and three technical repeats) and incubated at 37 °C for 24 h and 48 h respectively. A baseline row of wells were also seeded as a control for the starting amount of cells, each well containing a total volume of 100 µl. Dimethyl sulfoxide (DMSO) not exceeding 0.02% concentration was used as a vehicle control. A percentage of DMSO to total volume concentration higher than 0.02% becomes cytotoxic.

After the exposure time had elapsed, the live cell count and percentage viability was measured. A volume of 100 µL of Muse^{TM} Count and Viability kit solution were added to each well, mixed by pipetting then transferred to 1.5 mL Eppendorf tubes. Measurements were taken in duplicate on the MUSE Cell Analyser from Merck (Darmstadt, Germany) and analysed to directly calculate the SIRT-IC_{50}. The Muse^{TM} Count and Viability kit solution works through propidium iodide action to distinguish dead and live cells with no additional dye added. Each well was counted individually and values of total cell count (live and dead cells) were then recorded to determine the IC_{50} for all the compounds. Computer programs used to analyse raw data were Excel and Graphpad Prism 5.0 (GraphPad Software, Inc., CA, USA).

Morphology studies

1.16.1 Apoptosis and oncosis detection: Fluorescent microscopy and polarization-optical differential interference contrast

Polarization-optical differential interference contrast (PlasDIC) is a microscope based polarization-optical transmitted light contrasting method. PlasDIC light microscopy was used to recognize and display the integrity of specific cells when compared to other viable cells (147). This provides insight regarding the effects of the inhibitors on the comparative morphological changes in treated versus control cells. Cells in media only act as a negative control and cells exposed to Actinomycin D (0.2 µg/mL) acts as a positive control in successive experiments.

Fluorescent microscopy was done with the Zeiss Axiovert 25 inverted microscope (Carl Zeiss (Pty) Ltd., Johannesburg, South Africa), and used to distinguish between viable, apoptotic and oncotic cells. Hoechst 33345 (blue) and propidium iodide (PI) (red) fluorescent dyes as well as acridine orange (148) were used in this technique. Hoechst 33342 is a fluorescent dye which stains the nuclei of viable cells and apoptotic cells. This dye can penetrate cell membranes that are still intact. Under fluorescence light Hoechst 33342 staining of the nucleus is blue and Zeiss filter was used, with the light at an excitation of 352 nm and the emission at 455 nm. Propidium iodide, using Zeiss filter 15, is a fluorescent dye that is unable to penetrate an intact membrane and therefore stains the nucleus of only cells that have lost their membrane integrity due to oncotic and/or necrotic processes (149). Acridine orange, using Zeiss filter 9, is a lysosomotropic fluorescent compound that serves as a tracer for acidic vesicular organelles including autophagic vacuoles and lysosomes (150, 151). Cells undergoing autophagy have an increased tendency for acridine orange staining when compared to viable cells. However, acridine orange is not a specific marker for autophagy and therefore other techniques are needed to verify the appearance of increased autophagic activity. This technique was only performed on the SH-SY5Y cell line as the cells form an adhesive monolayer which is easily viewed under a microscope and practical to stain.

a) Materials

BisBenzimide (Hoechst 33342), acridine orange and propidium iodide were purchased from Sigma-Aldrich (St. Louis, MO, USA).

b) Methods

Exponentially growing SH-SY5Y cells were seeded at 150 000 cells per well in 6-well plates with 3 mL of medium. After the 24 h attachment period the medium was discarded and the cells exposed to the predetermined $IC_{50(SIRT1)}$ of the compound and incubated for 24 h and 48 h respectively. After the exposure time had elapsed, 0.5 mL of Hoechst 33342 solution (3.5 µg/mL in PBS) was added to the medium to give a final concentration of 0.9 µM and incubated for 30 min at 37 °C in a CO_2 incubator. After 25 min, 0.5 mL of acridine orange solution (4 µg/mL) and 0.5 mL of propidium iodide solution (40 µg/mL in PBS) was added to the medium to give a final concentration of 1 µg/mL and 12 µM respectively and then incubated for 5 min at 37 °C. After the full 30 min had elapsed, the medium was removed and the cells carefully rinsed three times with PBS before being immersed in clean PBS (1 mL). At least three biological replicated were performed in order to obtain representative images. The cells were examined with a Zeiss inverted Axiovert CFL40 microscope and Zeiss AxiovertMRm monochrome camera under Zeiss Filter 2 for Hoechst 33342 (blue) stained and Zeiss Filter 9 for acridine orange-stained (148) and Zeiss filter 15 for propidium iodide-stained (red) cells and the images subsequently overlaid and analysed using the Zeiss Axiovert 25 inverted microscope (Carl Zeiss (Pty) Ltd., Johannesburg, South Africa). In order to prevent fluorescent dye quenching, all procedures were performed in a dark room.

Flow cytometry studies

1.17.1 Cell Cycle progression: Flow cytometry and DNA staining with Propidium iodide after 24 h and 48 h

Flow cytometry was employed to analyse the influence of W137 on cell cycle progression on both SH-SY5Y and U937 cell lines. Quantifying the DNA content of the individual cells allows the correlation between percentages of cells at specific stages of the cell cycle and allows the analysis of cell cycle blockade of 24 h and 48 h exposed cells respectively. Analysis was conducted by ethanol fixation and membrane permeation followed by propidium iodide staining of cells. Propidium iodide was used to stain the nucleus in order to quantify the DNA. The amount of DNA present correlates with the stages of the cell cycle during cell division (Figure 2.3). In flow cytometry a laser beam of a single frequency is directed onto a hydrodynamically focused stream of cells in flowing fluid. A number of detectors are aimed at the point where the stream passes through the light beam; one in line with the light beam (Forward Scatter or FSC) and several perpendicular to the laser including the Side Scatter channel (SSC) and one or more fluorescent detectors. Each suspended particle passing through the laser beam scatters the light and fluorescent chemicals in the particle are excited into emitting light at a lower frequency than the light source. This combination of scattered and fluorescent light is detected by the detectors. By analysing fluctuations in brightness at each detector (one for each fluorescent emission peak) it is possible to deduce the size, quantity and fluorescent intensity (DNA content when stained with propidium iodide) of cells (Figure 1.17.1). FSC correlates with the cell volume and SSC depends on the inner complexity of the particle e.g. amount of DNA, shape of nucleus, etc.

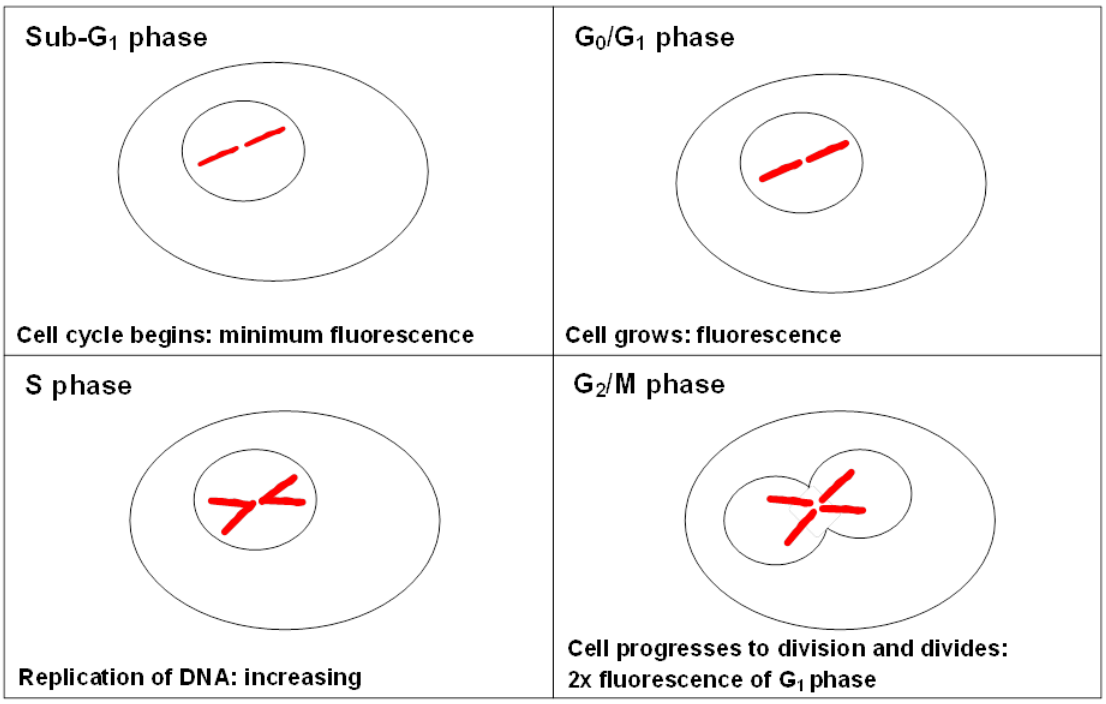

Figure 1.17.1: Graphical representation of the mechanism of cell cycle study through the application of propidium iodide fluorescence. During the sub-G_1 phase of the cell cycle fluorescence is due to a standard quantity of DNA as found in a non-dividing, viable cell. As the cell progresses through the phases leading to division, DNA duplication occurs as the cell enters mitosis and increase in fluorescence up to two fold can be detected.

a) Materials

The 99.9% ethanol was from Merck Co. (Darmstadt, Germany). Propidium Iodide was purchased from Sigma-Aldrich (St. Louis, MO, USA).

b) Methods

Exponentially growing U937 AML and SH-SY5Y neuroblastoma cells were seeded into 6-well plates at 150 000 cells per well and exposed to the $IC_{50(SIRT1)}$ of the test compounds and incubated at 37 °C for 24 h and 48 h respectively. After the exposure time has elapsed, $1x10^6$ of the U937 cells were centrifuged at 300 x*g* for 5 min in 15 mL tubes and the supernatant discarded. For the SH-SY5Y cell line, the cells were trypsinized and pipetted from the wells into 15 mL tubes before centrifuging as carried out with the U937 cells. The cells were resuspended in 200 µL

of ice-cold PBS containing 0.1% FCS. Thereafter, 3 mL of ice-cold 70% ethanol was added in a drop wise manner with gentle vortex mixing and the cells stored at 4ºC for 24 h. After 24 h, the cells were pelleted by centrifuging the samples at 300 x*g* for 5 min. The supernatant was removed and the cells resuspended in 1 mL of PBS containing propidium iodide (40 µg/mL). The samples were incubated at 37 ºC for 45 min in the dark.

Propidium iodide fluorescence (relative DNA content per cell) was measured with a FC500 System flow cytometer (Beckman Coulter South Africa (Pty) Ltd) equipped with an air-cooled argon laser of 488 nm. Data from at least 10 000 cells were analysed with CXP software (Beckman Coulter South Africa (Pty) Ltd). Data from cell debris (particles smaller than apoptotic bodies) and clumps of 2 or more cells was removed from further analysis through appropriate gating. Cell cycle distributions were calculated with WEASEL version 2.4 software (F. Battye, Walter and Eliza Hall Institute (WEHI), Melbourne, Australia) by assigning relative DNA content per cell to sub-G_1, G_1, S and G_2/M fractions. Propidium iodide molecules emit light at 617 nm therefore, data obtained from the log forward scatter detector nr 3 (Fl3 log, detects 600 nm emissions) was represented as histograms on the x-axis.

1.17.2 Apoptosis detection analysis: Phosphatidylserine externalization after 24 h and 48 h

To analyse the percentage dead cells, simultaneous FITC-conjugated Annexin V and propidium iodide staining were performed without membrane permeabilisation. Annexin V measures the translocation of the membrane phosphatidylserine (PS) from the inner side of the plasma membrane to the outer side (Figure 1.17.2) which is one of the earliest indications of apoptosis. Annexin V, a 35-36 kDa, Ca^{2+}-dependent, phospholipid binding protein with a high affinity for PS binds the exposed extracellular PS. Cells were counter-stained with propidium iodide in order to distinguish between necrotic and early apoptotic cells (96). Annexin V is conjugated to a fluorochrome, fluorescein isothiocyanate (FITC), and used for the identification of stages of apoptosis through flow cytometry. This procedure was performed following 24 h incubation as well as 48 h test compound exposure to compare the percentages of cells undergoing the various stages of death at respective times.

The mechanism of propidium iodide and Annexin V fluorescence for the study of cell death

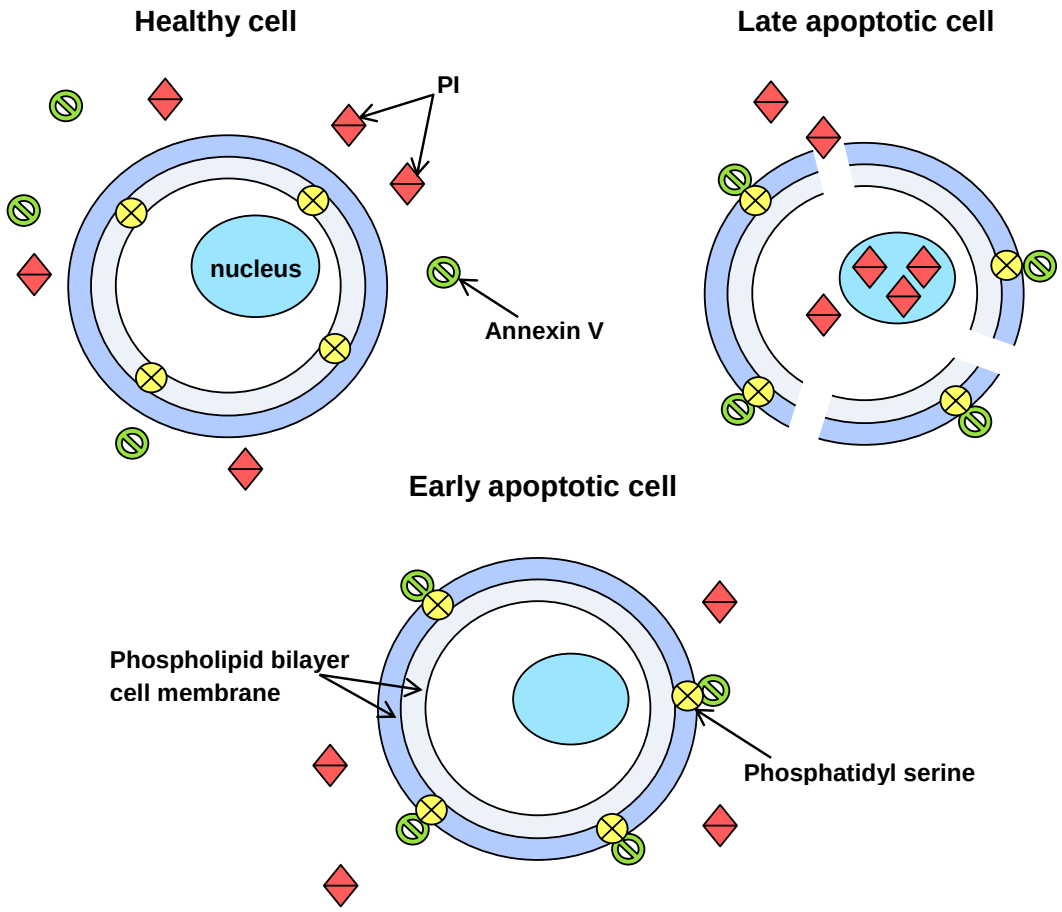

Figure 1.17.2: Graphical representation of the mechanism of cell death study through the application of propidium iodide and Annexin V fluorescence. Membrane phospholipid phosphatidylserine (PS) translocates from the inner to the outer leaflet of the plasma membrane during early apoptosis and once exposed to the extracellular environment, PS provides binding sites for the phospholipid binding protein Annexin V. Propidium iodide cannot penetrate viable cells or cells in early apoptosis with intact membranes and therefore propidium iodide staining distinguishes between early apoptotic, late apoptotic and necrotic cells when it is able to enter and fluoresce.

a) Materials

Annexin V-FITC Kit was purchased from BIOCOM biotech Pty (Ltd) (Clubview, South Africa).

b) Methods

Exponentially growing cells were seeded into 6-well plates at 150 000 cells per well and exposed to the $IC_{50(SIRT1)}$ concentrations of the compound and incubated at 37 °C for 24 h and 48 h respectively. For the SH-SY5Y cell line, the cells were trypsinized once the exposure time had elapsed and pipetted from the wells into 15 mL tubes before centrifuging. The U937 cells were centrifuged at 300 x*g* for 5 min in 15 mL tubes and the supernatant discarded. Thereafter, the cells from both cell lines were resuspended in 1 mL of 1x binding buffer in a test tube. The cells were centrifuged at 300 x*g* for 10 min and the supernatant was discarded. This was followed by the cells being resuspended in 100 µL of 1x binding buffer and 10 µL of Annexin V-FITC added to the samples, where after it was incubated for 15 min in a dark room at 25˚C (standard room temperature). Following the incubation time, the cells were washed with 1 mL 1x binding buffer and centrifuged again at 300 x*g* for 10 min. The supernatant was discarded, where after the cells were resuspended in 500 µL of 1x binding buffer solution. A volume of 5 µL of propidium iodide was added just before flow cytometry analysis using the FC500 System flow cytometer (Beckman Coulter South Africa (Pty) Ltd). Care was taken throughout the procedure to protect the samples from exposure to ambient light throughout the experimental procedure by covering test tubes with foil.

Propidium iodide fluorescence (oncotic cells) and annexin V fluorescence (apoptotic cells) was measured with an FC500 System flow cytometer (Beckman Coulter South Africa (Pty) Ltd) equipped with an air-cooled argon laser excited at 488 nm. Data from at least 30 000 cells were analysed with CXP software (Beckman Coulter South Africa (Pty) Ltd). Data from cell debris (particles smaller than apoptotic bodies) and clumps of 2 or more cells was removed from further analysis through gating. Propidium iodide molecules emit light at 617 nm and FITC emit at 530 nm therefore, data was obtained from the Fl1 detector for 515-545 nm emissions and Fl3 detector for 600 nm emissions. FL3 log (propidium iodide) was represented on the x-axis and FL1 log (FITC) was represented on the y-axis and the plot was divided into four quadrants. The bottom-left quadrant was assigned to measure the viable cells with minimal propidium iodide and FITC staining. Medium only (MO) control cells of both cell lines were calibrated to include 98% of cells within the viable cell quadrant. The top left quadrant was assigned to cells in the early stages of apoptosis, the bottom-

right quadrant was assigned to cells undergoing oncosis and the top-right quadrant was assigned to cells in the late stages of apoptosis which have become necrotic. Distributions of cells within the quadrants were calculated with WEASEL version 2.4 software (F. Battye, Walter and Eliza Hall Institute (WEHI), Melbourne, Australia).

1.17.3 Mitochondrial membrane depolarization: 3,3'-dihexyloxacarbocyanine Iodide

The differences in membrane potential (depolarization) were measured with 3,3'-dihexyloxacarbocyanine Iodide ($DiOC_6(3)$), which is a dye with cationic properties that accumulates in the mitochondria of viable cells to produce a bright green fluorescence (152). In cells undergoing apoptosis the dye is unable to aggregate within the mitochondrial as the membrane potential is altered, resulting in the dye remaining in the cytoplasm and therefore not fluorescing (Figure 1.17.3) (153).

a) Materials

$DiOC_6(3)$ was purchased from Sigma (St. Louis, MO, USA).

b) Methods

Exponentially growing U937 AML or SH-SY5Y cells were seeded into 6-well plates at 150 000 cells per well and exposed to the $IC_{50(SIRT1)}$ concentrations of the compound and incubated at 37 °C for 48 h. After the exposure time has elapsed, the U937 cells were centrifuged at 300 x*g* for 5 min in 15 mL tubes and the supernatant discarded. For the SH-SY5Y cell line, the cells were trypsinized and pipetted from the wells into 15 mL tubes before centrifuging. The cells were then resuspended in 1 mL medium to wash and centrifuged at 300 x*g* for 5 min. The supernatant was discarded and the cells resuspended in 1 mL of PBS. 100 nM of $DiOC_6(3)$ was added to the samples for 30 min (incubated at 37 ˚C), followed by washing twice with PBS to remove the unbound dye. Fluorescence analysis was conducted using the FC500 System flow cytometer (Beckman Coulter South Africa (Pty) Ltd). Data from at least 10 000 cells were analysed with WEASEL version 3.0 software (F. Battye, Walter and Eliza Hall Institute (WEHI), Melbourne, Australia).

The mechanism of $DiOC_6(3)$ fluorescence for the study of mitochondrial membrane potential as a measure for cell death

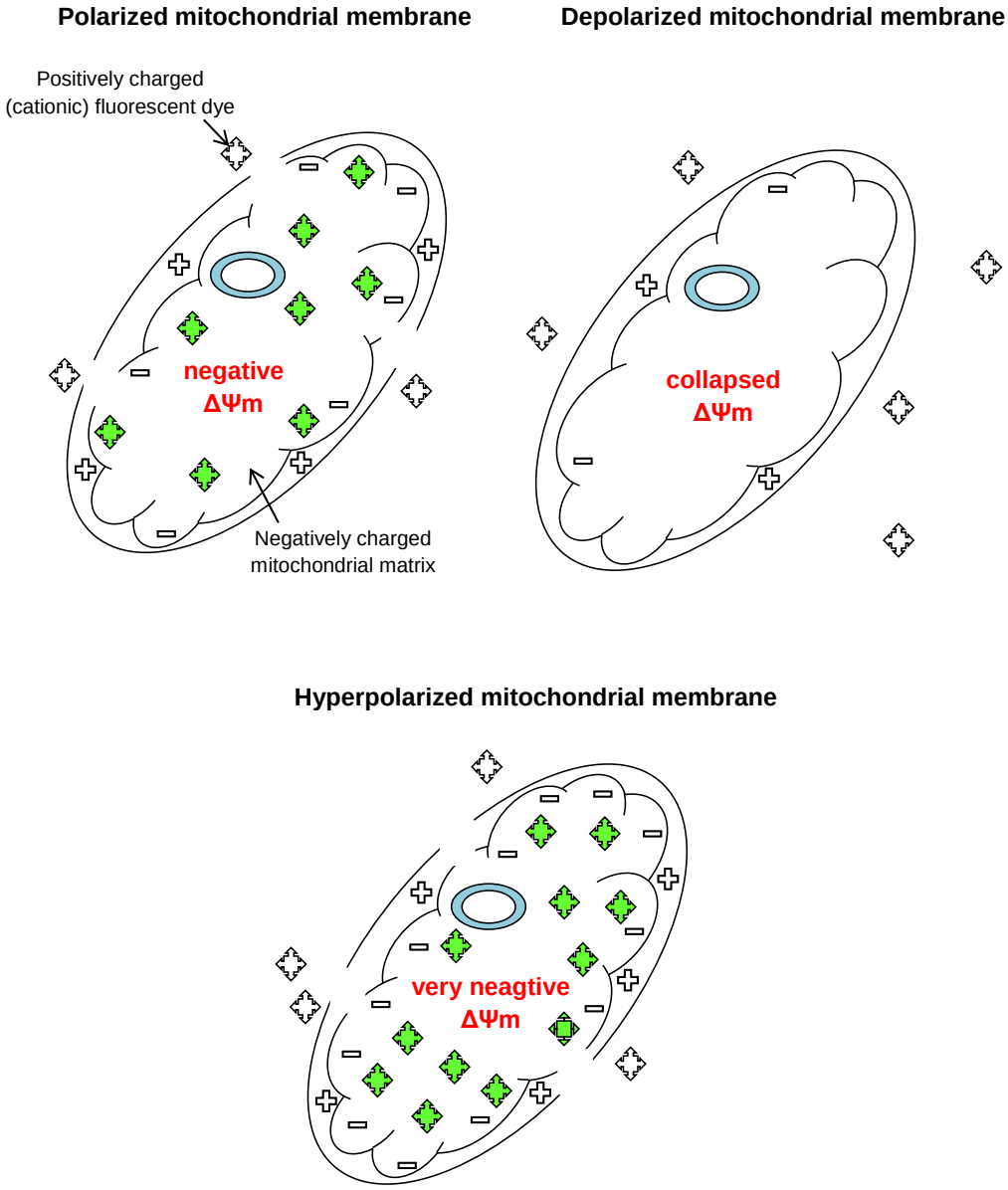

Figure 1.17.3: Graphical representation of various states of mitochondrial membrane potential and $DiOC_6(3)$ as an indicator of change in membrane polarity. 3,3'-dihexyloxacarbocyanine Iodide ($DiOC_6(3)$) is a cationic dye which fluoresces bright green when upon accumulation in the accessible mitochondria of viable cells. The dye does not aggregate in mitochondria of cells undergoing apoptosis as the mitochondrial membrane polarity is altered, therefore no fluorescence of the dye in the cytoplasm will be observed.

1.17.4 Reactive oxygen species formation: 2,7-dichlorofluorescein diacetate

Cells producing excessive amounts of reactive oxygen species (ROS) undergo oxidative stress that can be damaging to DNA structure and the mitochondria. To study the possibility of oxidative stress, a non-fluorescent probe, 2,7-dichlorodihydrofluorescein diacetate (H2DCF-DA), was used to indicate the levels of hydrogen peroxide (H_2O_2) generated within the cells. H2DCF-DA is de-esterified inside the cells and becomes the highly fluorescent derivative 2,7-dichlorofluorescein (DCF) upon oxidation (Figure 1.17.4).

a) Materials

H2DCF-DA was purchased from Sigma (St. Louis, MO, USA).

b) Methods

Exponentially growing cells were seeded into 6-well plates at 150 000 cells per well and exposed to the $IC_{50(SIRT1)}$ concentrations of the compound and incubated at 37 °C for 48 h. After the exposure time has elapsed the cells were centrifuged at 300 xg for 5 min, washed twice with PBS and the supernatant discarded. The cells were then resuspended in 1 mL PBS and 20 µM H2DCF-DA added, followed by incubation for 25 min at 37 °C. The analysis of DCF was measured in the flow cytometer. DCF fluorescence measurements were conducted using the FC500 System flow cytometer (Beckman Coulter South Africa (Pty) Ltd). Data from at least 10 000 cells were analysed with WEASEL version 3.0 (F. Battye, Walter and Eliza Hall Institute (WEHI), Melbourne, Australia).

The mechanism of DCFDA fluorescence for the study of ROS formation

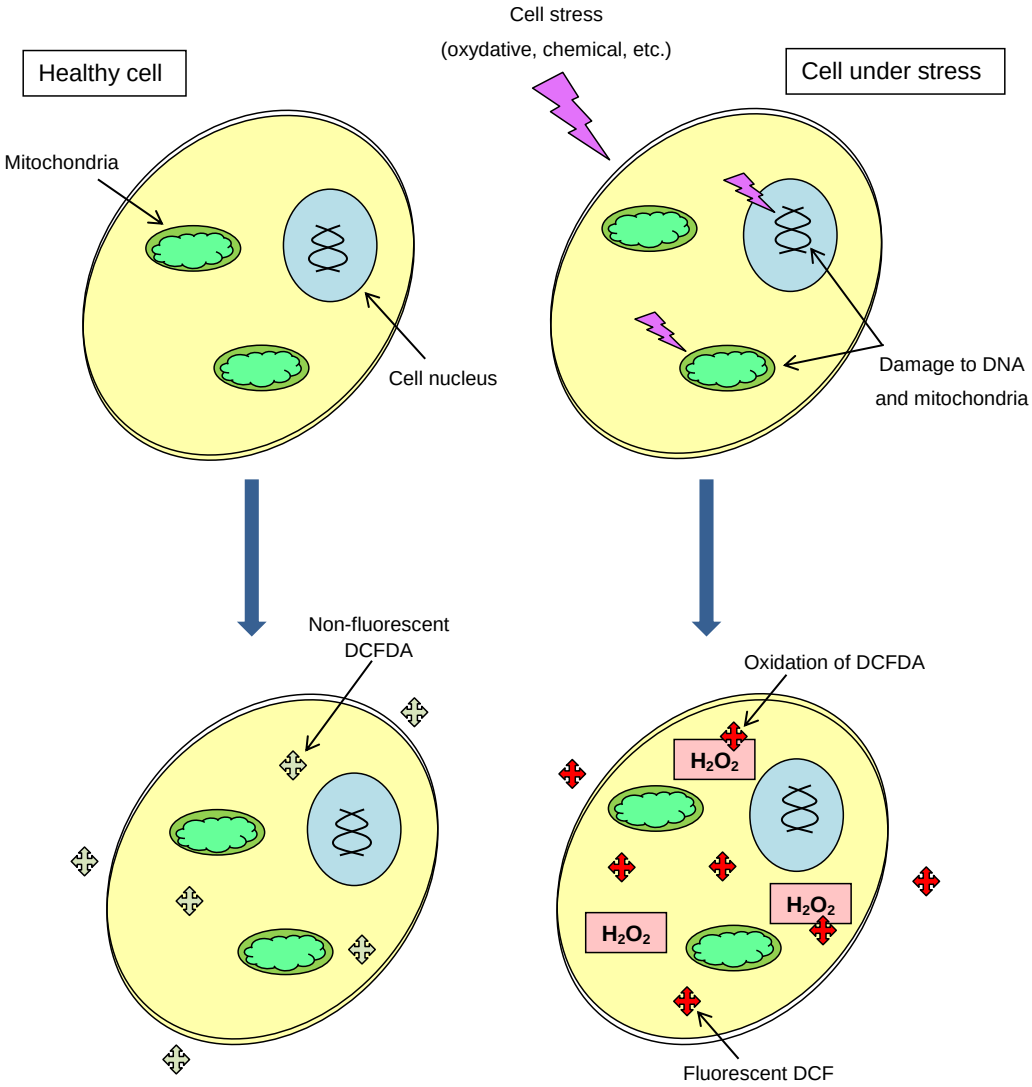

Figure 1.17.4: Change of the H2DCF-DA probe from non-fluorescence to fluorescence upon oxidation is an indicator of reactive oxygen species within cells. Excessive amounts of ROS produced by cells surviving in stressful conditions can damage DNA and the mitochondria. H2DCF-DA is used to measure levels of hydrogen peroxide (H_2O_2) generated within the cells as de-esterification of the H2DCF-DA molecules inside the cells results in formation of the highly fluorescent derivative 2,7-dichlorofluorescein (DCF).

Gene expression analysis: Reverse transcription quantitative polymerase chain reaction of *C-MYC* and *p53*

SIRT1 also positively influences *C-MYC* transcription and has been found to play a crucial role in cell proliferation of many cancer types (4, 41). Inhibition of SIRT1 by the inhibitory test compounds in this study were hypothesised to prevent the gene expression of *C-MYC*. *p53* is a key protein in inducing cell death via apoptosis (154, 155). Therefore examining the expression of *C-MYC* and *p53*, key proteins in cancer growth or inhibition respectively, was expected to provide insight into DNA to RNA transcription in both cancer cell lines and how W137 SIRT1 inhibitor compound influenced the expression of mRNA for these critical proteins.

Reverse transcription quantitative polymerase chain reaction (qRT-PCR) is the enzymatic amplification of a segment of mRNA between a pair of primers. The technique offers an accurate measurement of the mRNA level which correlates with the level of expression of the gene of interest, as it has been transcribed. The amount of increase or decrease in mRNA can be used as a measure of the amount of template present at the start of the PCR. The primers are two oligonucleotides, one on each side of the target DNA sequence. One primer is complementary to the one strand of double stranded DNA and the other primer complimentary to the other strand. Three house-keeping genes, a genomic DNA control, positive PCR control and reverse transcription controls were included.

Total RNA from the vehicle-control and the wells containing exposed cells (4 biological replicates) were isolated using Sigma Aldrich's RNAzol® RT (St. Louis, MO, USA) as per manufacturers instructions, which delivers pure, high quality RNA from cells. The RNA is considered pure of organic contamination (e.g. ethanol or phenol) with a 260/230 absorbance ratio greater than 1.5 and free of protein contamination with a 260/280 absorbance ratio greater than 2. cDNA was synthesized through reverse transcription and quantified using Roche's LightCycler® Nano instrument (Randburg, Gauteng, South Africa) and the SensiFAST™ SYBR® No-ROX Kit from Bioline (Celtic Molecular Diagnostics, Cape Town, South Africa), which is designed to yield superior results on fast-cycling instruments.

a) Materials

RNAzol® RT from Sigma (St. Louis, MO, USA) was used for total RNA extraction and the SensiFAST™ SYBR® No-ROX Kit from Bioline (Celtic Molecular Diagnostics, Cape Town, South Africa) for fast and efficient real-time PCR.

b) Methods

1.18.1 RNA extraction

In order to obtain high quality pure total RNA, Sigma Aldrich's RNAzol® RT reagent and an optimized protocol was used. Exponentially growing cells were seeded into 6-well plates at 150 000 cells per well, exposed to the $IC_{50(SIRT1)}$ concentrations of the test compound and incubated at 37 °C for 24 h and 48 h respectively. After the exposure time had elapsed, SH-SY5Y cells were lysed directly on the culture dish. The RNAzol® RT was added (1 mL per 10 cm^2 area of culture well) and mixed by pipetting to form a homogenous lysate. For the U937 cell line, cells were centrifuged at 300 x*g* for 5 min in 15 mL tubes and the supernatant discarded. At least 1 mL of RNAzol® RT was added per 15 mL tube and pipetted several times for thorough mixing. Samples were placed in sterile 1.5 mL RNAse free Eppendorf tubes for all subsequent steps of mixing, reagent addition, centrifuging and incubation.

For DNA, protein and polysaccharide precipitation, 0.4 mL RNase-free water was added per mL of RNAzol® RT. The samples were tightly capped, shaken vigorously for 15 sec and allowed to stand 10 min at room temperature. This was followed by centrifuging the mixture for 15 min at 12,000 x*g* at 4˚C. The mixture subsequently separates into a semisolid pellet consisting of DNA, protein and polysaccharides and a supernatant containing the required RNA. This upper layer was then transferred by pipette into new sterile tubes, leaving a thick layer of supernatant still covering the pellet. Extreme care is taken not to disturb the pellet and cause mixing of the layers in this step to avoid contamination.

An equal volume of 100% isopropanol was added to the new tubes to facilitate RNA precipitation. The mixture was allowed to stand for 10 min at room temperature and centrifuged at 12,000 x*g* for 10 min also at room temperature. A white or colourless pellet of RNA precipitate may be observed after this step depending on the amount

of RNA acquired. The pellet was washed twice with 0.4 mL freshly made 75% ethanol (per 1 mL of supernatant used for precipitation) in the centrifuge at 6,000 x*g* for 3 min at room temperature. The alcohol solution was carefully removed by pipetting and 35 µL RNase free water (2-6 µL) was used to solubilize the pellet without drying. The samples were vortex mixed for 2-5 min at room temperature and stored at -20˚C until quantification using the Nanodrop spectrophotometry instrument and subsequent qRT-PCR analysis of the samples.

1.18.2 PCR analysis

The RNA samples were used to conduct quantitative reverse transcriptase PCR analyses. PCR tubes (0.1 mL) were labelled as follows (Table 1.18.1):

Table 1.18.1: Tube orientation of samples for PCR analysis showing negative and positive controls as well as W137 compound exposed samples with three repeats of each.

Neg. ctrl (*GAP*)	Neg. ctrl (*C-MYC*)	Neg. ctrl (*p53*)	Test (*GAP*)	Test (*C-MYC*)	Test (*p53*)	Pos. ctrl (*GAP*)	Pos. ctrl (*C-MYC*)
Neg. ctrl (*GAP*)	Neg. ctrl (*C-MYC*)	Neg. ctrl (*p53*)	Test (*GAP*)	Test (*C-MYC*)	Test (*p53*)	Pos. ctrl (*GAP*)	Pos. ctrl (*C-MYC*)
Neg. ctrl (*GAP*)	Neg. ctrl (*C-MYC*)	Neg. ctrl (*p53*)	Test (*GAP*)	Test (*C-MYC*)	Test (*p53*)	Pos. ctrl (*GAP*)	Pos. ctrl (*C-MYC*)
					Pos. ctrl (*p53*)	Pos. ctrl (*p53*)	Pos. ctrl (*p53*)

The SensiFAST™ SYBR® No-ROX Kit from Bioline with an optimized protocol was used. The total contents of individual PCR tubes must add up to 20 µL, which includes primers (3 mL), mastermix (10.6 mL, which includes 10 µL 2x SensiFAST™ SYBR® No-ROX One-Step Mix, 0.2 mL Reverse transciptase and 0.4 mL RiboSafe RNase Inhibitor) and 6.4 mL RNA template and water mix (400 ng template; the volume calculated using RNA concentrations as obtained through Nanodrop spectrophotometry, and water to reach 6.4 mL). All volumes were adapted to compensate for pipetting error.

The primers were pipetted into PCR tubes, followed by the RNA template and water mix and lastly the mastermix. cDNA was synthesized through reverse transcription

and quantified using Roche's LightCycler® Nano instrument (Randburg, Gauteng, South Africa), set at basic 2 step cycling conditions lasting 54 min, as optimized using the SensiFAST™ SYBR® No-ROX Kit protocol and the LightCycler® Nano instrument specifications. The relative mRNA levels were calculated using the $\Delta\Delta C_q$ method for each target gene and GAPDH was used to normalize the data (156). The resulting data was analysed using Excel and the standard student's t-test was applied to determine statistical significance.

Protein expression quantification: Enzyme-Linked ImmunoSorbent Assay (ELISA) of the p53 protein

Gene expression data from the qRT-PCR experiments are a good indication of relative mRNA levels of genes associated with apoptosis at the time of cell termination. However, gene expression does not necessarily correlate with protein expression or activity. Therefore, the quantities of acetylated p53 were also analysed. p53 is an important regulator of apoptosis and inhibition or down-regulation of p53 is often observed in cancerous tissue (1-3). When p53 is acetylated, it is active and promotes cell maintenance and cancer protection. SIRT1 is a deacetylation enzyme and SIRT1 inhibition is therefore expected to result in p53 being in the acetylated stage and therefore active (4).

The ELISA, Enzyme-Linked Immuno-sorbent Assay, and antibodies specific to p53 (157) were applied to determine p53 protein quantities. The Ab 133987 p53 Acetyl K382 Human ELISA (Enzyme-Linked Immunosorbent Assay) kit, which was used for this experiment, is an *in vitro* enzyme-linked immunosorbent assay for the accurate quantitative measurement of acetylated Lysine at position 382 of the p53 protein in human cell and tissue lysates.

a) Materials

The p53 Acetyl K382 Human ELISA kit was purchased from Abcam (Milton, UK).

b) Methods

Exponentially growing U937 AML or SH-SY5Y cells were seeded into 6-well plates at 150 000 cells per well then exposed to the $IC_{50(SIRT1)}$ concentrations of the test compounds and incubated at 37 °C for 48 h.

The p53 Acetyl K382 Human ELISA assay employs a p53 protein specific antibody layered into well plate strips. Cells were collected and centrifuged at 500 x*g* for 10 min at 4 °C. The cell pellet was solubilized with the supplied Extraction Buffer. The protein concentration was measured with Pierce's BCA Protein Assay Reagent Kit. Prepared samples (as described in Chapters 2.9.1-2.9.2) were pipetted directly into the wells and p53 that is present in the sample binds to the wells through the

immobilized antibody. After washing, the wells were exposed to an anti-p53 Acetyl Lysine382 detector antibody which is manually added. Washing will then remove any unbound detector antibody and HRP-conjugated label specific for the detector antibody will then be pipetted into the wells, followed by a repeat washing. TMB substrate solution was subsequently added to the wells upon which a blue colour developed in correlation to the amount of acetylated Lysine382 of the antibody-bound p53. The colour intensity was measured at 600 nm and the results analysed using Excel and/or Graphpad Prism 5.0 (GraphPad Software, Inc., CA, USA). Actinomycin D was used as a positive control and at least three biological replicates with three technical replicates for each biological replicate (n=3) were carried, as for all other experiments, unless otherwise stated.

1.19.1 Preparation of cell extracts

Media was removed from samples of both cell lines and the cells were rinsed twice with PBS. Cells were solubilized by adding extraction buffer containing phosphatase, protease and kinase inhibitors directly to the well (0.75-1.5 mL per confluent 15 cm diameter plate) for SH-SY5Y cells, and through solubilisation of cell pellets at $2x10^7$ cells per mL extraction buffer, for U937 cells. Cells were scraped and transferred to tubes where the lysate was incubated on ice for 15-20 min. The supernatants were transferred into clean tubes and the pellets discarded. Samples were then stored at -80˚C until the determination of protein concentrations in preparation for the ELISA experiment.

1.19.2 Determination of protein concentrations

The protein quantitative assay BCA (Pierce BCA Protein Assay Kit, including BCA reagent A, BCA reagent B and Albumin Standard Ampules (2 mg/mL), a detergent-compatible formulation based on bicinchoninic acid (BCA) for the colorimetric detection and quantitation of total protein) was used. An albumin standard solution of 10 mg/mL concentration was made from 10 mg albumin weighed and added to 1 mL extraction buffer. The stock solution was used to make dilutions at a working range of 20-2000 ug/mL using the microplate procedure from the supplier protocol (Table 1.19.1).

Table 1.19.1: Creation of BSA standards concentration samples to determine concentrations of unknown protein samples and to test efficacy of the BCA kit.

Albumin standard solution (µL)	Extraction buffer (µL)	Final diluted albumin (BSA) standards (µg/mL)
20	80	2000
15	85	1500
10	90	1000
7.5	92.5	750
5	95	500
2.5	97.5	250
1.25	98.75	125
0.25	99.75	25

A volume of 25 µL of each standard or unknown sample of was added in replicate microplate wells. The plate layout was as follows (Table 1.19.2,

Table 1.19.3):

Table 1.19.2: Plate layout the BSA standard concentrations to act as guidelines for the analysis of the concentrations of the unknown samples. Samples in green columns were diluted with extraction buffer and samples in purple columns were diluted with Tris buffer (100 mg/mL) to test this replacement for feasibility to be used in future projects.

2000	2000	2000		2000	2000	2000								
1500	1500	1500		1500	1500	1500								
1000	1000	1000		1000	1000	1000								
750	750	750		750	750	750								
500	500	500		500	500	500								
250	250	250		250	250	250								
125	125	125		125	125	125								
25	25	25		25	25	25								

Table 1.19.3: Plate layout of the unknown protein samples for concentration determination, in triplicate. Blue indicates the SH-SY5Y cell line and pink indicates the U937 cell line.

MO 1	MO 1	AcD 3	AcD 3	W137 + AcD 2	W137 + AcD 2		MO 1	MO 1	AcD 3	AcD 3	
MO 2	MO 2			W137 + AcD 3	W137 + AcD 3		MO 2	MO 2	W137 + AcD 1	W137 + AcD 1	
MO 3	MO 3						MO 3	MO 3	W137 + AcD 2	W137 + AcD 2	
W137 1	W137 1						W137 1	W137 1	W137 + AcD 3	W137 + AcD 3	
W137 2	W137 2						W137 2	W137 2			
W137 3	W137 3						W137 3	W137 3			
AcD 1	AcD 1						AcD 1	AcD 1			
AcD 2	AcD 2						AcD 2	AcD 2			

The working reagent was made using Reagent A (consisting of sodium carbonate, sodium bicarbonate, bicinchoninic acid and sodium tartrate in 0.1 M sodium hydroxide) and Reagent B (consisting of 4% cupric sulfate) in a 50:1 ratio and 200 µL was then added to each well. The plate was mixed by pipetting and slight shaking for 30 sec. Thereafter, the plate was covered and incubated at 37˚C for 30 min and thereafter cooled to room temperature and the absorbance measured at 562 nm using the spectrophotometer (Bio-Tek Instruments Inc., Vermont, USA).

A dilution series of a positive control sample was made using the Actinomycin D exposed extract samples of both cell lines. The sample tubes were each labelled as 1, with seven more tubes labelled 2 to 8 for each sample. Sample 1 was diluted to an upper concentration limit of the assay in incubation buffer. A half serial dilution was carried out by adding a volume of 150 uL of the incubation buffer to each tube

labelled 2 to 7. Thereafter, 150 uL from tube 1 was added to tube 2, then from 2 to 3 using fresh tip, mixing thoroughly with each transfer. The step was repeated for tubes 4 to 7. The incubation buffer was used as the zero standard, labelled tube 8. All reagents were room temperature when used. The p53 specific antibody was precoated into well plate strips included in the kit. A volume of 50 uL standard/sample/positive control dilution series/ negative control was pipetted into individual wells so that the p53 protein present would bind to the immobilized antibody. The plate was then sealed and covered for a two hour incubation period at room temperature and shaken lightly at 15 min intervals. The wells were aspirated and washed twice by decanting the contents from the wells and dispensing 300 uL wash buffer (prepared from 10x wash buffer and nanopure water) into the wells, washing by pipetting and removing the remaining buffer by aspiration and then inverting the plate to remove all excess liquid. A volume of 50 uL anti-p53 antibody Acetyl Lysine 382 detector antibody (prepared 10x detector antibody diluted with incubation buffer) was added to each well and the plate was sealed to incubate for 1 h at room temperature. The wells were then aspirated and washed twice as previously described. A volume of 50 uL HRP-conjugated label (prepared from 10x HRP label diluted with incubation buffer) specific for the detector antibody was pipetted into the wells then the plate was sealed for 1 hour incubation at room temperature. The wells were aspirated and washed twice. A volume of 100 uL of TMB substrate solution was added to the wells and the developing blue colour was recorded immediately through spectrophotometry with the elapsed time in proportion to amount of acetylated Lysine 382 of bound p53. The microplate reader was prepared at the following settings (Table 1.19.4):

Table 1.19.4: Settings of the micro-plate reader for spectrophotometry analyses of protein.

Mode	Kinetic
Wavelength	600 nm
Time	Up to 15 min (double cycle, totalling 30 min)
Interval	20 sec to 1 min (1 min intervals were chosen)
Shaking	Shake between readings

End-point results were analysed using Excel and Graphpad Prism 5.0 (GraphPad Software, Inc., CA, USA).

Statistical analysis of data

Statistical analysis of the data was done as prescribed by Mr C Janse van Rensburg of the Unit for Biostatistics at the Medical Research Council, Pretoria. Data was obtained from 3 independent experiments. Means are presented in bar charts, with error-bars referring to standard deviations. P-values, 0.05 were regarded as statistically significant and indicated by an * or number as indicated in the legends.

Qualitative studies: Microscopy

Morphological studies performed by means of fluorescent microscopy and light microscopy was conducted with a minimum of three representative images captured from each sample.

Quantitative studies: Spectrophotometry, flow cytometry and qRT-PCR

For the determination of the $IC_{50(SIRT1)}$, at least three biological replicates with three technical replicates for each biological replicate (n=3) were carried out with the relevant vehicle-treated controls. The $IC_{50(SIRT1)}$ values were calculated from the resulting sigmoidal dose–response curves using GraphPad Prism (158). For mechanistic studies, three treatment groups (vehicle-treated group, BRD4 inhibitor group (CC2 and CC6 individually treated) and sirtuin 1 inhibitor group (W137)), individually treated, were assessed respectively using an analysis of variance (ANOVA with 30 degrees of freedom). This translates to 3 technical and 3 biological replicates therefore resulting in a total of 9 experimental outcomes for each mechanistic study. The vehicle control was normalized to 100% and all comparisons were relative to the vehicle control in a percentage ratio. Data obtained from independent experiments was shown as the mean ± SD. Means were presented in bar charts mostly, with error-bars referring to standard deviations. P-values lower than 0.05 (<0.05) were regarded as statistically significant. All data captured was frequently monitored by the supervisor and co-supervisors.

Chapter 3: Results

Computer-Aided Drug Design

Potent pan SIRT1, 2 and 3 inhibitors with thieno carboximide moieties have previously been described (Figure 1.21.1A). Selectivity towards SIRT1 and SIRT2 could be achieved by changing the Y atom to a carbon and the Z atom to a nitrogen or vice versa (Figure 1.21.1A). The most potent and selective combination where Z is a nitrogen and Y a carbon atom and this configuration was then used and optimisation of the B moiety to further increase selectivity towards SIRT1 without losing inhibition activity.

Optimal activity was obtained with a nitrogen at position 6 (Figure 1.21.1A and B) and therefore various chemical moieties containing this feature were generated with Chemsketch. The SMILES annotations were converted to 3D structures using Open Babel 2.3.2 and balloon. Drug-likeness properties such as Lipinski and QED parameters were monitored with DruLiTo.

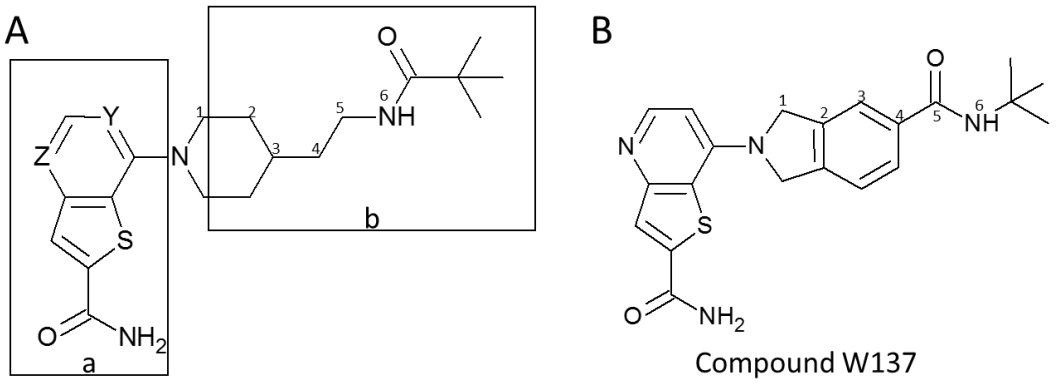

Figure 1.21.1: Structures of ligand 1NR from the 4jt8 protein structure from www.rcsb.org (A) and compound W137 (B). 1NR is a potent thieno carboximide pan SIRT 1, 2 and 3 inhibitor discovered by Disch *et al.* (2013) (159) .

Autodock Vina, rDOCK and Autodock docking suite software programs were used to perform *in silico* docking analysis of the ligands into the receptor pockets. The lowest energy conformation for each test structure from each docking suite was selected and the RMSD of the crystal pose and docked pose was calculated using the *match* module in Chimera(148). All the docking software reproduced the correct binding

pose (RMSD < 1.5) (Table 1.21.1) and predicted selectivity of W137 towards SIRT1 and 2 compared to SIRT3 (Table 1.21.1).

Table 1.21.1: Binding energies rDOCK, Autodock and Autodock Vina for W137 and the ligands 1NQ, 1NR and 1NS from the SIRT3 crystal structures 4JSR, 4JT8 and 4JT9 respectively.

	SIRT1			SIRT2			SIRT3		
Ligand	**rDOCK (kcalJ/mol)**	**Autodock (kcal/mol)**	**Vina (kcal/mol)**	**rDOCK**	**Autodock**	**Vina**	**rDOCK (RMSD)**	**Autodock (RMSD)**	**Vina (RMSD)**
4JSR (1NQ)	-19.89	-12.48	-10.6	-83.005	-12.49	-10.4	-19.35 (1.239)	-12.29 (1.45)	-10.4 (1.17)
4JT8 (1NR)	-15.72	-11.53	10.3	-66.501	-11.72	-10.2	-14.49 (0.925)	-11.56 (0.99)	-10.3 (0.701)
4JT9 (1NS)	-14.33	-11.86	-9.5	-59.678	-11.45	-9.2	-13.62 (0.524))	-11.26 (1.03)	-9.4 (0.516)
W137	-13.65	-11.57	-10.6	-59.018	-11.67	-10.6	-12.81	-11.12	-10.3

The binding pose of W137 predicts several conserved interactions among thieno pyridine-6-carboxamides including hydrogen bond interactions with the carboxamide group of W137 and the backbone nitrogen hydrogens of ILE347 and PHE273, and the sidechain oxygen of ASP348 (Figure 1.21.2). A hydrophobic interaction between PHE273 and the pyridine moiety of W137 is predicted (Figure 1.21.2). Additionally, hydrophobic interactions are predicted between PHE297 and the 2,3-dihydro-isoindole moiety and VAL412 and the trimethyl group of W137 (Figure 1.21.2).

To conclude, this section only describes the design of compound W137. While two other newly designed BRD4 inhibitor compounds, CC2 and CC6 were also tested in this study, only W137 showed positive cytotoxic results for the two model cell lines tested (see Section 3.4). Compound CC6 showed good activity against breast cancer cells as part of a different study and will be reported elsewhere.

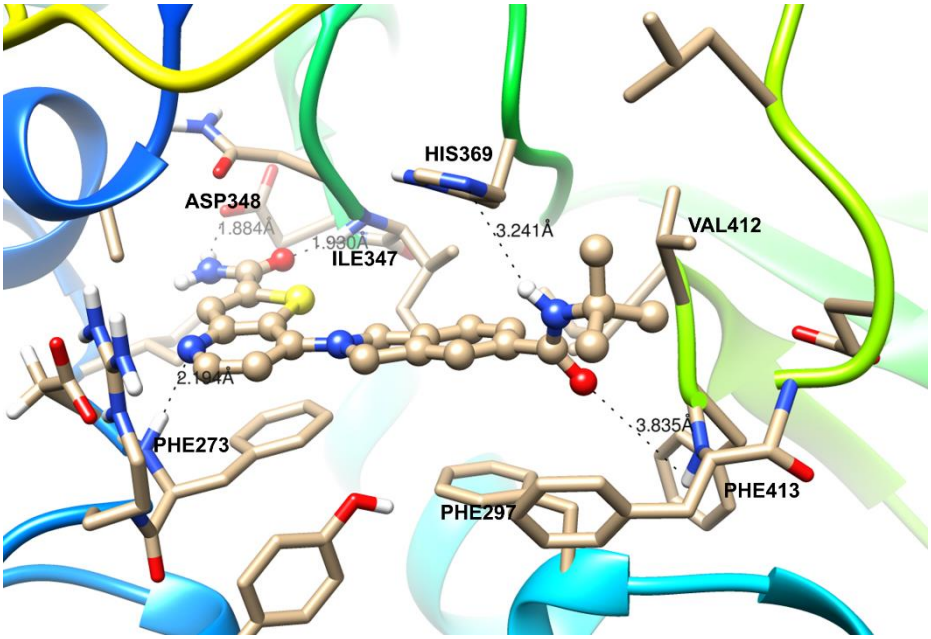

Figure 1.21.2: Binding pose of W137 bound to SIRT1 as predicted by Autodock. The carboxamide group of W137 interacts with the backbone nitrogen hydrogens of ILE347 and PHE273, and the sidechain oxygen of ASP348. The pyridine moiety of W137 shows a hydrophobic interaction with PHE273 and the 2,3-dihydro-isoindole moiety interacts with PHE297 are predicted between PHE297 and VAL412 and the trimethyl group of W137.

Ligand-binding analysis of W137

Biochemical assays against SIRT1, SIRT2 and SIRT3 were conducted by Reaction Biology Corp. (Malvern, PA) in order to determine whether W137 inhibits SIRT1, SIRT2 and SIRT3 deacetylase activity. The positive control for inhibition of SIRT1 and 2, Suramin, inhibited SIRT1 and SIRT2 activity to 50% at 2.86 μM and 15.97 μM respectively. The positive control for SIRT3, nicotinamide, inhibited SIRT3 50% at 53.67 μM. The $IC_{50(SIRT1)}$ concentrations for W137 against SIRT1, SIRT2 and SIRT3 was 14.8 μM and 14.6 μM and >100 μM respectively (Figure 1.22.1). W137 is >6x more selective against SIRT1 and SIRT2 activity compared to SIRT3.

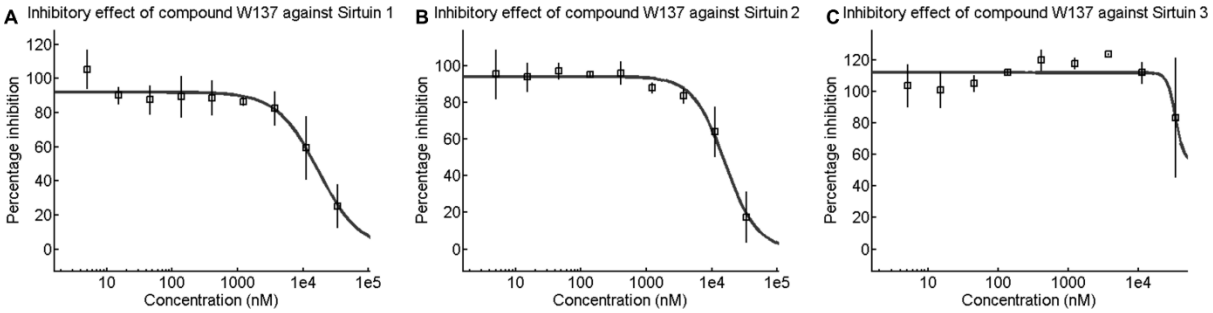

Figure 1.22.1: Inhibitory effect of W137 on SIRT1, 2 and 3 deacetylase activity. The **$IC_{50(SIRT1)}$** concentrations for W137 against SIRT1, SIRT2 and SIRT3 was 14.8 μM and 14.6 μM and >100 μM respectively.

Cell growth studies

Cellular quantification was determined by employing crystal violet as a DNA stain and spectrophotometry to measure staining for the fixed monolayer SH-SY5Y cells and flow cytometry counting for the suspended U937 cells. Cell numbers were expressed as a percentage of the negative control in order to determine the anti-proliferative effects of the W137 compound on SH-SY5Y and U937 cells.

For quantification of the SH-SY5Y cell line, crystal violet assay and spectrophotometry was applied. Cell counting was done using the MUSE Cell Analyser (Merck, Darmstadt, Germany) for accurate and reproducible quantification of cell numbers and viability measurements for cell seeding. The MUSE Cell Analyser system applies the principles of propidium iodide cell penetrance, clearly distinguishing between live and dead cells by means of viability percentages and live cell counting.

Quantification of the fixed cell monolayer was determined using crystal violet as a DNA stain and spectrophotometry for quantitative analysis. Staining cell nuclei of fixed cells with crystal violet allows for rapid, accurate and reproducible quantification of cell numbers in cultures inoculated and exposed in 96-well plates. Dye absorbance measured at 570 nm corresponds to cell numbers, providing closely accurate readings (background values subtracted, etc.). According to Berry *et al.* (1996), crystal violet staining of samples containing an abnormally high proportion (>30%) of stationary cells (as in the case of the SH-SY5Y cell line), results in more accurate concentration readings than trypan blue.

For the U937 cell line, flow cytometry was applied for quantification. The concentrations of the individual compounds required to inhibit 50% of the cell population ($IC_{50(SIRT1)}$) when compared to control samples was calculated as described by the National Cancer Institute in order to determine the growth inhibition induced by the inhibitors for the two cell lines. The following formula was applied:

$$IC50 = \frac{Number\ of\ cells\ exposed\ to\ test\ condition}{Number\ of\ cells\ exposed\ to\ vehicle - treated\ condition} * 100 = 50$$

The inhibitory effects of the SIRT1 inhibitor W137 as well as the BRD4 inhibitors CC2 and CC6 were assessed to determine the $IC_{50(SIRT1)}$ values on both the U937 and the SH-SY5Y cell lines, as indicated (Table 1.23.1).

The W137 compound showed the highest efficacy in reducing cell proliferation in both the SH-SY5Y and the U937 cell line in a dose-dependent manner. The lowest concentrations of the W137 compound is seen to inhibit 50% of the exposed cells (SIRT1-IC_{50}) compared to negative control samples (Figure 1.23.1, Table 1.23.1). A statistical significant difference (Student's t-test: p-value < 0.05) in growth inhibition was observed between the cell lines at all the concentrations 6.25 µM, 12.5 µM, 25 µM, 50 µM and 100 µM (Figure 1.23.1). The compound reduced cell proliferation at all tested concentrations in both the U937 and the SH-SY5Y cell lines. A 65% reduction in U937 cell viability/proliferation was observed at 100 µM, 58% reduction at 50 µM, 50% reduction at 25 µM, 17% reduction at 12,5 µM and 9% reduction at 6,25 µM when compared to medium-only negative control cells. The $IC_{50(SIRT1)}$ of W137 for the U937 cell line is calculated to be 25 µM. For the SH-SY5Y cell line, a 71% reduction in cell viability/proliferation was observed at 100 µM, 69% reduction at 50 µM, 55% reduction at 25 µM, 16% reduction at 12,5 µM and 14% reduction at 6,25 µM when compared to medium-only negative control cells. The $IC_{50(SIRT1)}$ of W137 for the SH-SY5Y cell line is calculated to be 20 µM (Figure 1.23.1).

The BRD4 inhibitors were the least active and only showed at above 25 uM. This is in contrast to the activity of the BRD4 inhibitor compound showing activity below 10 uM against MDA-MB-231 breast cancer cells (160). This indicates that the cell llines are more sensitive to the Sirtuin inhibitors compared to the tested BRD4 inhibitors. It was decided to focus on the SIRT inhibitor, W137, in order to determine it mechanism of action.

Table 1.23.1: The $IC_{50(SIRT1)}$ values obtained for the compounds tested on the U937 and SH-SY5Y cell lines respectively.

Compounds	$IC_{50(SIRT1)}$
SIRT1 inhibitors	
W137	SH-SY5Y: 20 µM
	U937: 25 µM
BRD4 Inhibitors	
CC2	SH-SY5Y: >100 µM (n/a)
	U937: 25 µM
CC6	SH-SY5Y: 30 µM
	U937: 90 µM (n/a)

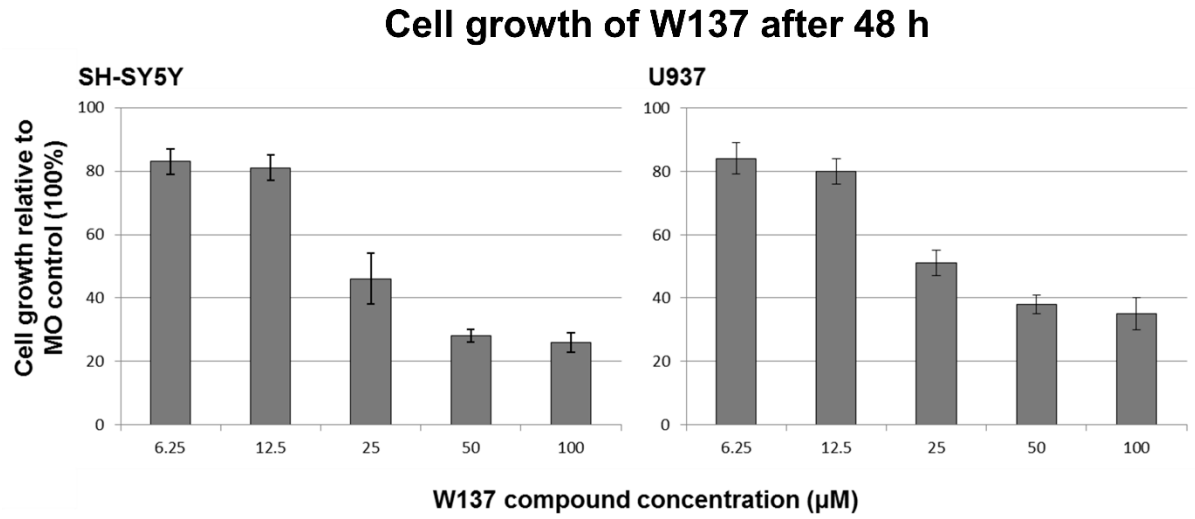

Figure 1.23.1: Column charts of the one-way ANOVA data acquired through Graphpad Prism 5.0 software (GraphPad Software, Inc., CA, USA). The tested concentrations of the W137 compound is shown and the cell viability as a percentage of the control (100%). The SH-SY5Y cell line chart illustrates a column reaching an $IC_{50(SIRT1)}$ value of 20 µM (calculated) and the U937 cell line chart illustrates a column reaching an $IC_{50(SIRT1)}$ value of 25 µM (calculated).

Qualitative analyses: Morphology studies

1.24.1 Fluorescent microscopy – Polarization-optical differential interference contrast and staining for apoptosis, autophagy and oncosis detection

Fluorescent microscopy was employed to differentiate between the observable condition of viable, apoptotic, autophagic and possibly oncotic cells. A triple fluorescent dye staining method, consisting of acridine orange, Hoechst 33345 (blue) and propidium iodide (red) fluorescent dyes, were applied in this technique and the Zeiss Axiovert 25 inverted microscope was used. Negative (medium only) control and positive control (Actinomycin D exposed) as well as W137-exposed SH-SY5Y cells were subjected to this study. This technique was performed only on the SH-SY5Y cell line as the cells form an adhesive monolayer which is easily viewed microscope and practical to stain, while the U937 cells are free floating cells (Figure 1.24.1).

Medium only negative control cells showed normal nuclear morphology and residual acridine orange staining (Figure 1.24.1 A and B). W137-treated and especially Actinomycin D exposed positive control SH-SY5Y cells presented with an increased acridine orange staining (Figure 1.24.1 C - F) indicating increased acidity as a possible result of lysosome formation during autophagy and/or loss of cell membrane integrity during apoptosis. Higher cell density was observed in the medium only negative control sample (Figure 3.5 A) when compared to the compound exposed samples (Figure 1.24.1 C). There was an increase of apoptotic bodies detected through propidium iodide staining in the compound exposed cell sample (Figure 1.24.1 D and E) compared to the negative medium only control (Figure 1.24.1B). The decrease in cell numbers reflects the ability of the compound to inhibit cell growth and the presence of apoptotic bodies show that the compound induces cell death. However, the increase in apoptotic bodies is insignificant and this may indicate that the cell membranes are largely intact, that oncotic processes may be absent and that compound induced cell inhibition and/or death may be through different mechanisms. When cell size and membrane structure of exposed cells (Figure 1.24.1 D) were compared to the negative control (Figure 1.24.1 B), the exposed cells appeared smaller in size possibly due to loss of membrane structure (Figure 1.24.1 D). The medium only sample cells appeared structurally intact. The Actinomycin D

exposed positive control cells (Figure 1.24.1 F) indicated higher levels of acridine orange staining compared to the test compound exposed cells (Figure 1.24.1 D and E).

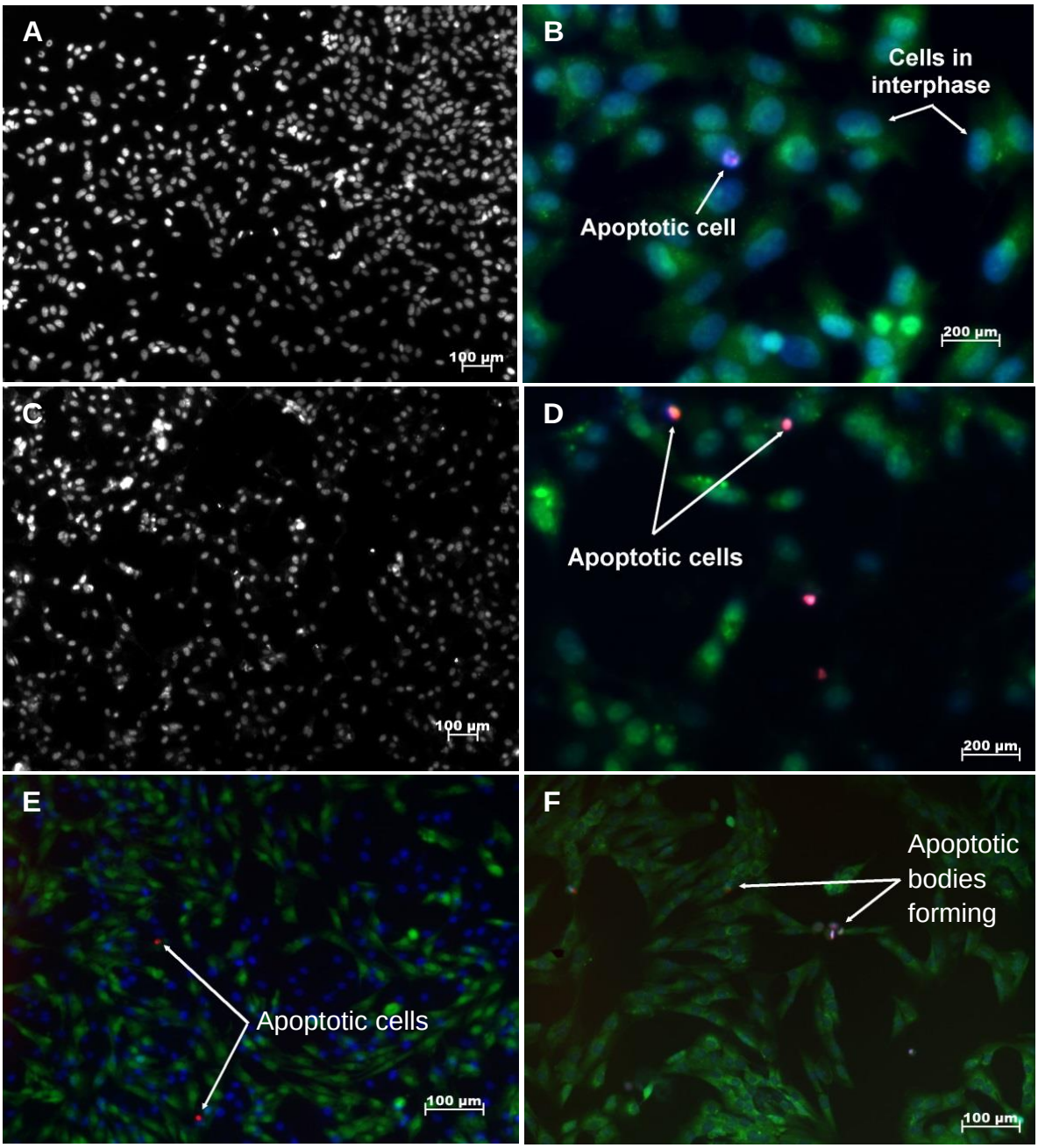

Figure 1.24.1: The morphological effect of The SIRT1 inhibitor compound W137 on SH-SY5Y cells. Hoechst 33324 (blue), acridine orange (148) and propidium iodide (red) staining and fluorescent microscopy imaging of the SH-SY5Y cells are shown. The medium-only negative control cells (A and B) showed normal nuclear morphology and residual acridine orange staining and appeared to be structurally intact. High cell density is also observed, indicating cellular proliferation. The W137-exposed cells (C-E) indicated loss of membrane structure, increased apoptosis, hightened acidity and lowered cell density. The Actinomycin D –exposed positive control cells had a high affinity

for acridine orange staining, possibly indicating acidic vacuole and/or lysosome formation during autophagy and increased apoptosis when compared to healthy, unexposed control cells (A and B).

Quantitative analyses: Flow cytometry studies

1.25.1 Cell cycle progression after 24 h and 48 h

The relative DNA content of cells was quantified as an indication of the percentage cells in various stages of the cell cycle in order to determine the effect that the W137 compound has on the progression of cells through the stages of the cell cycle. Staining was done using fluorescent propidium iodide dye and flow cytometry analysis.

For the SH-SY5Y cells after 24 h the analysis of medium only samples indicated an average sub-G_1 phase population percentage of 9.16%, compared to Actinomycin D-exposed samples indicating 4.97% and W137-exposed samples indicating 13.52% (Figure 1.25.1 A-C and G, Table 1.25.1). The results were not statistically significant. A statistically significant increase in the G_1-phase of Actinomycin D-exposed control (73.42%) was observed compared to the medium only control (52.02%) (Figure 1.25.1 A, B and G, Table 1.25.1). A statistically significant decrease in the G_2/M-phase for Actinomycin D-exposed cells (17%) was observed compared to the medium only control (24.04%) (Figure 1.25.1 A, B and G, Table 1.25.1). A statistically significant decrease in the S-phase for Actinomycin D-exposed cells (8.37%) was observed compared to the medium only control (14.78%) (Figure 1.25.1 A, B and G, Table 1.25.1). For the W137-exposed samples only a statistically significant decrease in the G_2/M phase (18.24%) was observed after 24 h compared to the medium only control (24.04%) (Figure 1.25.1 A, C and G, Table 1.25.1).

After 48 h a statistically significant increase in the sub-G_1 phase was observed for both the Actinomycin D- (7.92%) and W137-exposed (15.76%) samples compared to the medium only control (4.2%) (Figure 1.25.1 D-F and H, Table 1.25.1). The G_2/M phase population of medium only samples averaged 18.68%, compared to Actinomycin D-exposed samples at 19.28% (not statistically significant) and W137-exposed samples at 15.07% (statistically significant) (Figure 1.25.1 D-F and H, Table 1.25.1).

When comparing analyses of Actinomycin D-exposed samples after 24 h to Actinomycin D-exposed samples after 48 h, results were statistically significant for all phases (Figure 1.25.1 B and E, Table 1.25.1). When comparing W137-exposed

samples after 24 h to W137-exposed samples after 48 h, the S-phase decreased statistically significantly from 24 h (13.93%) to 48 h (8.19%) and the G_2/M -phase decreased statistically significantly from 24 h (18.24%) to 48 h (15.07%) (Figure 1.25.1 C and F, Table 1.25.1).

For the U937 cells after 24 h there was a statistically significant increase in the sub-G_1 population of Actinomycin D- (59.1%) and W137-exposed (21.6%) samples compared to the medium only control (2.82%) (Figure 1.25.2 A-C and G, Table 1.25.2). In Actinomycin D-exposed cells there was a corresponding statistically significant decrease in the G_1-, S- and G_2/M phase (36%, 4.2%, 1.17%) compared to the medium only control (61.09%, 13.72%, 22.44%) (Figure 1.25.2 A, B and G, Table 1.25.2). In the W137-exposed a statistically significant decrease in the S- and G_2/M phase (8.80%, 5.79%) compared to the medium only control (13.72%, 22.44%) (Figure 1.25.2 A, C and G, Table 1.25.2).

After 48 h there was a statistically significant increase in the sub-G_1 population of Actinomycin D- (65.47%) and W137-exposed (41.02%) samples compared to the medium only control (10.51%) (Figure 1.25.2 D-F and H, Table 1.25.2). A corresponding statistically significant decrease in the G_1-, S- and G_2/M phase was observed for the Actinomycin D-exposed cells (31.76%, 3.01%, 0.19%) and W137-exposed cells (44.63%, 8.8%, 5.79%) compared to the medium only control (56.02%, 17.43%, 16.05%) (Figure 1.25.2 D-F and H, Table 1.25.2).

When comparing analyses of Actinomycin D-exposed samples after 24 h to Actinomycin D-exposed samples after 48 h, results were statistically significant for all phases (Figure 1.25.2 B, E and H, Table 1.25.2). When comparing W137-exposed samples after 24 h to W137-exposed samples after 48 h, there was statistically significant increase in the sub-G_1 phase from 24 h (24.6%) to 48 h (41.0%) and the G_1 and G_2/M -phases decreased statistically significantly from 24 h (57.77%, 12.15%) to 48 h (44.63%, 5.79%) (Figure 1.25.2 C, F and H, Table 1.25.2).

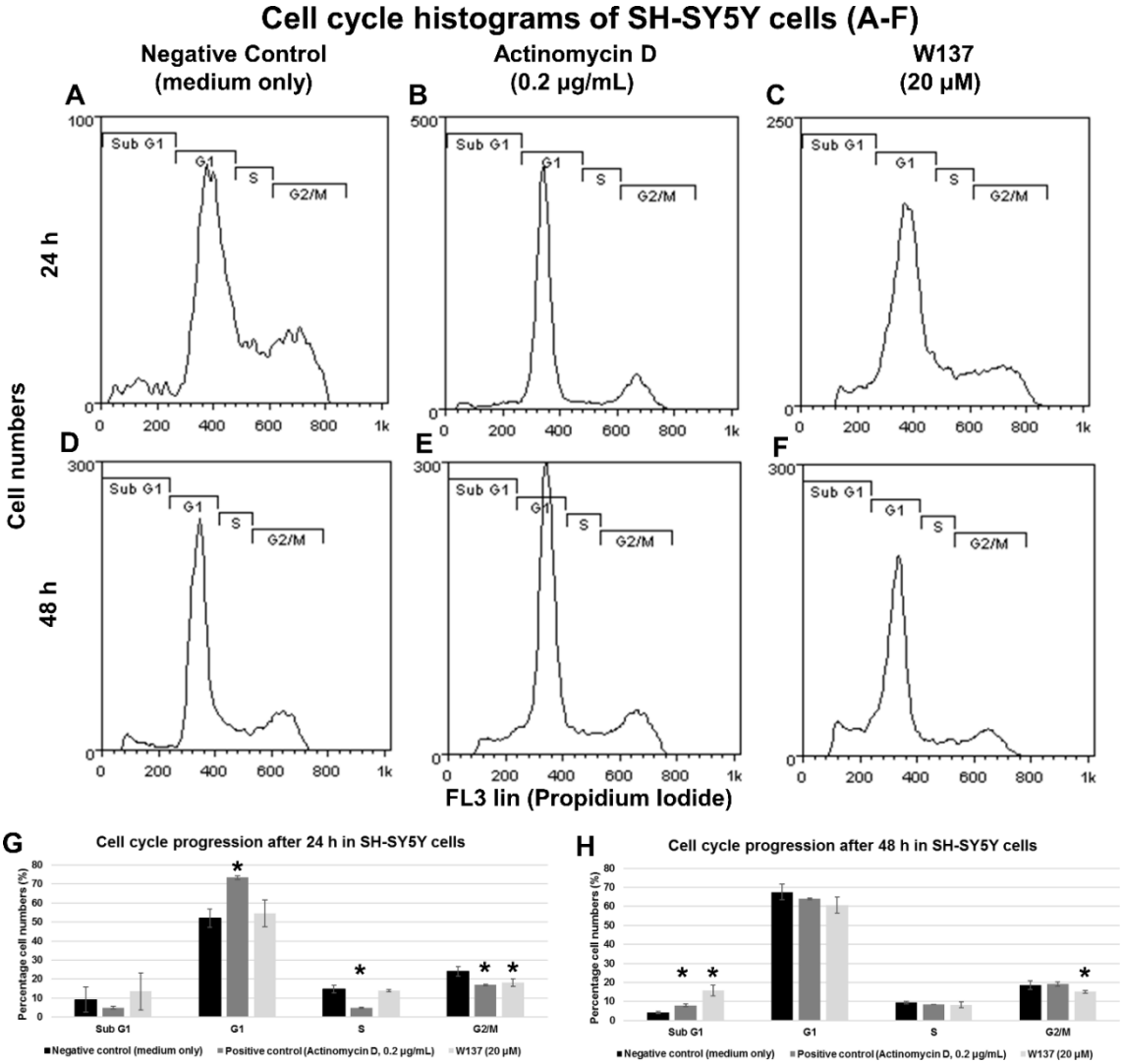

Figure 1.25.1: Histograms (A-F) and graphic representation (G-H) of cell cycle progression of SH-SY5Y cells after 24 h and 48 h exposure. A statistically significant increase in the sub-G_1 population in Actinomycin D- and W137-exposed cells after 48 h but not 24 h was observed, suggesting apoptosis was induced after 48 h. * indicates p-value < 0.05 between MO and test samples after 24 h and 48 h respectively.

Table 1.25.1: Measurement of relative DNA content of negative MO, positive Actinomycin D-exposed controls and W137-exposed SH-SY5Y cells after 24 h and 48 h exposure as an indication of cells in various stages of the cell cycle.

	Negative control (medium only)				Positive control (Actinomycin D, 0.2 µg/mL)				W137 (20 µM)			
	24 h		48 h		24 h		48 h		24 h		48 h	
	Mean	STDEV	Mean	STDEV	Mean	STDEV	Mean	STDEV	Mean	STDEV	Mean	STDEV
Sub G1	9.16	6.6	4.20	0.6	4.97	0.7	7.92 ‡	0.7	13.52	9.7	15.76 *	2.9
G1	52.02	4.9	67.48 †	4.1	73.42 *	1.0	63.95 †	0.5	54.63	7.1	60.59	4.2
S	14.78	2.0	9.42 †	0.8	4.92 *	0.2	8.37 ‡	0.1	13.93	0.5	8.19 †	1.5
G2/M	24.04	2.6	18.68	2.2	17 *	0.4	19.28 †	1.1	18.24 *	2.0	15.07 ‡	0.6

* indicates p-value < 0.05 between MO and test samples after 24 h and 48 h respectively. † indicates p-value < 0.05 between 24 h and 48 h samples.

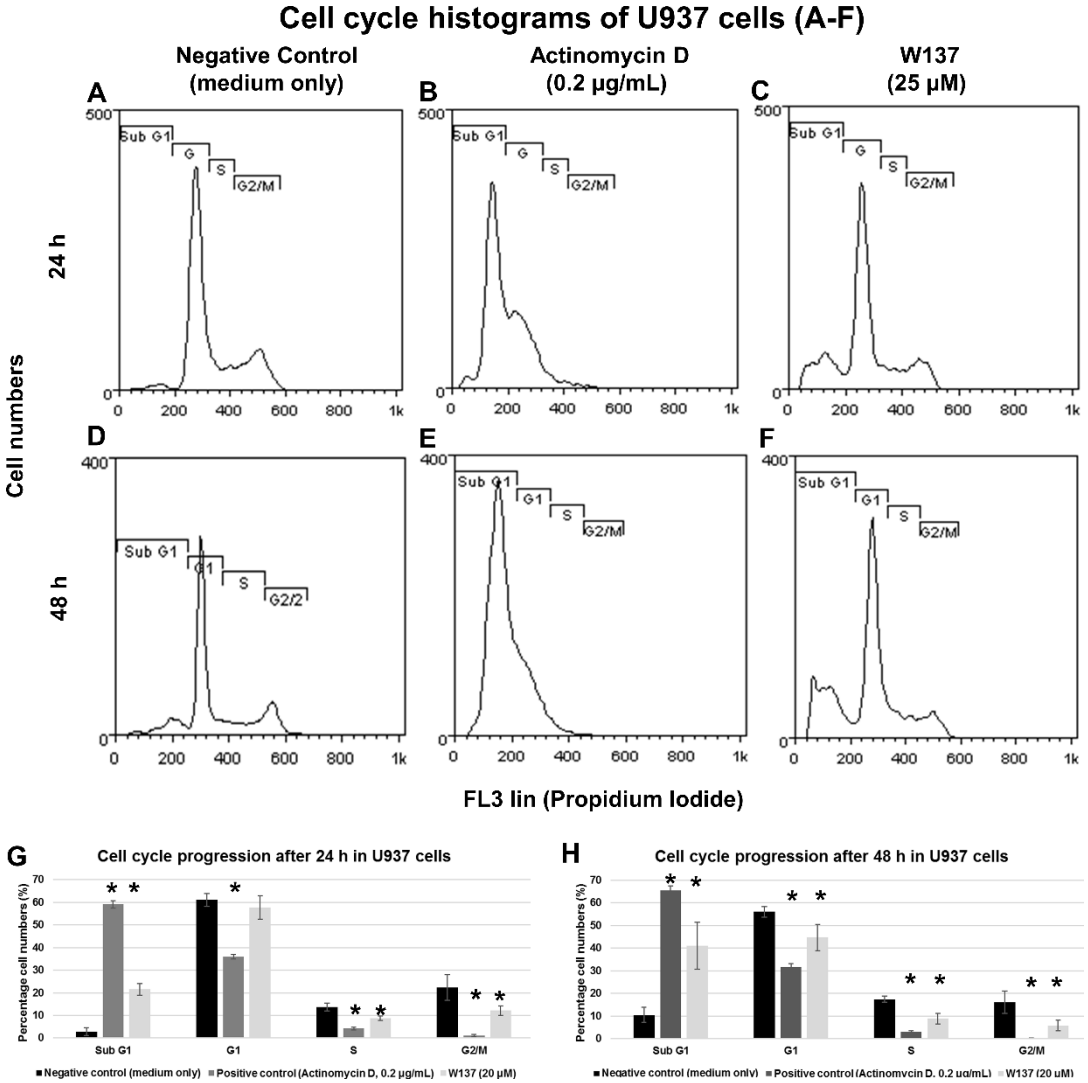

Figure 1.25.2: Histograms (A-F) and graphic representation (G-H) of cell cycle progression of U937 cells after 24 h and 48 h exposure. A statistically significant increase in the sub-G_1 population in Actinomycin D- and W137-exposed cells after 24 h and 48 h was observed, suggesting apoptosis was induced. * indicates p-value < 0.05 between MO and test samples after 24 h and 48 h respectively.

Table 1.25.2: Measurement of relative DNA content of negative MO, positive Actinomycin D-exposed controls and W137-exposed U937 cells after 24 h and 48 h exposure as an indication of cells in various stages of the cell cycle.

	Negative control (medium only)				Positive control (Actinomycin D, 0.2 µg/mL)				W137 (25 µM)			
	24 h		48 h		24 h		48 h		24 h		48 h	
	Mean	STDEV	Mean	STDEV	Mean	STDEV	Mean	STDEV	Mean	STDEV	Mean	STDEV
Sub G1	2.82 †	1.7	10.51	3.3	59.10*	1.6	65.47 *†	2.0	21.60*	2.6	41.02 *†	10.3
G1	61.09	2.9	56.02	2.4	36.00*	0.9	31.76 *†	1.5	57.77*	5.1	44.63 *†	5.7
S	13.72	1.7	17.43	1.3	4.20 *	0.6	3.01 *†	0.5	8.76 *	1.1	8.80 *	2.4
G2/M	22.44	5.7	16.05	5.0	1.17 *	0.4	0.19 *†	0.1	12.15*	2.1	5.79 *†	2.4

* indicates p-value < 0.05 between MO and test samples after 24 h and 48 h respectively† indicates p-value < 0.05 between 24 h and 48 h samples.

1.25.2 Apoptosis detection analysis: Phosphatidylserine externalization after 24 h and 48 h

Translocation of the membrane phosphatidyl serine externalization (PS) from the inner to the outer leaflet of the plasma membrane is normally one of the earliest indications of apoptosis and was measured with fluorescein isothiocyanate conjugated Annexin V. Annexin V is a 35-36 kDa, Ca^{2+}-dependent, phospholipid binding protein with a high affinity for PS. Propidium iodide is used to distinguish between necrotic and apoptotic cells. Late apoptotic cells are Annexin V- and propidium iodide positive. Dot plots of the results indicated the various stages (viable, early apoptotic, late apoptotic and necrotic) and the percentage of cells undergoing the specific stage.

For the SH-SY5Y cells following 24 h and 48 h exposure to the W137 compound (20 µM), a statistically significant increase in early apoptotic (29.33%, 35.4%), late apoptotic (7.29%, 11.28%) and necrotic (1.16%, 4.13%) cells when compared to negative control (medium only) for early apoptotic (17.93%, 18.06%), late apoptotic (0.78%, 0.19%) and necrotic (0.01%, 0.04%) cells (Figure 1.25.3 A and C, D and F, G, H, Table 1.25.3). A corresponding statistically significant decrease was observed in the viable cells of W137-exposed cells (62.23%, 41.82%) compared to the medium only control (81.29%, 81.72%) (Figure 1.25.3 A and C, D and F, G, H, Table 1.25.3).

The positive control, Actinomycin D-exposed cells showed a statistically significant decrease in viable cells for 24 h and 48 h (41.14%, 31.07%) compared to the medium only control (81.29%, 81.72%) (Figure 1.25.3 A and B, D and E, G, H, Table 1.25.3). Exposure to Actinomycin D for 24 h and 48 h resulted in a statistically significant increase in early apoptotic (53.2%, 28.51%), late apoptotic (5.38%,

26.9%) and necrotic (0.29%, 13.59%) cells when compared to negative control (medium only) for early apoptotic (17.93%, 18.06%), late apoptotic (0.78%, 0.19%) and necrotic (0.01%, 0.04%) cells (Figure 1.25.3 A and B, D and E, G, H, Table 1.25.3).

When comparing cell death of Actinomycin D-exposed SH-SY5Y samples after 24 h to Actinomycin D-exposed samples after 48 h, there was a statistically significant decrease in viable cells from 24 h (41.14%) to 48 h (31.07%) and early apoptotic cells from 24 h (53.2%)(p-value < 0.0001) to 48 h (28.51%) (Figure 1.25.3 B and E, G, H, Table 1.25.3). There was a corresponding statistically significant increase in late apoptotic cells from 24 h (5.38%) to 48 h (26.9%) and necrotic cells from 24 h (0.29%) to 48 h (13.59%) (Figure 1.25.3 B and E, G, H, Table 1.25.3). For the W137-exposed samples after 24 h to 48 h, there was a statistically significant decrease in viable cells from 24 h (62.23%) to 48 h (41.82%) (Figure 1.25.3 C and F, G, H, Table 1.25.3). There was a statistically significant increase in late apoptotic cells from 24 h (7.29%) to 48 h (11.28%) and necrotic cells from 24 h (1.16%) to 48 h (4.13%) for W137-exposed cells (Figure 1.25.3 C and F, G, H, Table 1.25.3).

For the U937 cells the positive control, Actinomycin D-exposed cells showed a statistically significant decrease in viable cells for 24 h and 48 h (41.03%, 49.63%) compared to the medium only control (77.39%, 93.1%) (Figure 1.25.4 A and B, D and E, G, H, Table 1.25.4). Exposure to Actinomycin D for 24 h resulted in a statistically significant increase in late apoptotic cells (25.33%) compared to negative control (3.74%) (Figure 1.25.4 A and B, G, Table 1.25.4). After 48 h exposure to Actinomycin D there was a statistically significant increase in early apoptotic (18.37%), late apoptotic (22.73%) and necrotic (9.26%) cells when compared to negative control (medium only) for early apoptotic (3.17%), late apoptotic (3.08%) and necrotic (0.01%) cells (Figure 1.25.4 D and E, H, Table 1.25.4).

The W137-exposed cells showed a statistically significant decrease in viable cells for 24 h and 48 h (42.97%, 55.75%) compared to the medium only control (77.39%, 93.10%) (Figure 1.25.4 A and C, D and F, G, H, Table 1.25.4). Exposure to W137 for 24 h resulted in a statistically significant increase in early apoptotic (52.93%) compared to the negative control (16.88%) (Figure 1.25.4 A and C, G, Table 1.25.4).

After 48 h exposure to W137 there was a statistically significant increase in late apoptotic cells (29.88%) compared to the negative control (3.08%) (Figure 1.25.4 D and F, H, Table 1.25.4).

When comparing cell death of W137-exposed U937 samples after 24 h to W137-exposed samples after 48 h, there was a statistically significant increase in viable cells from 24 h (42.97%) to 48 h (55.75%) and late apoptotic cells from 24 h (2.39%) to 48 h (29.88%) (Figure 1.25.4 C and F, G, H, Table 1.25.4). There was statistically significant decrease in early apoptotic cells from 24 h (52.93%) to 48 h (12.68%) (Figure 1.25.4 C and F, G, H, Table 1.25.4). For the Actinomycin D-exposed samples after 24 h to 48 h, there was no statistically significant difference (Figure 1.25.4 B and E, G, H, Table 1.25.4).

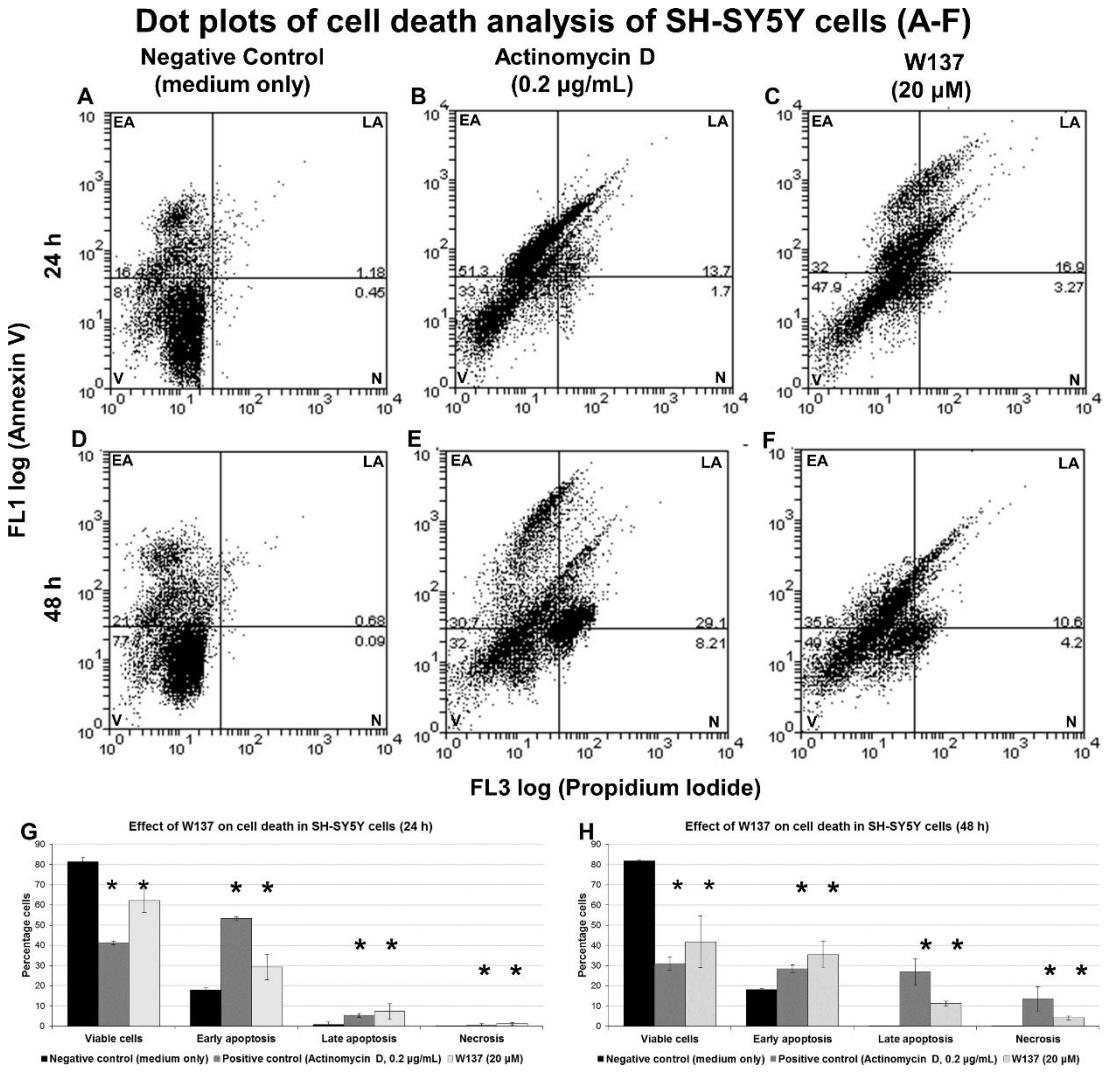

Figure 1.25.3: Dot plots (A-F) and graphical representation of cell death analyses for SH-SY5Y cells after 24 h and 48 h. A statistically significant increase in early and late apoptosis in W137- and Actinomycin D-exposed cells after 24 h and 48 h was observed. * indicates p-value < 0.05 between MO and test samples after 24 h and 48 h respectively.

Table 1.25.3: Measurement of phosphatidylserine externalization and membrane permeability of negative (media only) and positive (Actinomycin D) controls and W137-treated SH-SY5Y cells 24 h and 48 h after exposure as an indication of the percentages of cells in the various stages of cell death.

	Negative control (medium only)				Positive control (Actinomycin D, 0.2 µg/mL)				W137 (20 µM)			
	24 h		48 h		24 h		48 h		24 h		48 h	
	Mean	STDEV	Mean	STDEV	Mean	STDEV	Mean	STDEV	Mean	STDEV	Mean	STDEV
Viable cells	81.29	2.3	81.72	0.8	41.14*	4.4	31.07*†	3.3	62.23*	6.0	41.82*†	12.7
Early apoptosis	17.93	1.1	18.06	0.7	53.20*	6.5	28.51*†	1.9	29.33*	6.3	35.40*†	6.5
Late apoptosis	0.78	1.2	0.19	0.0	5.38*	3.3	26.90*†	6.7	7.29*	3.9	11.28*†	1.2
Necrosis	0.01	0.0	0.04	0.0	0.29*	0.2	13.59*†	6.05	1.16*	0.8	4.13*†	0.9

* indicates p-value < 0.05 between MO and test samples after 24 h and 48 h respectively. † indicates p-value < 0.05 between 24 h and 48 h samples.

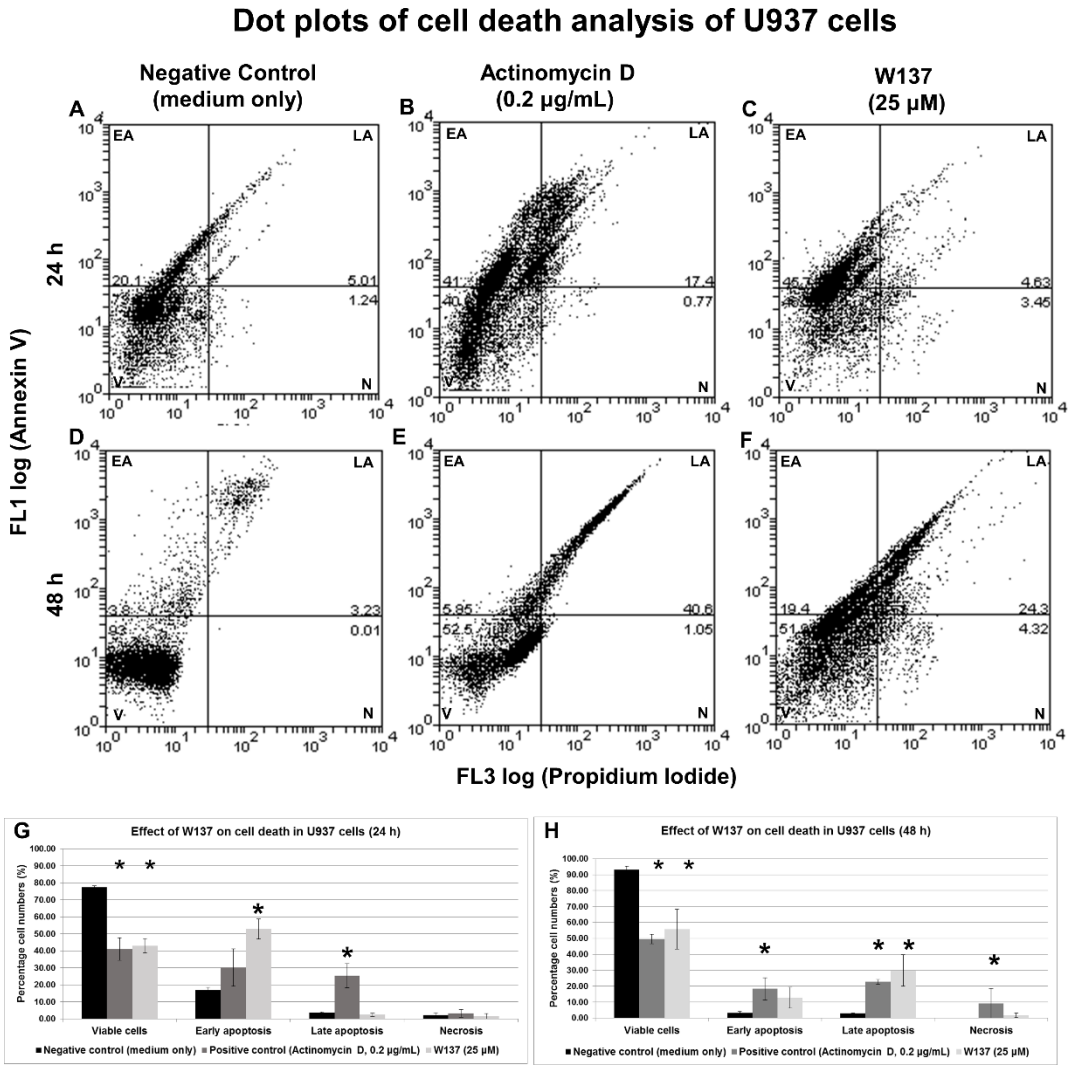

Figure 1.25.4: Dot plots (A-F) and graphical representation of cell death analyses for U937 cells after 24 h and 48 h. A statistically significant increase in early and late apoptosis in W137- and Actinomycin D-exposed cells after 24 h and 48 h was observed. * indicates p-value < 0.05 between MO and test samples after 24 h and 48 h respectively.

Table 1.25.4: Measurement of phosphatidylserine externalization and membrane permeability of negative (media only) and positive (Actinomycin D) controls and W137-treated SH-SY5Y cells 24 h and 48 h after exposure as an indication of the percentages of cells in the various stages of cell death.

	Negative control (medium only)				Positive control (Actinomycin D, 0.2 µg/mL)				W137 (25 µM)			
	24 h		48 h		24 h		48 h		24 h		48 h	
	Mean	STDEV	Mean	STDEV	Mean	STDEV	Mean	STDEV	Mean	STDEV	Mean	STDEV
Viable cells	77.39	0.9	93.10	2.2	41.03 *	6.7	49.63 *	3.0	42.97 *	4.1	55.75 *†	12.4
Early apoptosis	16.88	1.6	3.17 †	1.0	30.20	11.0	18.37 *†	7.0	52.93 *	5.9	12.68 †	6.6
Late apoptosis	3.74	0.4	3.08	0.0	25.33 *	7.1	22.73 *	1.6	2.39	0.9	29.88 *†	9.7
Necrosis	2.33	1.2	0.01†	0.0	3.14	2.3	9.26 *†	9.31	1.43	1.8	1.72	1.5

* indicates p-value < 0.05 between MO and test samples after 24 h and 48 h respectively† indicates p-value < 0.05 between 24 h and 48 h samples.

1.25.3 Cell death: Mitochondrial membrane depolarization

Cells in the process of undergoing apoptosis may have a loss of integrity in the membrane of the mitochondria. This change in the electrical gradient of the membrane may result in the release of pro-apoptotic proteins such as cytochrome c and in turn activate signals for the initiation of programmed cell death. Fluorescent probes applied for monitoring mitochondrial membrane potential are frequently used for the assessment of mitochondrial function, particularly in the determination of cell fate in molecular and biomedical research. Mitochondrial membrane depolarization was measured with the cell-permeant, lipophilic dye 3,3'-dihexyloxacarbocyanine iodide ($DiOC_6(3)$), which selectively stains the mitochondria of live cells when used at low concentrations. In apoptotic cells the dye is unable to aggregate as the mitochondrial membrane potential is lost, resulting in the dye being impounded in the cytoplasm, unbound, and therefore not fluorescing green.

The analysed fluorescence data that was obtained from each sample is illustrated through histograms. The M1 region indicates cells with decreased green fluorescence and thus cells with increased mitochondrial membrane depolarization, whereas the M2 region shows cells that had not undergone a change in membrane potential. For the M1 region of the W137-exposed SH-SY5Y (26.53%) and U937 (43.07%) cells there was a statistically significant increase after 48 h exposure compared to the medium only control for the SH-SY5Y (22.32%) and U937 (24.52%) cells (Figure 1.25.5). Actinomycin D-treated cells also showed an increase in the M1 region in the SH-SY5Y (51.26%) and U937 (52.39%) cells there was a statistically significant increase after 48 h exposure compared to the medium only control for the SH-SY5Y (22.32%) and U937 (24.52%) cells (Figure 1.25.5). The p values were less than 0.0001 (p-value < 0.0001), indicating highly significant results.

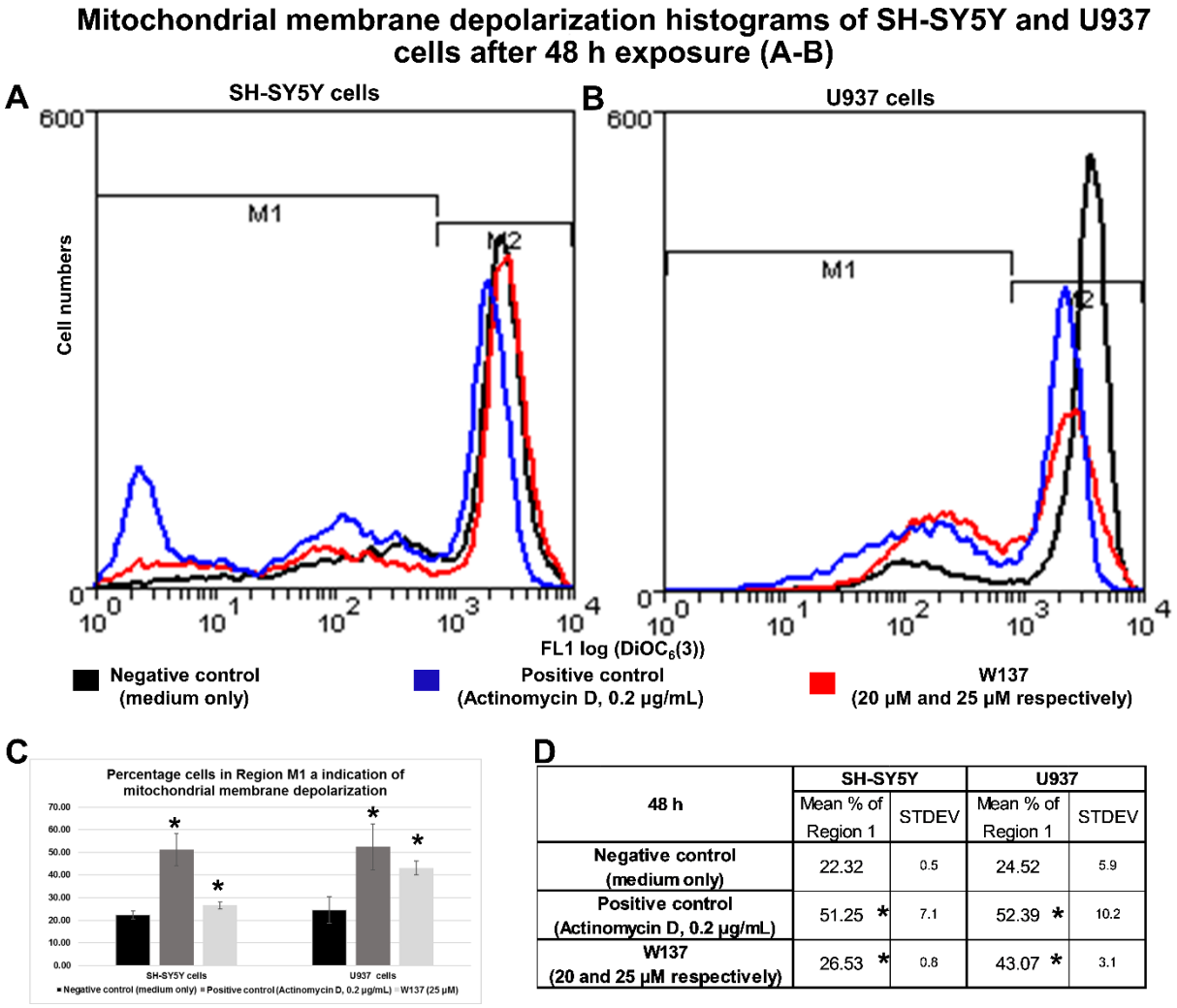

48 h	SH-SY5Y		U937	
	Mean % of Region 1	STDEV	Mean % of Region 1	STDEV
Negative control (medium only)	22.32	0.5	24.52	5.9
Positive control (Actinomycin D, 0.2 µg/mL)	51.25 *	7.1	52.39 *	10.2
W137 (20 and 25 µM respectively)	26.53 *	0.8	43.07 *	3.1

Figure 1.25.5: Histograms (A and B), graphical representation (C) and tabular representation (D) of the effect of Actinomycin D- and W137-exposed cells on membrane potential on SH-SY5Y cells and on U937 cells after 48 h exposure. A statistically significant difference in the M1 region was found in all the treated samples, indicating cell death via mitochondrial depolarization. * indicates p-value < 0.05 between MO and test samples after 24 h and 48 h respectively.

1.25.4 Reactive oxygen species formation: 2,7-dichlorofluorescein diacetate

To study the effects of oxidative stress, a non-fluorescent probe, 2′,7′-Dichlorodihydrofluorescein diacetate (H2DCFDA) was used to indicate the levels of hydrogen peroxide (H_2O_2) generated within the cells. H2DCFDA only becomes the highly fluorescent derivative 2,7-dichlorofluorescein (DCF) upon de-esterification and oxidation within the cells. Fluorescence was studied from results obtained from each sample and illustrated through dot plots and histograms. Analysis of the forward scatter (indication of size) and side scatter (indication cell granularity) dot plots identified two populations of cells (Region 1 and Region 2 respectively). Region 1 cells appear to be greater in cell size and smaller in terms of granularity.

In medium only SH-SY5Y cells the number of cells in Region 1 (74.2%) is statistically significant higher when compared Actinomycin D- (9.3%) and W137-exposed (34.3%) cells (Figure 1.25.6 A-D, F, Table 1.25.5). When looking at the Fl1 (green) fluorescence of Region 1 no difference was observed for the W137-exposed cells (91.3) compared to the medium only cells (96.1) and a statistically significant decrease was observed in the Actinomycin D-exposed cells (70.4) (Figure 1.25.6 A-D, G, Table 1.25.5). The Fl1 (green) fluorescence mean intensity of Region 2 of Actinomycin D-exposed cells (92.5) was statistically significantly greater compared to the medium only control (40) while the fluorescence mean intensity of W137-exposed cells (13.4) was statistically significantly smaller compared to the medium only control (40) (Figure 1.25.6 A-C, E, F, G, Table 1.25.5).

In medium only U937 cells the number of cells in Region 1 (87.6%) is statistically significant higher when compared Actinomycin D- (57%) and W137-exposed (71.2%) cells (Figure 1.25.7 A-D, F, Table 1.25.6). When looking at the Fl1 (green) fluorescence of Region 1 no difference was observed for the W137-exposed cells (561.8) compared to the medium only cells (499.4) and a statistically significant increase was observed in the Actinomycin D-exposed cells (717.5) (Figure 1.25.6 A-D, G, Table 1.25.6). The Fl1 (green) fluorescence mean intensity of Region 2 of Actinomycin D-exposed cells (432.7) was statistically significantly greater compared to the medium only control (251.4) while the fluorescence mean intensity of W137-

exposed cells (259.8) was not statistically significantly different compared to the medium only control (251.4) (Figure 1.25.6 A-C, E, F, G, Table 1.25.6).

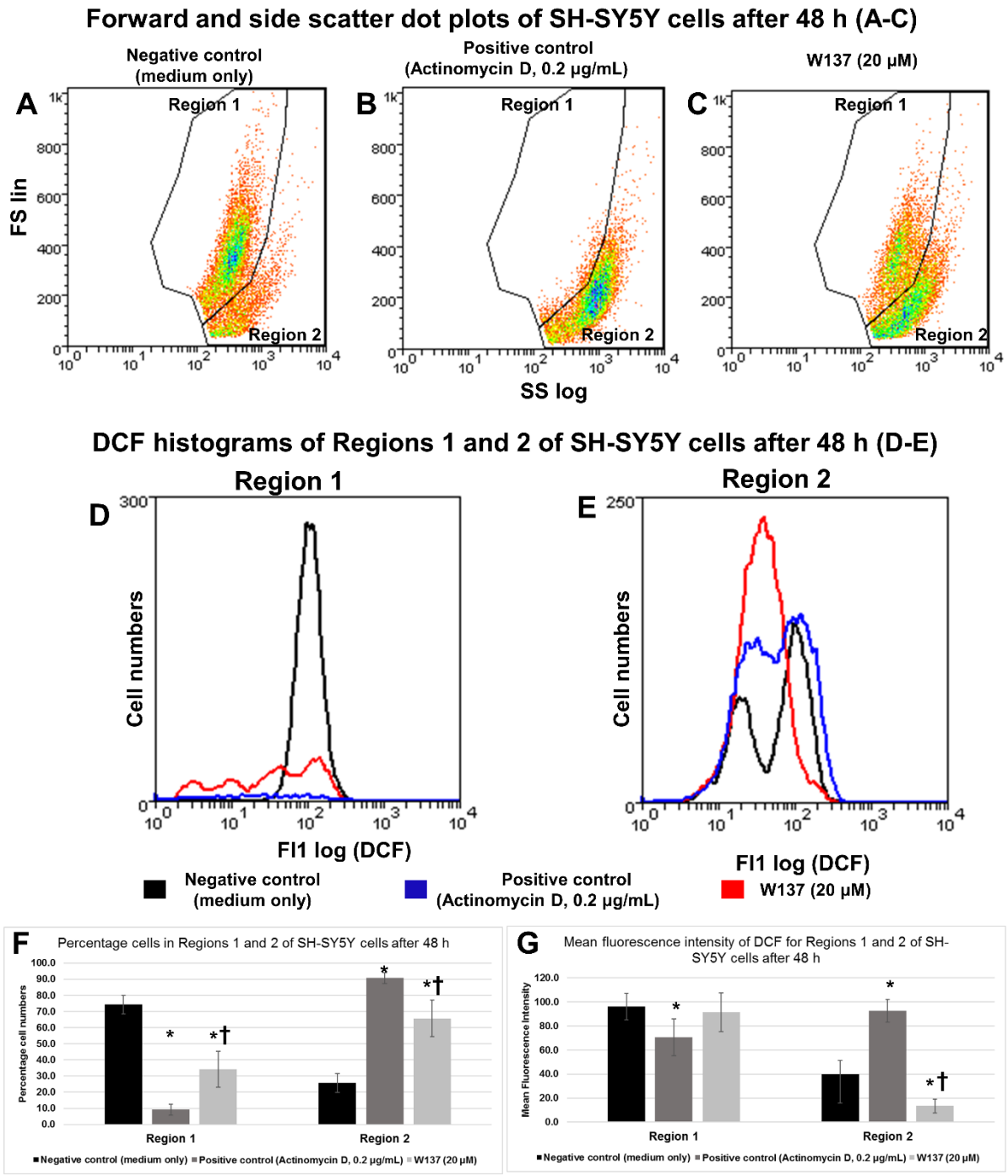

Figure 1.25.6: Dot plot (A-C), histogram (D and E) and graphical representation (F and G) of the effect of Actinomycin D- and W137-exposed cells on reactive oxygen species formation on SH-SY5Y cells after 48 h exposure.

Table 1.25.5: Measurement of reactive oxygen species of negative control (media only) and positive (Actinomycin D) controls and W137-treated SH-SY5Y cells 24 h and 48 h after exposure.

	Region 1				Region 2			
	Percentage cells	STDEV	Fluorescence Mean	STDEV	Percentage cells	STDEV	Fluorescence Mean	STDEV
Negative control (medium only)	74.2	5.8	96.1	11.1	25.8	5.8	40.0	24.1
Positive control (Actinomycin D, 0.2 µg/mL)	9.3 *	3.4	70.4 *	15.3	90.7 *	3.4	92.5 *	9.3
W137 (20 µM)	34.3 * †	11.2	91.3	16.2	65.7 * †	11.2	13.4 * †	5.7

* indicates p-value < 0.05 between MO and test samples after 24 h and 48 h respectively. † indicates p-value < 0.05 between 24 h and 48 h samples.

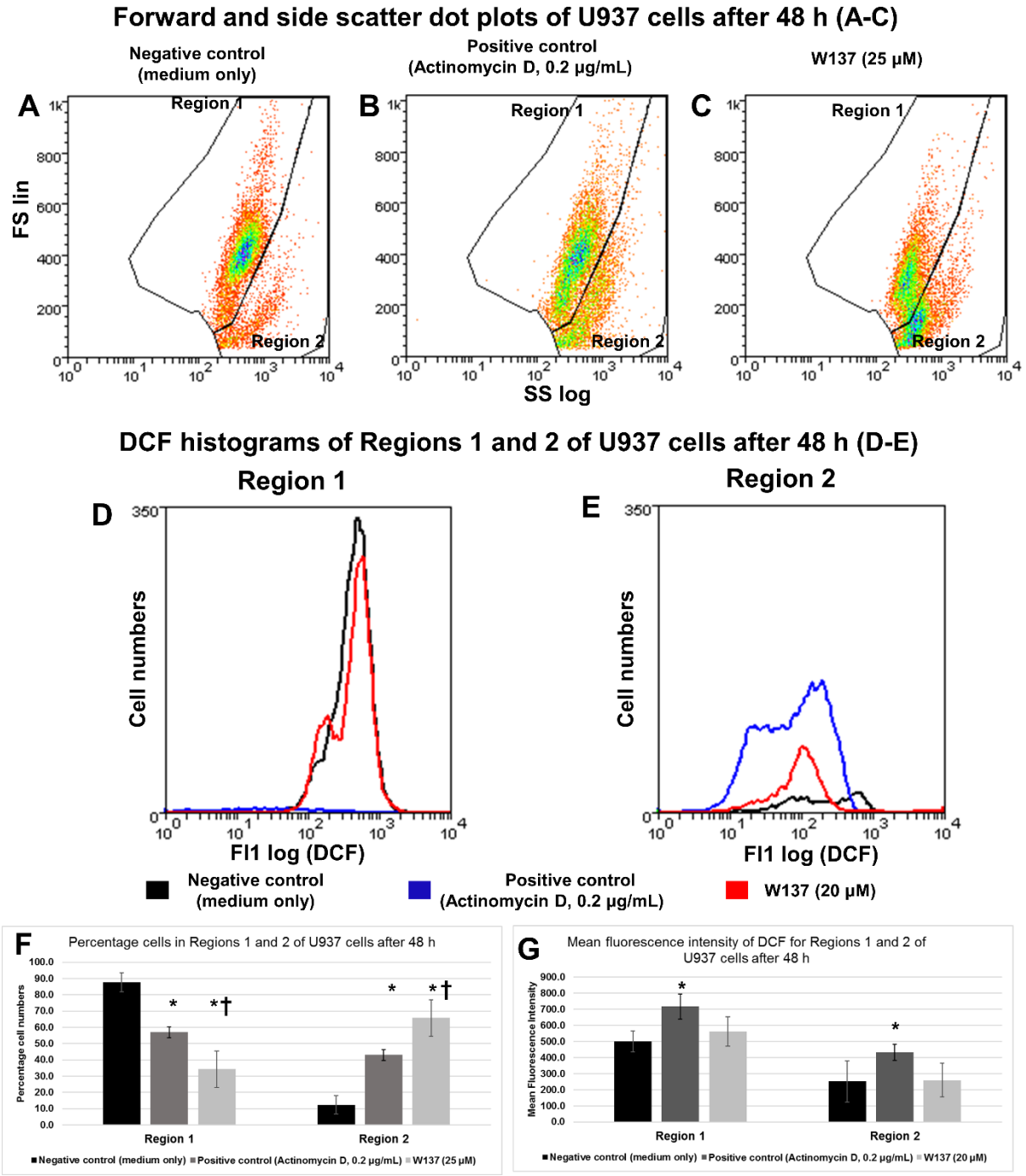

Figure 1.25.7: Dot plot (A-C), histogram (D and E) and graphical representation (F and G) of the effect of Actinomycin D- and W137-exposed cells on reactive oxygen species formation on SH-SY5Y cells after 48 h exposure. * indicates p-value < 0.05 between MO and test samples after 24 h and 48 h respectively. † indicates p-value < 0.05 between 24 h and 48 h samples.

Table 1.25.6: Measurement of reactive oxygen species of negative control (media only) and positive (Actinomycin D) controls and W137-treated SH-SY5Y and U937 cells 24 h and 48 h after exposure.

	Region 1				Region 2			
	Percentage cells	STDEV	Fluorescence Mean	STDEV	Percentage cells	STDEV	Fluorescence Mean	STDEV
Negative control (medium only)	87.6	4.3	499.4	64.4	12.4	4.3	251.4	127.3
Positive control (Actinomycin D, 0.2 µg/mL)	57.0 *	6.1	717.5 *	78.1	43.0 *	6.1	432.7 *	49.5
W137 (25 µM)	71.2 * †	4.9	561.8	92.7	28.8 * †	4.9	259.8	105.6

* indicates p-value < 0.05 between MO and test samples after 24 h and 48 h respectively. † indicates p-value < 0.05 between 24 h and 48 h samples.

Gene expression analysis: Reverse transcription quantitative polymerase chain reaction of *C-MYC* and *p53*

To quantify the expression of the selected genes and thereby determine the effect of the compound on gene expression, quantitative reverse transcription polymerase chain reaction (qRT-PCR) technique was applied. RNA was considered pure of organic contamination (e.g. ethanol or phenol) with a 260/230 ratio greater than 1.5 and pure of protein contamination with a 260/280 ratio greater than 2. Only pure total RNA was used for labelled cDNA synthesis. The *C-MYC* and *p53* genes were selected as the genes of interest and *GAPDH* was used as a housekeeping gene.

For SH-SY5Y cells the *C-MYC* gene after Actinomycin D exposure statistically significantly decreased expression after 24 h (0.03) compared to negative medium only control (Figure 1.26.1 A, C). W137 exposure decreased statistically significantly *C-MYC* expression after 24 h (0.41) compared to negative medium only control (Figure 1.26.1 A, C). For the *p53* gene, Actinomycin D exposure statistically significantly decreased expression after 24 h (0.13) and W137 exposure statistically significantly increased *p53* expression after 24 h (1.32) and after 48 h (2.82) compared to negative medium only control (Figure 1.26.1 B, C).For U937 cells the *C-MYC* gene after Actinomycin D exposure statistically significantly increased expression after 24 h (3.05) and 48 h (6.32) compared to negative medium only control (Figure 1.26.2 A, C). For the *p53* gene, Actinomycin D exposure statistically significantly increased expression after 24 h (4.13) and 48 h (7.45) and W137 exposure statistically significantly increased *p53* expression after 24 h (2.66) compared to negative medium only control (Figure 1.26.2 B, C).

A

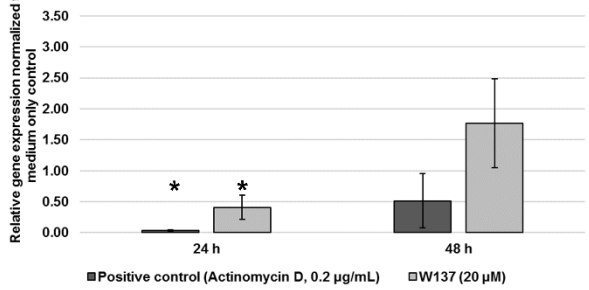

B

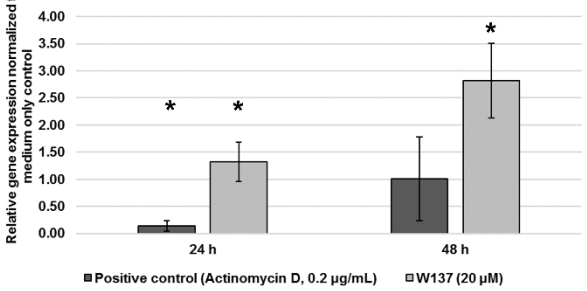

C

SH-SY5Y	*C-MYC*				*p53*			
	Positive control (Actinomycin D, 0.2 µg/mL)		W137 (20 µM)		Positive control (Actinomycin D, 0.2 µg/mL)		W137 (20 µM)	
	Average	STDEV	Average	STDEV	Average	STDEV	Average	STDEV
24 h	0.03 *	0.01	0.41 *	0.2	0.13 *	0.1	1.32 *	0.4
48 h	0.52	0.4	1.77	0.7	1.01	0.8	2.82 *	0.7

Figure 1.26.1: Graphic (A and B) and tabular (C) representation of the effects of W137 and Actinomycin D exposure on gene expression of *C-MYC* and *p53* in SH-SY5Y cells after 24 h and 48 h. For the *C-MYC* gene only statistically significant differences were observed after 24 h. P53 gene expression statistically significant increased for W137-exposed cells after 24 h and 48 h.* Indicates a *p-value* <0.05.

A

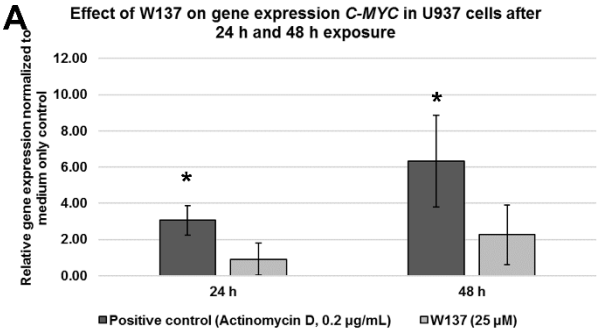

B

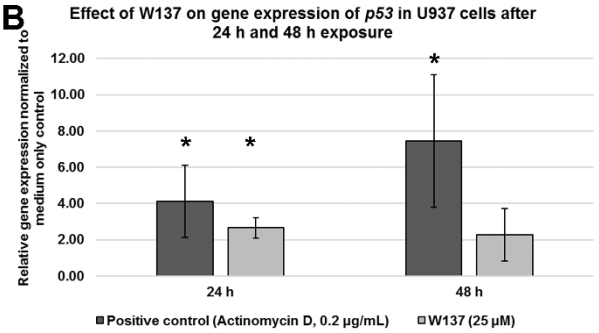

C

U937	*C-MYC*				*p53*			
	Positive control (Actinomycin D, 0.2 µg/mL)		W137 (25 µM)		Positive control (Actinomycin D, 0.2 µg/mL)		W137 (25 µM)	
	Average	STDEV	Average	STDEV	Average	STDEV	Average	STDEV
24h	3.05 *	0.8	0.91	0.9	4.13 *	2.0	2.66 *	0.6
48h	6.32 *	2.5	2.26	1.7	7.45 *	3.7	2.27	1.5

Figure 1.26.2: Graphic (A and B) and tabular (C) representation of the effects of W137 and Actinomycin D exposure on gene expression of *C-MYC* and *p53* in U937 cells after 24 h and 48 h. For the *C-MYC* gene, Actinomycin D exposure statistically significantly increased expression after 24 h and 48 h compared to negative medium only control. The *p53* gene expression increased statistically significantly after in response Actinomycin D exposure after 24 h and 48 h.* Indicates a *p-value* <0.05.

Protein quantification: Enzyme-Linked Immunosorbent Assay (ELISA) of the p53 protein

The Ab 133987 p53 Acetyl K382 Human ELISA kit, a sensitive *in vitro* enzyme-linked immunosorbent assay for the accurate and prompt quantification of acetylated Lysine 382 of the p53 protein in human cell lysates, was utilized for this experiment. After 48 h exposure to Actinomycin D and to W137 a statistically significant increase in acetylation of K382 was observed. No significant difference was seen in Actinomycin D and W137 combination results compared to the negative medium only control. In U937 cells 48 h exposure resulted in statistically significantly increased p53 acetylation only in Actinomycin D exposed samples.

Analyses of the SH-SY5Y cell line after 48 h indicated a statistically significant increase in expression of K382 acetylated p53 protein in Actinomycin D (1.17-fold) and W137 (1.12-fold) exposed samples after 48 h (Figure 1.27.1). No statistically significant difference was observed in Actinomycin D and W137 combination exposed samples when compared to the negative medium only control (Figure 1.27.1). U937 cells indicated a statistically significant increase in Actinomycin D (1.18-fold) exposed samples after 48 h (Figure 1.27.1).

A

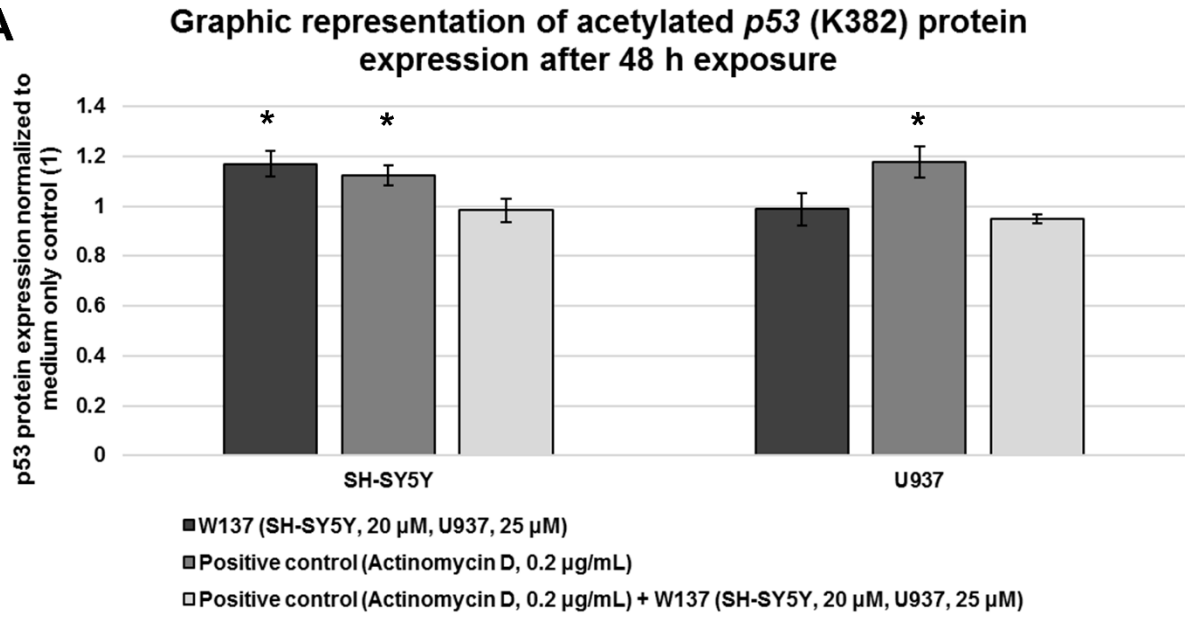

B

	Positive control (Actinomycin D, 0.2 µg/mL)		W137 (SH-SY5Y, 20 µM, U937, 25 µM)		Positive control (Actinomycin D, 0.2 µg/mL) + W137 (SH-SY5Y, 20 µM, U937, 25 µM)	
	Average	STDEV	Average	STDEV	Average	STDEV
SH-SY5Y	1.17 *	0.05	1.12 *	0.04	0.98	0.05
U937	0.99	0.06	1.18 *	0.06	0.95	0.02

Figure 1.27.1: Analyses of the expression of the acetylated (K382) p53 protein. In SH-SY5Y cells p53 acetylation increased statistically significantly after both 48 h exposure to W137 (1.17) and 48 h exposure to Actinomycin D (1.12). In U937 cells p53 acetylation increased statistically significantly after 48 h exposure to Actinomycin D (1.18). * Indicates a *p-value* <0.05 compared to the negative control.

Chapter 4: Discussion and Conclusion

In this novel study, the differential effects of the *in silico* designed sirtuin 1 inhibitor compound W137 on cellular growth and death was investigated in the neuroblastoma SH-SY5Y and acute myeloid leukemia U937 cell lines. This work is the first to study and report findings on the newly designed compound. The mechanistic effects of W137 was studied *in vitro* through the analysis of cell numbers, morphology, cell cycle progression, cell death through phosphatidylserine externalization and mitochondrial membrane depolarization, ROS species formation as well as the expression of crucial cancer-related genes and protein.

The diverse roles of sirtuin 1 (SIRT1), a class lll histone and non-histone deacetylase primarily located in the nucleus, seems to be dependent on cell- and tumour type as well as the nature of the maintenance genes in the genome (4). Sirtuins are thought to act as cancer suppressors in normal cells and cancer promoters in tumorigenic cells in most cases and play a significant role in the survival and drug resistance of tumor cells during chemotherapy, classifying them as high priority targets for new treatments (161). The newly designed SIRT1 inhibitory compound W137 was tested on two human cancer cell lines with the purpose of determining the value of SIRT1 as a future anti-cancer treatment for human cancers.

Through the inhibition of SIRT1, which functions by deactivating or down-regulating anti-cancer proteins through deacetylation, the regulation of cancer associated gene expression may be possible in SIRT1-advantaged cancers such as in neuroblastoma and acute myeloid leukemia. If the activity of the oncogene *C-MYC* and the tumour suppressor gene *p53* can be regulated by the admission of a SIRT1 inhibitory drug, cancer cell survival and death evasion as well as mutation and cancer metastasis could potentially be treated more effectively. The purpose of the study was first to determine the anti-proliferative effects of the newly designed compound on two human cancer cell lines and second to elucidate cell death inducing properties, possible mechanistic action and other *in vitro* effects of the compound. Positive findings motivate further research into SIRT1 as a cancer treatment target and the

development of new drugs using newly designed high-efficiency, low-toxicity compounds.

Recently, the potency, specificity, and cellular targets of the sirtuin 1 and 2 inhibitors Sirtinol, Salermide and the sirtuin 1 inhibitor EX527 were investigated on MCF-7 cells by Peck *et al.* (2010). The results indicated that Sirtinol and Salermide effectively induced cell death at concentrations of 25 uM and higher. EX527, a potent and selective SIRT1 inhibitor with SIRT1 $IC_{50(SIRT1)}$ of 38 nM, is more selective (200-500-fold) for SIRT1 than for SIRT2 or SIRT3 and has been shown to be a potent SIRT6 inhibitor (162). Peck *et al.* (2010) had found that EX527 has an $IC_{50(SIRT1)}$ of 50 uM against MCF-7 cells and exposure to EX527 caused cell cycle arrest at the G_1 phase of MCF-7 cells. Sirtinol and Salermide treatment resulted in the acetylation of p53, a target protein of SIRT1 and SIRT2 as well as the SIRT2 target tubulin in MCF-7 cells. It was found that using small interfering RNA to silence both SIRTs, but not SIRT1 and SIRT2 individually can induce cell death in MCF-7 cells. These findings indicate that EX527 is ineffective in inhibiting SIRT2 and that the tumour suppressor p53 is the mediator of Sirtinol and Salermide cytotoxic function. Solomon *et al.* (2006) had also observed that treating primary human mammary epithelial cells and other cell lines with EX527 dramatically increased acetylation at lysine 382 of p53 after various types of DNA damage (163). However, the work of Peck *et al.* (2010) indicated that the acetylation of p53 was also increased by the histone deacetylase (HDAC) class I/II inhibitor trichostatin A (TSA) (162). EX-527 and TSA acted synergistically to increase acetyl-p53 levels, confirming that p53 acetylation is regulated by both SIRT1 and HDACs. The combination of EX-527 and TSA had no further effect on cell viability and growth. These results show that, although SIRT1 deacetylates p53, this does not play a role in cell survival following DNA damage in certain cell lines and primary human mammary epithelial cells (162, 163). The results of these study conducted by Peck *et al.* (2010) and Solomon *et al.* (2006) therefore suggest that SIRT inhibitors require combined targeting of both SIRT1 and SIRT2 to induce p53 acetylation and cell death.

A recent study conducted by Dan *et al.* (2011) identified significant up-regulation of sirtuin 2 and nicotinamide phosphoribosyltransferase (NAMPT) (an enzyme that enables NAD+ biosynthesis in humans) in primary acute myeloid leukemia cells

compared to hematopoietic progenitor cells from healthy individuals. Results indicated that inhibition of either nicotinamide phosphoribosyltransferase or SIRT2 significantly reduced proliferation and induced apoptosis in human acute myeloid leukemia cell lines and primary blasts (109). The anti-leukemic effects of the inhibition of nicotinamide phosphoribosyltransferase or sirtuin 2, such as deacetylation of the protein kinase B/AKT, ultimately lead to ß-catenin inactivation through phosphorylation. These results provide strong evidence that SIRT2 (or the NAMPT enzyme, or both) participate in proliferation and survival of leukemic cells and suggests that the protein kinase B/AKT/ Glycogen synthase kinase-3 ß/ß-catenin pathway is a target for inhibition of nicotinamide phosphoribosyltransferase or sirtuin 2 of leukemia cell proliferation. This is another case illustrating the significance of SIRT2 in cancer cell survival and how targeting SIRT2 and SIRT1 for inhibition simultaneously might be the most effective route to take towards treating leukemia and other cancers (108, 109). The ligand-binding assay in the present study confirmed that W137 is a selective inhibitor of SIRT1 and SIRT2 compared to SIRT3 with inhibitory activity against SIRT1, 2 and 3 being 2.86 µM, 15.97 µM and 53.67 µM respectively.

On the SH-SY5Y cell line using crystal violet as a DNA stain revealed that the W137 compound inhibited cell proliferation to varying degrees depending on compound concentration. Flow cytometry was employed to study cell growth in the U937 cell line, revealing that cell inhibition also occurs in a concentration-dependent manner. An $IC_{50(SIRT1)}$ value of 20 µM was obtained for SH-SY5Y cells and a value of 25 µM for U937 cells after 48 h. This is more potent than the SIRT1 inhibitor EX527 (SIRT1 $IC_{50(SIRT1)}$=38 nM) with an $IC_{50(SIRT1)}$ of 50 uM against MCF-7 cells (162, 163). W137 show similar activity compared to the dual SIRT1 and 2 inhibitors Salermide and Sirtinol ($IC_{50(SIRT1)}$ of <25 µM against MCF-7 cells) indicating promising levels of inhibition and motivating further experimentation (162, 163).(162) The W137 compound therefore inhibited growth at slightly lower concentrations in the SH-SY5Y cell line than in the U937 cell line. These findings are the results of the first tests done on the anti-proliferative effects of the newly designed SIRT1 inhibitor compound W137 on two human cancer cell lines. These concentrations were used throughout subsequent experimentation.

Qualitative studies on cell morphology employing fluorescent microscopy and triple dye staining indicated a decrease in cell density and loss of cellular membrane integrity. The adhesive SH-SY5Y cell line indicated a slight increase in propidium iodide staining of DNA after 48 h exposure to the W137 compound, suggesting either necrosis and/or late stages of apoptosis. Flow cytometry and the DNA stain propidium iodide was employed to study the progression of the cell cycle after 24 and 48 h respectively. Following 24 h and 48 h exposure to the W137 compound, the SH-SY5Y cell line exhibited increased cell numbers in the sub-G_1 phase suggesting cell death is induced by W137. No significant cell cycle block in either the G_1 or G_2/M phase was observed for the W137-exposed cells, suggesting that the compound does not work by modulating the cycle in SH-SY5Y cells. Analysis of the U937 cell line after 24 h and 48 h exposure to W137 indicated also an increase in the sub-G_1 without any apparent block in any of the stages of the cell cycle. The efficacy of W137 does not vary significantly after 24 h exposure compared to 48 h exposure for the SH-SY5Y cell line in terms of causing an increase in the sub G_1 fraction, while an increase in compound efficacy seems to be observed after an extended exposure period (48 h) for the U937 cell line.

Flow cytometry using the DNA stain propidium iodide in conjunction with Annexin V was used to analyse cell death induced via apoptosis and/or necrosis. Following 24 h exposure to the W137 compound, the SH-SY5Y cells shifted towards an increase in early and late apoptosis with a slight increase in necrosis. This trend continued after 48 h exposure, confirming that cell death occurs via apoptosis in the SH-SY5Y cell line when exposed to W137. Analysis of the U937 cell line indicated the W137-exposed cell population shifted slightly towards early apoptosis after the 24 h. Following 48 h exposure, the W137-exposed cell population shifted slightly towards late apoptosis and necrosis, also confirming that cell death occurs via apoptosis in the U937 cell line when exposed to W137.

Cells in the process of undergoing apoptosis may undergo a loss of integrity in the membrane of the mitochondria due to change in the transport of electrons and the membrane polarity (164, 165). This change in the electrical gradient of the membrane may result in the release of pro-apoptotic proteins such as cytochrome *c* and in turn activate signals for the initiation of programmed cell death. Mitochondrial

dysfunction has been shown to participate in the induction of apoptosis and has even been suggested to be central to the apoptotic pathway. When the mitochondrial permeability transition pores are open it has been demonstrated to induce depolarization of the transmembrane potential ($\Delta\psi_m$), release of apoptogenic factors and loss of oxidative phosphorylation (164). Cell death was studied by means of mitochondrial membrane potential analyses through the application of flow cytometry and $DiOC_6(3)$ dye and indicated that a loss of membrane integrity did occur in both cell lines. SH-SY5Y and U937 cells exhibited increased mitochondrial membrane depolarization and therefore the intrinsic mitochondrial pathway as the likely means to achieve apoptosis. $DiOC_6(3)$ stains the mitochondria of live cells and not apoptotic cells due to its membrane permeability characteristics when used at low concentrations (166). SH-SY5Y and U937 cells indicated significant increase in cells with decreased green fluorescence and thus cells with loss of membrane polarity. Although this may be an early event in the apoptotic process in many systems, emerging data also suggests that this might not be the case in all models of apoptosis. The loss of mitochondrial membrane potential may not be an essential early requirement for apoptosis and in some cases may be a direct consequence of the apoptotic-signalling pathway (164). Furthermore, it has also been observed that loss of mitochondrial membrane potential may not be required for cytochrome *c* release, whereas release of apoptosis inducing factor (AIF) is dependent upon disruption of mitochondrial membrane potential early in the apoptotic pathway. Therefore, while dissipation of mitochondrial membrane potential is observed in W137-exposed cells further studies are needed to confirm whether this an early event in the apoptotic pathway or as a result of other upstream pro-apoptotic pathways being induced by W137 (164).

Chemically reactive species containing oxygen are crucial in many aspects of cell functionality and an increase or decrease to unhealthy levels of ROS can lead to molecular damage, decreased cell growth and/or apoptosis and disease acquisition (167-169). Levels of hydrogen peroxide (H_2O_2) generated within W137-exposed cells after the 48 h exposure time had elapsed was measured using DH2CF-DA and flow cytometry. Using front and side scatter plots, two populations (Region 1 and Region 2) of cells could be identified. More cells were observed to be in Region 1 in healthy, negative control cells compared to W137- and Actinomycin D-exposed cells,

suggesting this population represents healthy cells. When looking at Region 1, no statistically significant difference was observed in DCF fluorescence in W137-exposed SH-SY5Y and U937 cells. For Region 2, W137-exposed cells showed a statistically significant decrease in DCF-fluorescence SH-SY5Y cells but not U937 cells. This data suggests that ROS was not induced in response to W137 exposure after 48 h. This study was conducted after 48 h exposure and does not negate the possibility of ROS being induced at earlier stages and future studies will explore this possibility. For Actinomycin D a statistically significant increase in ROS compared to the negative control was observed in Region 2 in both cell lines after 48 h. This confirms results from other studies showing Actinomycin D induces ROS and is part of its mechanism in inducing cell death (170).

To study the effect of exposure to the W137 compound on the expression of the *p53* and *C-MYC* genes, both key factors in healthy and cancerous cells, the quantitative reverse transcriptase polymerase chain reaction (qRT-PCR) technique was employed. The quantity of high quality pure total RNA is, in some cases, an indication of the level of expression of the genes of interest. The SH-SY5Y cell line indicated a decrease in *C-MYC* levels upon Actinomycin D and W137 exposure after 24 h compared to negative medium only control, while expression of the *p53* gene was decreased after 24 h Actinomycin D exposure. Exposure to W137, however, increased *p53* expression after 24 h as well as 48 h. p53 is crucial in programming cells for death and probably induces SH-SY5Y cells to enter apoptosis. Increased *C-MYC* gene expression was observed in U937 cells after Actinomycin D exposure after 24 h 48 h. For the *p53* gene, Actinomycin D exposure increased expression after 24 h as well as 48 h. W137 exposure increased *p53* expression after 24 h indicating that apoptosis induction probably occurs upon increased *p53* activity. Repression of SIRT1 therefore possibly resulted in the activation or increased expression of the pro-apoptotic gene *p53*, possibly enhancing cancer cell susceptibility to death and repair mechanisms. MYC oncoproteins, which are commonly up-regulated in human cancers of different organ origins, exert oncogenic effects by modulating gene and protein expression.

The protein structures of N-MYC and C-MYC are stabilized by Aurora A, a mitotic kinase enzyme integral to healthy cell proliferation and degraded through the

ubiquitin proteolysis pathway. Liu *et al.* (2012) recently demonstrated that SIRT2 was up-regulated by N-MYC in neuroblastoma cells and that SIRT2 then enhanced N-MYC and C-MYC protein stability which promoted cancer cell proliferation. The NEDD4 protein, a ubiquitin-protein ligase, is directly repressed by SIRT2 through histone deacetylation. The NEDD4 molecule was found to directly bind to MYC proteins to be targeted for ubiquitination and degradation, and application of small-molecule SIRT2 inhibitors resulted in NEDD4 gene expression, reduced N-MYC and C-MYC protein expression and suppressed neuroblastoma cancer cell proliferation. Additionally, Aurora A expression was up-regulated by SIRT2 and therefore indirectly down-regulated with administration of small-molecule SIRT2 inhibitors. This newly discovered pathway appears to be critical to MYC oncoprotein stability and stresses the importance of research into potential SIRT2 inhibitors in the prevention and treatment of MYC-induced malignancies. The importance of SIRT2 in neuroblastoma proliferation, and possibly that of many more cancers, is stressed by the work of Liu *et al.* (2012), again illustrating the importance of future tests in combinational targeting of SIRT1 and SIRT2 (45, 106).

The ELISA technique for protein analysis was employed to test for change in p53 protein K382 acetylation and activity following 48 h exposure to W137. Gene expression data from the qRT-PCR experiments are a good indication of relative RNA levels within the cells but are not necessarily directly proportional to protein levels. The active, acetylated p53 protein is a crucial component in cell maintenance, damage detection and programmed cell death, and inhibition or down-regulation of p53 has been detected in many cancer types (1-3). Deacetylation of p53 by SIRT1 results in protein deactivation or down-regulation and therefore SIRT1 inhibition is expected to result in p53 being in the acetylated stage and active (4). Following 48 h exposure, analyses of the SH-SY5Y cells indicated a small but statistically significant increase in the expression of K382 acetylated p53 protein in Actinomycin D and W137 exposed cells. No significant difference was observed in Actinomycin D and W137 combination exposed samples when compared to the negative medium only control. U937 cells only indicated an increase in Actinomycin D exposed samples after 48 h while no significant effects was observed in W137-exposed cells, suggesting the possibility of a different mechanism of achieving cell death than increased p53 protein activity. The variable results of the U937 cell line and the SH-

SY5Y cell line obtained this experiment and others may indicate cell line specificity and a variation of efficacy of the compound and the possibility of future anti-cancer drugs with varying mechanisms of action on different cancer types.

In conclusion, the novel dual SIRT1 and 2 inhibitor W137 inhibited cell proliferation in both the U937 and SH-SY5Y cell lines in a dose-dependent manner through the inhibition of cell growth and the induction of cell death *in vitro*. The $IC_{50(SIRT1)}$ values obtained for the compound as tested on the two cell lines were comparable to other well-known SIRT 1 and 2 inhibitors and low enough to merit further experimentation. The two cell lines exhibited different reactions to the compound in some experiments but similar reactions in others, motivating the importance of further study into the cell line specificity and mechanistic variation of W137. Induction of cell death through apoptosis was confirmed via cell cycle, Annexin V and mitochondrial membrane permeability studies using flow cytometry. The results obtained for the SH-SY5Y cell line was consistent over the 24 h and 48 h exposure periods, with the W137-exposed cell population shifted towards late apoptosis and necrosis and a percentage of cells still viable. The confirmation of these results by that obtained from the fluorescent microscopy study leads to the conclusion that apoptosis is the most likely cause of cell death for this cell line but that necrotic activity plays a role as well. This is a mechanism of autolysis with greater risk to nearby healthy cells through damage caused by leaking of products of cell death and initiating an inflammatory response in the patient and is therefore not the preferred route to inducing cell death in cancer cells.

With a large percentage of U937 cells still viable after 24 h exposure to the compound, a postponed mechanism of cell death is expected (highest level of lethality reached after 48 h, not 24 h). Following 48 h exposure, the W137-exposed cell population had shifted slightly towards late apoptosis and necrosis. A different mechanism may also explain the low $IC_{50(SIRT1)}$ values obtained with high percentages of cells still testing viable after exposure. The results confirmed apoptosis as being the most probably mechanism of cell death. The presence of autophagy was not tested in this cell death study and may be an informative future step in determining the mechanism of cell death induced by the compound, as autophagy is often induced by common chemotherapeutic drugs (162, 163) and

acridine orange staining observed through fluorescent microscopy might indicate autophagic cell death.

Understanding of *in vitro* molecular mechanisms of SIRT1 and how this is influenced by molecular inhibition enables researchers to focus on affected cellular mechanisms and to subsequently evaluate the W137 compound as a possible candidate for use in anticancer therapy. Several questions regarding the action mechanism of W137 and its basis for differential effects on non-tumorigenic cells remain unanswered. The current study contributes to the unravelling of the *in vitro* molecular mechanisms associated with and influenced by SIRT1 and SRT2 providing a basis for further research on this multi-functional cellular component and its diverse role in disease regulation. The W137 compound could potentially be an effective component in a drug against more than one type of cancer.

References

1. Kruse J-P, Gu W. Modes of p53 regulation. Cell. 2009;137(4):609-22.

2. Huang M-J, Cheng Y-c, Liu C-R, Lin S, Liu HE. A small-molecule c-Myc inhibitor, 10058-F4, induces cell-cycle arrest, apoptosis, and myeloid differentiation of human acute myeloid leukemia. Experimental hematology. 2006;34(11):1480-9.

3. Brodeur GM, Seeger RC, Schwab M, Varmus HE, Bishop JM. Amplification of N-myc in untreated human neuroblastomas correlates with advanced disease stage. Science. 1984;224(4653):1121-4.

4. Yi J, Luo J. SIRT1 and p53, effect on cancer, senescence and beyond. Biochimica et Biophysica Acta (BBA)-Proteins and Proteomics. 2010;1804(8):1684-9.

5. Dranitsaris G, Truter I, Lubbe MS, Amir E, Evans W. Advances in cancer therapeutics and patient access to new drugs. Pharmacoeconomics. 2011;29(3):213-24.

6. Hanahan D, Weinberg RA. The hallmarks of cancer. Cell. 2000;100(1):57-70.

7. Ferreira D, Adega F, Chaves R. The importance of cancer cell Lines as in vitro models in cancer methylome analysis and anticancer drugs testing: INTECH Open Access Publisher; 2013.

8. Döhner H, Weisdorf DJ, Bloomfield CD. Acute myeloid leukemia. N Engl J Med. 2015;373(12):1136-52.

9. Jemal A, Bray F, Center MM, Ferlay J, Ward E, Forman D. Global cancer statistics. CA: a cancer journal for clinicians. 2011;61(2):69-90.

10. Estey E, Hartmut D. Acute myeloid leukaemia. Lancet. 2006;368:1894-907.

11. Stone RM, O'Donnell MR, Sekeres MA. Acute Myeloid Leukemia. Hematology 2004;117:98-117.

12. Joshua L, Butera JN. Acute myelogenous leukemia. Experimental Hematology. 2009;37:649-58.

13. Herrmann H, Blatt K, Shi J, Gleixner KV, Cerny-Reiterer S, Müllauer L, et al. Small-molecule inhibition of BRD4 as a new potent approach to eliminate leukemic stem- and progenitor cells in acute myeloid leukemia (AML). Oncotarget. 2012;3(12).

14. Acute myeloid leukemia: National Cancer Institute; 2006 [Available from: http://www.seer.cancer.gov/statfacts/html/amyl.htm?statfacts_page=amyl.html&x=15&y=17.

15. Esteve J, Parker L, Roy P, Herrmann F, Duffy S, Frappaz D, et al. Is neuroblastoma screening evaluation needed and feasible? British journal of cancer. 1995;71(6):1125.

16. Yang B, Reynolds CP. Tirapazamine cytotoxicity for neuroblastoma is p53 dependent. Clinical cancer research. 2005;11(7):2774-80.

17. Wang Y, Zhou BP. Epithelial-Mesenchymal Transition—A Hallmark of Breast Cancer Metastasis. Cancer Hallmarks. 2013;1(1):38-49.

18. Berdasco M, Esteller M. Aberrant epigenetic landscape in cancer: how cellular identity goes awry. Developmental cell. 2010;19(5):698-711.

19. Jackson SP, Bartek J. The DNA-damage response in human biology and disease. Nature. 2009;461(7267):1071-8.

20. DeNardo DG, Andreu P, Coussens LM. Interactions between lymphocytes and myeloid cells regulate pro-versus anti-tumor immunity. Cancer and Metastasis Reviews. 2010;29(2):309-16.

21. Jiang BH, Liu LZ. PI3K/PTEN signaling in angiogenesis and tumorigenesis. Advances in cancer research. 2009;102:19-65.

22. Hugo H, Ackland ML, Blick T, Lawrence MG, Clements JA, Williams ED, et al. Epithelial—mesenchymal and mesenchymal—epithelial transitions in carcinoma progression. Journal of cellular physiology. 2007;213(2):374-83.

23. Yang J, Weinberg RA. Epithelial-mesenchymal transition: at the crossroads of development and tumor metastasis. Developmental cell. 2008;14(6):818-29.

24. Maxwell PH, Wiesener MS, Chang G-W, Clifford SC, Vaux EC, Cockman ME, et al. The tumour suppressor protein VHL targets hypoxia-inducible factors for oxygen-dependent proteolysis. Nature. 1999;399(6733):271.

25. McDonnell TJ, Korsmeyer SJ. Progression from lymphoid hyperplasia to high-grade malignant lymphoma in mice transgenic for the t (14; 18). Nature. 1991;349(6306):254.

26. Folkman J, Kalluri R. Cancer without disease. Nature. 2004;427(6977):787-.

27. Azam F, Mehta S, Harris AL. Mechanisms of resistance to antiangiogenesis therapy. European Journal of cancer. 2010;46(8):1323-32.

28. Ebos JM, Lee CR, Kerbel RS. Tumor and host-mediated pathways of resistance and disease progression in response to antiangiogenic therapy. Clinical Cancer Research. 2009;15(16):5020-5.

29. Ellis LM, Reardon DA. Cancer: The nuances of therapy. Nature. 2009;458(7236):290-2.

30. Medema RH, Bos JL. The role of p21ras in receptor tyrosine kinase signaling. Critical reviews in oncogenesis. 1993;4(6):615-61.

31. Saha J. Novel Chemotherapeutic Agents Against Inflammation and Carcinogenesis. 2004.

32. Hartwell LH, Kastan MB. Cell cycle control and cancer. Science. 1994;266:1821-7.

33. Israels ED, Israels LG. The Cell Cycle. STEM CELLS. 2001;19(1):88-91.

34. Latchman DS. Gene Control. New York: Garland Science, Taylor and Francis Group; 2010.

35. Bates S, Bonetta L, MacAllan D, Parry D, Holder A, Dickson C, et al. CDK6 (PLSTIRE) and CDK4 (PSK-J3) are a distinct subset of the cyclin-dependent kinases that associate with cyclin D1. Oncogene. 1994;9(1):71-9.

36. Galluzzi L. No death without life: vital functions of apoptotic effectors. Cell Death and Differentiation. 2008;15:1113-23.

37. Sherr CJ. Cancer cell cycles. Science. 1996;274:1672-7.

38. Klug WS, Cummings MR. Concepts of genetics: Pearson Education, Inc; 2003.

39. Brown MA. Tumor suppressor genes and human cancer. Advances in Genetics. 1997;36:4-135.

40. Nussbaum RL, Roderick RM, Huntington FW. Genetics in medicine. 7 ed. Philadelphia: Saunders: Elsevier; 2007.

41. Dang CV. MYC on the path to cancer. Cell. 2012;149(1):22-35.

42. Dang CV, Le A, Gao P. MYC-induced cancer cell energy metabolism and therapeutic opportunities. Clinical cancer research. 2009;15(21):6479-83.

43. Filippakopoulos P, Qi J, Picaud S, Shen Y, Smith WB, Fedorov O, et al. Selective inhibition of BET bromodomains. Nature Reviews. 2010(468):1067-73.

44. Li L, Osdal T, Ho Y, Chun S, McDonald T, Agarwal P, et al. SIRT1 Activation by a c-MYC Oncogenic Network Promotes the Maintenance and Drug Resistance of Human FLT3-ITD Acute Myeloid Leukemia Stem Cells. Cell Stem Cell. 2014;15(4):431-46.

45. Liu PY, Xu N, Malyukova A, Scarlett CJ, Sun YT, Zhang XD, et al. The histone deacetylase SIRT2 stabilizes Myc oncoproteins. Cell Death And Differentiation. 2012;20:503.

46. R. Connolly VS. Epigenetics as a Therapeutic Target in Breast Cancer. J Mammary Gland Biol Neoplasia. 2012;17(3):191-204.

47. Li B, Carey M, Workman JL. The role of chromatin during transcription. Cell. 2007;128(4):707-19.

48. Sanchez R, Zhou M-M. The role of human bromodomains in chromatin biology and gene transcription. Current opinion in drug discovery & development. 2009;12(5):659.

49. Latchman D, Latchman DS. Eukaryotic transcription factors: Academic press; 2010.

50. Kozako T, Suzuki T, Yoshimitsu M, Arima N, Honda S-i, Soeda S. Anticancer agents targeted to sirtuins. Molecules. 2014;19(12):20295-313.

51. Cardaci S, Desideri E, Ciriolo MR. Targeting aerobic glycolysis: 3-bromopyruvate as a promising anticancer drug. Journal of bioenergetics and biomembranes. 2012;44(1):17-29.

52. Koa YH, Smitha BL, Wanga Y, Pompera MG, Rinic DA, Torbensond MS, et al. Advanced cancers: eradication in all cases using 3-bromopyruvate therapy to deplete ATP. Biochemical and Biophysical Research Communications. 2004;324:269-75.

53. Bustamante E, Pedersen PL. High aerobic glycolysis of rat hepatoma cells in culture: role of mitochondrial hexokinase. Proceedings of the National Academy of Sciences. 1977;74:3735-9.

54. Kim W, Yoon JH, Jeong JM, Cheon GJ, Lee TS, Yang JI, et al. Apoptosis-inducing antitumor efficacy of hexokinase II inhibitor in hepatocellular carcinoma. Molecular Cancer Therapeutics. 2007;6(9).

55. Nakashima RA, Mangan PS, Colombini M, Pedersen PL. Hexokinase receptor complex in hepatomamitochondria: evidence fromN,N′-dicyclohexylcarbodiimidelabeling studies for the involvement of the pore-forming protein VDAC. Biochemistry. 1986;25:1015-21.

56. Devasagayam TPA, Tilak JC, Boloor KK, Sane Ketaki S, Ghaskadbi Saroj S, Lele RD. Free Radicals and Antioxidants in Human Health: Current Status and Future Prospects. Journal of Association of Physicians of India. 2004;52:796-800.

57. Andreyev AY, Kushnareva YE, Starkov AA. Mitochondrial metabolism of reactive oxygen species. Biochemistry. 2005;70:200-14.

58. Chen Z, Zhang H, Lu W, Huang P. Role of mitochondria-associated hexokinase II in cancer cell death induced by 3-bromopyruvate. Biochimica et Biophysica Acta (BBA)-Bioenergetics. 2009;1787(5):553-60.

59. Ganapathy-Kanniappan S, Vali M, Kunjithapatham R, Buijs M, Syed L, Rao P, et al. 3-bromopyruvate: a new targeted antiglycolytic agent and a promise for cancer therapy. Current pharmaceutical biotechnology. 2010;11(5):510-7.

60. Sladek T. E2F transcription factor action, regulation and possible role in human cancer. Cell proliferation. 1997;30(3-4):97-105.

61. Hartwell L, Weinert T. Checkpoints: controls that ensure the order of cell cycle events. Science. 1989;246(4930):629-34.

62. Adams PD. Regulation of the retinoblastoma tumor suppressor protein by cyclin/cdks. Biochimica et Biophysica Acta (BBA) - Reviews on Cancer. 2001;1471(3):M123-M33.

63. Sladek TL. E2F transcription factor action, regulation and possible role in human cancer. Cell Proliferation. 1997;30(3-4):97-105.

64. Bell SP, Dutta A. DNA Replication in Eukaryotic Cells. Annual Review of Biochemistry. 2002;71(1):333-74.

65. Henneke G, Koundrioukoff S, Hübscher U. Multiple roles for kinases in DNA replication. EMBO reports. 2003;4(3):252-6.

66. McMahon SB. MYC and the control of apoptosis. Cold Spring Harbor perspectives in medicine. 2014;4(7):a014407.

67. Lei M, Tye BK. Initiating DNA synthesis: from recruiting to activating the MCM complex. Journal of Cell Science. 2001;114(8):1447-54.

68. Sherr CJ, Roberts JM. CDK inhibitors: positive and negative regulators of G1-phase progression. Genes & development. 1999;13(12):1501-12.

69. Draetta G, Luca F, Westendorf J, Brizuela L, Ruderman J, Beach D. cdc2 protein kinase is complexed with both cyclin A and B: Evidence for proteolytic inactivation of MPF. Cell. 1989;56(5):829-38.

70. Nigg EA. Mitotic kinases as regulators of cell division and its checkpoints. Nature Reviews Molecular Cell Biology. 2001;2:21.

71. Lowe M, Rabouille C, Nakamura N, Watson R, Jackman M, Jämsä E, et al. Cdc2 Kinase Directly Phosphorylates the cis-Golgi Matrix Protein GM130 and Is Required for Golgi Fragmentation in Mitosis. Cell. 1998;94(6):783-93.

72. Kimura K, Hirano M, Kobayashi R, Hirano T. Phosphorylation and Activation of 13S Condensin by Cdc2 in Vitro. Science. 1998;282(5388):487-90.

73. Rubin CI, Atweh GF. The role of stathmin in the regulation of the cell cycle. Journal of Cellular Biochemistry. 2004;93(2):242-50.

74. Adams J, Cory S. The Bcl-2 apoptotic switch in cancer development and therapy. Oncogene. 2007;26(9):1324-37.

75. Lowe SW, Cepero E, Evan G. Intrinsic tumour suppression. Nature. 2004;432(7015):307-15.

76. Evan G, Littlewood T. A matter of life and cell death. Science. 1998;281(5381):1317-22.

77. Willis SN, Adams JM. Life in the balance: how BH3-only proteins induce apoptosis. Current opinion in cell biology. 2005;17(6):617-25.

78. Junttila MR, Evan GI. p53—a Jack of all trades but master of none. Nature Reviews Cancer. 2009;9(11):821-9.

79. Nakashima RA, Mangan PS, Colombini M, Pedersen PL. Hexokinase receptor complex in hepatoma mitochondria: evidence from N,N'-dicyclohexylcarbodiimide-labeling studies for the involvement of the pore-forming protein VDAC. Biochemistry. 1986;25(5):1015-21.

80. Veldhoen RA, Banman SL, Hemmerling DR, Odsen R, Simmen T, Simmonds AJ, et al. The chemotherapeutic agent paclitaxel inhibits autophagy through two distinct mechanisms that regulate apoptosis. Oncogene. 2012;32:736.

81. Majno G, Joris I. Apoptosis, oncosis, and necrosis. An overview of cell death. The American Journal of Pathology. 1995;146(1):3-15.

82. Golstein P, Kroemer G. Cell death by necrosis: towards a molecular definition. Trends in Biochemical Sciences. 2007;32(1):37-43.

83. Levine B, Kroemer G. Autophagy in the pathogenesis of disease. Cell. 2008;132(1):27-42.

84. Mizushima N. Autophagy: process and function. Genes & development. 2007;21(22):2861-73.

85. Bröker LE, Huisman C, Span SW, Rodriguez JA, Kruyt FAE, Giaccone G. Cathepsin B Mediates Caspase-Independent Cell Death Induced by Microtubule Stabilizing Agents in Non-Small Cell Lung Cancer Cells. Cancer Research. 2004;64(1):27-30.

86. Hensel T, Giorgi C, Schmidt O, Calzada-Wack J, Neff F, Buch T, et al. Targeting the EWS-ETS transcriptional program by BET bromodomain inhibition in Ewing sarcoma. Oncotarget. 2015.

87. Sinha S, Levine B. The autophagy effector Beclin 1: a novel BH3-only protein. Oncogene. 2008;27:S137-S48.

88. Mathew R, Karantza-Wadsworth V, White E. Role of autophagy in cancer. Nature Reviews Cancer. 2007;7(12):961-7.

89. . !!! INVALID CITATION !!! (Galluzzi, 2008 #55;Zong, 2006 #56;Golstein, 2007 #131;Murakami, 2014 #146).

90. Galluzzi L, Kroemer G. Necroptosis: a specialized pathway of programmed necrosis. Cell. 2008;135(7):1161-3.

91. Zong W-X, Thompson CB. Necrotic death as a cell fate. Genes & development. 2006;20(1):1-15.

92. Grivennikov SI, Greten FR, Karin M. Immunity, inflammation, and cancer. Cell. 2010;140(6):883-99.

93. White E, Karp C, Strohecker AM, Guo Y, Mathew R. Role of autophagy in suppression of inflammation and cancer. Current opinion in cell biology. 2010;22(2):212-7.

94. Murakami Y, Matsumoto H, Roh M, Giani A, Kataoka K, Morizane Y, et al. Programmed necrosis, not apoptosis, is a key mediator of cell loss and DAMP-mediated inflammation in dsRNA-induced retinal degeneration. Cell death and differentiation. 2014;21(2):270.

95. Cheson BD, Bennett JM, Kopecky KJ, Büchner T, Willman CL, Estey EH, et al. Revised recommendations of the international working group for diagnosis, standardization of response criteria, treatment outcomes, and reporting standards for therapeutic trials in acute myeloid leukemia. Journal of Clinical Oncology. 2003;21(24):4642-9.

96. Travis LB, Li C-Y, Zhang Z-N, Li D-G, Yin S-N, Chow W-H, et al. Hematopoietic malignancies and related disorders among benzene-exposed workers in China. Leukemia & lymphoma. 1994;14(1-2):91-102.

97. Winum JY, Scozzafava A, Montero JL, Supuran CT. Sulfamates and their therapeutic potential. Medicinal research reviews. 2005;25(2):186-228.

98. Roth M, Chen W. Sorting out functions of sirtuins in cancer. Oncogene. 2014;33(13):1609-20.

99. Cantó C, Auwerx J. Targeting sirtuin 1 to improve metabolism: all you need is NAD+? Pharmacological reviews. 2012;64(1):166-87.

100. Glozak MA, Sengupta N, Zhang X, Seto E. Acetylation and deacetylation of non-histone proteins. gene. 2005;363:15-23.

101. Spange S, Wagner T, Heinzel T, Krämer OH. Acetylation of non-histone proteins modulates cellular signalling at multiple levels. The international journal of biochemistry & cell biology. 2009;41(1):185-98.

102. Glozak M, Seto E. Histone deacetylases and cancer. Oncogene. 2007;26(37):5420.

103. Jing H, Lin H. Sirtuins in Epigenetic Regulation. Chemical reviews. 2015;115(6):2350-75.

104. Macedo de Oliveira MV, Andrade JMO, Paraíso AF, Santos SHS. Sirtuins and cancer: new insights and cell signaling. Cancer investigation. 2013;31(10):645-53.

105. Trapp J, Jochum A, Meier R, Saunders L, Marshall B, Kunick C, et al. Adenosine Mimetics as Inhibitors of NAD+-Dependent Histone Deacetylases, from Kinase to Sirtuin Inhibition. Journal of Medicinal Chemistry. 2006;49(25):7307-16.

106. Liu H, Jiang C, Xiong C, Ruan J. DEDC, a new flavonoid induces apoptosis via a ROS-dependent mechanism in human neuroblastoma SH-SY5Y cells. Toxicology in Vitro. 2012;26(1):16-23.

107. Radogna F, Cerella C, Gaigneaux A, Christov C, Dicato M, Diederich M. Cell type-dependent ROS and mitophagy response leads to apoptosis or necroptosis in neuroblastoma. Oncogene. 2015;35:3839.

108. Levis M. FLT3 mutations in acute myeloid leukemia: what is the best approach in 2013? Hematology / the Education Program of the American Society of Hematology American Society of Hematology Education Program. 2013;2013:220-6.

109. Dan L, Klimenkova O, Klimiankou M, Klusmann J-H, van den Heuvel-Eibrink MM, Reinhardt D, et al. The role of Sirtuin 2 activation by nicotinamide phosphoribosyltransferase in the aberrant proliferation and survival of myeloid leukemia cells. Haematologica. 2011.

110. Pedersen PL. 3-Bromopyruvate (3BP) a fast acting, promising, powerful, specific, and effective “small molecule” anti-cancer agent taken from labside to

bedside: introduction to a special issue. Journal of bioenergetics and biomembranes. 2012;44(1):1-6.

111. Sanchez R, Meslamani J, Zhou M-M. The bromodomain: from epigenome reader to druggable target. Biochimica et Biophysica Acta (BBA)-Gene Regulatory Mechanisms. 2014;1839(8):676-85.

112. Gibson AW, Cheng T, Johnston RN. Apoptosis Induced by c-Myc Overexpression Is Dependent on Growth Conditions. Experimental Cell Research. 1995;218(1):351-8.

113. Hoffman B, Liebermann DA. Apoptotic signaling by c-MYC. Oncogene. 2008;27:6462.

114. Phesse TJ, Myant KB, Cole AM, Ridgway RA, Pearson H, Muncan V, et al. Endogenous c-Myc is essential for p53-induced apoptosis in response to DNA damage in vivo. Cell Death And Differentiation. 2014;21:956.

115. Sarosiek KA, Fraser C, Muthalagu N, Bhola PD, Chang W, McBrayer SK, et al. Developmental Regulation of Mitochondrial Apoptosis by c-Myc Governs Age- and Tissue-Specific Sensitivity to Cancer Therapeutics. Cancer Cell. 2017;31(1):142-56.

116. Chung C-w. 1 Small Molecule Bromodomain Inhibitors: Extending the Druggable Genome. Progress in medicinal chemistry. 2012;51:1.

117. Ember SW, Zhu J-Y, Olesen SH, Martin MP, Becker A, Berndt N, et al. Acetyl-lysine binding site of bromodomain-containing protein 4 (BRD4) interacts with diverse kinase inhibitors. ACS chemical biology. 2014;9(5):1160-71.

118. Dey A, Nishiyama A, Karpova T, McNally J, Ozato K. Brd4 marks select genes on mitotic chromatin and directs postmitotic transcription. Molecular Biology of the Cell. 2009;20:4899–909.

119. Dang CV, Le A, Gao P. MYC-induced cancer cell energy metabolism and therapeutic opportunities. Clinical Cancer Research. 2009;15:6479-83.

120. Tong W-G, Chen R, Plunkett W, Siegel D, Sinha R, Harvey RD, et al. Phase I and pharmacologic study of SNS-032, a potent and selective Cdk2, 7, and 9

inhibitor, in patients with advanced chronic lymphocytic leukemia and multiple myeloma. Journal of clinical oncology. 2010;28(18):3015-22.

121. Meitar D, Crawford SE, Rademaker AW, Cohn SL. Tumor angiogenesis correlates with metastatic disease, N-myc amplification, and poor outcome in human neuroblastoma. Journal of clinical oncology. 1996;14(2):405-14.

122. Vargo-Gogola T, Rosen JM. Modelling breast cancer: one size does not fit all. Nature Reviews Cancer. 2007;7(9):659-72.

123. Van Staveren W, Solís DW, Hebrant A, Detours V, Dumont JE, Maenhaut C. Human cancer cell lines: Experimental models for cancer cells in situ? For cancer stem cells? Biochimica et Biophysica Acta (BBA)-Reviews on Cancer. 2009;1795(2):92-103.

124. Louzada S, Adega F, Chaves R. Defining the sister rat mammary tumor cell lines HH-16 cl. 2/1 and HH-16. cl. 4 as an in vitro cell model for Erbb2. PloS one. 2012;7(1):e29923.

125. Engel LW, Young NA, Tralka TS, Lippman ME, O'Brien SJ, Joyce MJ. Establishment and characterization of three new continuous cell lines derived from human breast carcinomas. Cancer research. 1978;38(10):3352-64.

126. Webb B, Sali A. Comparative protein structure modeling using Modeller. Current protocols in bioinformatics. 2014:5.6. 1-5.6. 32.

127. Acdlabs.com. Advanced Chemistry Development, Inc. ACD/Chemsketch 12.0 ed. Toronto, Canada2015.

128. OLBoyle NM, Banck M, James CA, Morley C, Vandermeersch T, Hutchison G. Open Babel: An open chemical toolbox. Journal of Cheminformatics. 2011;3:33.

129. Vainio MJ, Johnson MS. Generating conformer ensembles using a multiobjective genetic algorithm. The Journal of Chemical Physics. 2007;47(6):2462-74.

130. Puranen JS, Vainio MJ, Johnson MS. Accurate conformation-dependent molecular electrostatic potentials for high-throughput in silico drug discovery. Journal of computational chemistry. 2010;31(8):1722-32.

131. Trott O, Olson AJ. AutoDock Vina: improving the speed and accuracy of docking with a new scoring function, efficient optimization, and multithreading. Journal of Computational Chemistry. 2010;31(2):455-61.

132. Ruiz-Carmona S, Alvarez-Garcia D, Foloppe N, Garmendia-Doval AB, Juhos S, Schmidtke P, et al. rDock: a fast, versatile and open source program for docking ligands to proteins and nucleic acids. PLoS computational biology. 2014;10(4):e1003571.

133. Huey R, Morris G. AutoDock tools. La Jolla, CA, USA: The Scripps Research Institute. 2003.

134. Pronk S, Páll S, Schulz R, Larsson P, Bjelkmar P, Apostolov R, et al. GROMACS 4.5: a high-throughput and highly parallel open source molecular simulation toolkit. Bioinformatics. 2013:btt055.

135. Lindorff-Larsen K, Piana S, Palmo K, Maragakis P, Klepeis JL, Dror RO, et al. Improved side-chain torsion potentials for the Amber ff99SB protein force field. Proteins: Structure, Function, and Bioinformatics. 2010;78(8):1950-8.

136. Jämbeck JP, Lyubartsev AP. An extension and further validation of an all-atomistic force field for biological membranes. Journal of Chemical Theory and Computation. 2012;8(8):2938-48.

137. Nickolls J, Buck I, Garland M, Skadron K. Scalable parallel programming with CUDA. Queue. 2008;6(2):40-53.

138. da Silva AWS, Vranken W. ACPYPE-Antechamber python parser interface. BioMed Central Research Notes. 2012;5(1):367.

139. Jämbeck JP, Lyubartsev AP. Update to the General Amber Force Field for small solutes with an emphasis on free energies of hydration. The Journal of Physical Chemistry B. 2014;118(14):3793-804.

140. Kumari R, Kumar R, Lynn A. g_mmpbsa・ A GROMACS Tool for High-Throughput MM-PBSA Calculations. Journal of Chemical Information and Modeling. 2014;54(7):1951-62.

141. Biasini M, Bienert S, Waterhouse A, Arnold K, Studer G, Schmidt T, et al. SWISS-MODEL: modelling protein tertiary and quaternary structure using evolutionary information. Nucleic acids research. 2014;42(W1):W252-W8.

142. Trott O, Olson AJ. AutoDock Vina: improving the speed and accuracy of docking with a new scoring function, efficient optimization, and multithreading. J Comput Chem. 2010;31(2):455-61.

143. Gillies R, Didier N, Denton M. Determination of cell number in monolayer cultures. Analytical biochemistry. 1986;159(1):109-13.

144. Kueng W, Silber E, Eppenberger U. Quantification of cells cultured on 96-well plates. Analytical biochemistry. 1989;182(1):16-9.

145. Berry J, Huebner E, Butler M. The crystal violet nuclei staining technique leads to anomalous results in monitoring mammalian cell cultures. Cytotechnology. 1996;21(1):73-80.

146. Johnson G. Automated handled instrument improves counting precision across multiple cell lines. BioTechniques. 2010;48:325-7.

147. Rowland S, Jacobson J, Patton W, King A, PJ. C. Dual fluorescence analysis of DNA apoptosis in sperm. American Journal of Obstetrics and Gynecology. 2003;188(5):1156-7.

148. Pettersen EF, Goddard TD, Huang CC, Couch GS, Greenblatt DM, Meng EC, et al. UCSF Chimera—a visualization system for exploratory research and analysis. Journal of computational chemistry. 2004;25(13):1605-12.

149. Latt SA, Langlois RG, Melamed MR, Lindmo T, Mendelsohn ML. Fluorescent probes of DNA microstructure and DNA synthesis. . 2nd ed. New York: John Wiley & Sons; 1990.

150. Danz R, Vogelgsang A, Käthner R. PlasDIC–a useful modification of the differential interference contrast according to Smith/Nomarski in transmitted light arrangement. Photonik. 2004;1:42.

151. Klionsky DJ, Cuervo AM, Seglen PO. Methods for monitoring autophagy from yeast to human. Autophagy. 2007;3(3):181-206.

152. Guthrie H, Welch G. Determination of high mitochondrial membrane potential in spermatozoa loaded with the mitochondrial probe 5,5',6,6'-tetrachloro-1,1',3,3'-tetraethylbenzimidazolyl-carbocyanine iodide (JC-1) by using fluorescence-activated flow cytometry. Methods in Molecular Biology. 2008;477:89-97.

153. Mandy F, Bergeron M, Minkus T. Principles of flow cytometry. Transfusion Science. 1995;16(4):303-14.

154. Kroemer G. The proto-oncogene Bcl-2 and its role in regulating apoptosis. Nature Medicine. 1997;3(6):614-20.

155. Haupt S, Berger M, Goldberg Z, Haupt Y. Apoptosis - the p53 network. Journal of Cell Science. 2003;116(Pt 20):4077-85.

156. Haimes J, Kelley M, Dharmacon. Demonstration of a ΔΔCq Calculation Method to Compute Relative Gene Expression from qPCR Data. [Research article]. In press 2014.

157. Dallas P, Gottardo N, Firth M, Beesley A, Hoffmann K, Terry P, et al. Gene expression levels assessed by oligonucleotide microarray analysis and quantitative real-time RT-PCR -- how well do they correlate? BMC Genomics. 2005;6(1):59.

158. Cui H, Kamal Z, Ai T, Xu Y, More SS, Wilson DJ. Discovery of potent and selective sirtuin 2 (SIRT2) inhibitors using a fragment-based approach. J Med Chem. 2014;57.

159. Disch JS, Evindar G, Chiu CH, Blum CA, Dai H, Jin L, et al. Discovery of thieno [3, 2-d] pyrimidine-6-carboxamides as potent inhibitors of SIRT1, SIRT2, and SIRT3. Journal of medicinal chemistry. 2013;56(9):3666-79.

160. Tembo T. Mechanistic studies on paired drug combinations using a BRD4 inhibitor, a SIRT1 inhibitor, and an antimitotic drug on breast cancer cell lines. MSc, University of Pretoria. 2016.

161. Hu J, Jing H, Lin H. Sirtuin inhibitors as anticancer agents. Future Medicinal Chemistry. 2014;6(8):945-66.

162. Peck B, Chen C-Y, Ho K-K, Di Fruscia P, Myatt SS, Coombes RC, et al. SIRT Inhibitors Induce Cell Death and p53 Acetylation through Targeting Both SIRT1 and SIRT2. Molecular Cancer Therapeutics. 2010.

163. Solomon JM, Pasupuleti R, Xu L, McDonagh T, Curtis R, DiStefano PS, et al. Inhibition of SIRT1 Catalytic Activity Increases p53 Acetylation but Does Not Alter Cell Survival following DNA Damage. Molecular and Cellular Biology. 2006;26(1):28-38.

164. Ly JD, Grubb DR, Lawen A. The mitochondrial membrane potential (Δψm) in apoptosis; an update. Apoptosis. 2003;8(2):115-28.

165. Gertz M, Steegborn C. Function and regulation of the mitochondrial Sirtuin isoform Sirt5 in Mammalia. Biochimica et Biophysica Acta (BBA) - Proteins and Proteomics. 2010;1804(8):1658-65.

166. Métivier D, Dallaporta B, Zamzami N, Larochette N, Susin SA, Marzo I, et al. Cytofluorometric detection of mitochondrial alterations in early CD95/Fas/APO-1-triggered apoptosis of Jurkat T lymphoma cells. Comparison of seven mitochondrion-specific fluorochromes. Immunology letters. 1998;61(2-3):157-63.

167. Hole PS, Zabkiewicz J, Munje C, Newton Z, Pearn L, White P, et al. Overproduction of NOX-derived ROS in AML promotes proliferation and is associated with defective oxidative stress signaling. Blood. 2013.

168. Mochizuki T, Furuta S, Mitsushita J, Shang WH, Ito M, Yokoo Y, et al. Inhibition of NADPH oxidase 4 activates apoptosis via the AKT/apoptosis signal-regulating kinase 1 pathway in pancreatic cancer PANC-1 cells. Oncogene. 2006;25:3699.

169. Yu SJ, Yoon J-H, Yang J-I, Cho EJ, Kwak MS, Jang ES, et al. Enhancement of hexokinase II inhibitor-induced apoptosis in hepatocellular carcinoma cells via augmenting ER stress and anti-angiogenesis by protein disulfide isomerase inhibition. Journal of bioenergetics and biomembranes. 2012;44(1):101-15.

170. Wang M-J, Liu S, Liu Y, Zheng D. Actinomycin D enhances TRAIL-induced caspase-dependent and-independent apoptosis in SH-SY5Y neuroblastoma cells. Neuroscience research. 2007;59(1):40-6.

The Research Ethics Committee, Faculty Health Sciences, University of Pretoria complies with ICH-GCP guidelines and has US Federal wide Assurance.
- FWA 00002567, Approved dd 22 May 2002 and Expires 03/20/2022.
- IRB 0000 2235 IORG0001762 Approved dd 22/04/2014 and Expires 03/14/2020.

UNIVERSITEIT VAN PRETORIA
UNIVERSITY OF PRETORIA
YUNIBESITHI YA PRETORIA

Faculty of Health Sciences Research Ethics Committee

29/06/2017

Approval Certificate
New Application

Ethics Reference No.: 244/2017

Title: In vitro study of in silico designed sirtuin 1 and bromodomain 4 inhibitors on human neuroblastoma SH-SY5Y and acute myeloid leukemia U937 cells.

Dear Miss Monique Otto

The **New Application** as supported by documents specified in your cover letter dated 1/06/2017 for your research received on the 1/06/2017, was approved by the Faculty of Health Sciences Research Ethics Committee on its quorate meeting of 28/06/2017.

Please note the following about your ethics approval:
- Ethics Approval is valid for 2 years
- Please remember to use your protocol number (**244/2017**) on any documents or correspondence with the Research Ethics Committee regarding your research.
- Please note that the Research Ethics Committee may ask further questions, seek additional information, require further modification, or monitor the conduct of your research.

Ethics approval is subject to the following:
- The ethics approval is conditional on the receipt of **6 monthly written Progress Reports**, and
- The ethics approval is conditional on the research being conducted as stipulated by the details of all documents submitted to the Committee. In the event that a further need arises to change who the investigators are, the methods or any other aspect, such changes must be submitted as an Amendment for approval by the Committee.

We wish you the best with your research.

Yours sincerely

Dr R Sommers, MBChB; MMed (Int); MPharMed,PhD
Deputy Chairperson of the Faculty of Health Sciences Research Ethics Committee, University of Pretoria

The Faculty of Health Sciences Research Ethics Committee complies with the SA National Act 61 of 2003 as it pertains to health research and the United States Code of Federal Regulations Title 45 and 46. This committee abides by the ethical norms and principles for research, established by the Declaration of Helsinki, the South African Medical Research Council Guidelines as well as the Guidelines for Ethical Research: Principles Structures and Processes, Second Edition 2015 (Department of Health).

☎ 012 356 3084 deepeka.behari@up.ac.za / fhsethics@up.ac.za http://www.up.ac.za/healthethics
✉ Private Bag X323, Arcadia, 0007 - Tswelopele Building, Level 4, Room 60, Gezina, Pretoria